TOWARD AN IN VITRO BIOEQUIVALENCE TEST

by

Jie Sheng

A dissertation submitted in partial fulfillment
of the requirements for the degree of
Doctor of Philosophy
(Pharmaceutical Sciences)
In The University of Michigan
2007

Doctoral Committee:

Professor Gordon L. Amidon, Chair
Professor Henry Y. Wang
Associate Professor Nair Rodriguez-Hornedo
Associate Professor Steven P. Schwendeman

To Kurt Q. Zhu, my husband and my very best friend,

and

to Diana S. Zhu and Brandon D. Zhu, my lovely children.

Acknowledgements

Most of all, I thank Prof. Gordon L. Amidon, for his support, guidance, and inspiration during my graduate studies at the University of Michigan. Being his student is the best step happened in my career. I am always amazed by his vision, energy, patience and dedication to the research and his students. He trained me to grow as a scientist and as a person.

I also wish to thank all of my committee members, Professors David Fleisher, Nair Rodriguez-Hornedo, Steven Schwendeman and Henry Wang, for their very insightful and constructive suggestions to my research. It took all their efforts to raise me as a professional scientist in pharmaceutical field. They all contributed significantly to development and improvement of my graduate work. Especially, Prof. Wang has also guided me in thinking of career development as if 20-year later. I felt to be his student in many ways.

I thank mentors, colleagues and friends, Prof. John Yu from Ohio State University, Paul Sirois from Eli Lilly, Kurt Seefeldt, Chet Provoda, Jonathan Miller, John Chung, Chris Landoswki, Haili Ping and Yasuhiro Tsume from College of Pharmacy, for many interesting discussions throughout the graduate program. I thank L.D. and Pat for facilitating my research in the college. I also thank Iris Templin and Gail for their administrative help along the way.

I thank Prof. David Smith for his support and guidance during the PSTP fellowship, and beyond. I thank Prof. Kyung-Dall Lee for his perspectives in teaching, science and research.

Lastly, I am grateful to my husband, Kurt Zhu, for his endless love and patience. I wish that I had supported him the same way when he was in graduate school. I thank my children, Diana and Brandon, for being so close to me.

TABLE OF CONTENTS

DEDICATION……...ii

ACKNOWLEDGEMENTS……iii

LIST OF TABLES……...vii

LIST OF FIGURES……..ix

ABSTRACT……...xi

CHAPTER

I. INFLUENCE OF FASTED STATE GASTROENTEROLOGICAL FACTORS ON *IN VIVO* DISSOLUTION OF POORLY SOLUBLE DRUGS……...1

Introduction……..1
Gastrointestinal Factors……...2
Motility……2
pH……..4
Bile Salts…….....4
Buffer Species……...6
Other Gastrointestinal Factors……..7
Effects of GI Factors on BCS II drugs……7
Selection of Model Compounds…….11
Implications of GI Factors in Establishing Bioequivalence Dissolution Methodology……..12
Summary……15
Specific Aims……16
References……..21

II. PARTICLE DIFFUSIONAL LAYER THICKNESS IN A USP DISSOLUTION APPARATUS II: A COMBINED FUNCTION OF PARTICLE SIZE AND PADDLE SPEED……27

Abstract……..27
Introduction……28

Theoretical Section……31
Experimental Section……34
Results……...37
Discussion……..41
Conclusions……51
References……..63

III. SOLUBILIZATION AND DISSOLUTION OF INSOLUBLE WEAK ACID, KETOPROFEN: EFFECTS OF PH COMBINED WITH SURFACTANT……66

Abstract……..66
Introduction……67
Methods……69
Results and Discussion ……76
Conclusions……83
References……..93

IV. A COMPARISON OF PHOSPHATE AND BICARBONATE BUFFERS: RELEVANCE TO IN VIVO DISSOLUTION……96

Abstract……..96
Introduction……97
Theoretical Section……..100
Experimental Section……...105
Results……..107
Discussion……114
Conclusions……..120
References……131

V. SUMMARY……134

LIST OF TABLES

Table 1.1. Biopharmaceutical Classification System (BCS)……..17

Table 1.2. pH in the small intestine in healthy humans in the fasted state…….18

Table 1.3. Biopharmaceutical properties of fenofibrate, ketoprofen and indomethacin……..19

Table 2.1. Physical characteristics of various size fractions of fenofibrate powder...52

Table 2.2. Comparison of the relationship between h_{app} and r in: Higuchi-Hiestand's work, Hintz-Johnson's work and the current work in a USP dissolution apparatus II…….……53

Table 2.3. Particle sizes and Re: comparison of fenofibrate powder dissolution in a USP dissolution apparatus II and previous studies using the function form of Eq 2……54

Table 3.1. Equilibrium solubility (mg/mL ± S.D.) of ketoprofen at various pH and SLS concentrations……85

Table 3.2. Solubilization power (C_{SN}) of various pH and SLS concentrations on ketoprofen……..86

Table 3.3. The intrinsic dissolution rate ($J/\omega^{1/2},\ \times 10^4\ mg/cm^2/s^{1/2}/rad^{1/2} \pm S.D.$) of ketoprofen at various pH and SLS concentrations……87

Table 4.1. Commonly used pharmaceutical dissolution media/buffers for simulating upper small intestine……121

Table 4.2. Parameters used in theoretical analysis……122

Table 4.3. Intrinsic flux of ketoprofen in the phosphate and in the bicarbonate buffer systems, experimental and theoretical results……..123

Table 4.4. Intrinsic flux ratios of indomethacin in the phosphate versus in the bicarbonates, experimental and theoretical results……..124

Table 4.5. Intrinsic dissolution rates of ketoprofen in 50mM pH 6.8 phosphate and bicarbonate buffers……..125

Table 4.6-1. Drug flux ratio in USP 50 mM phosphate and 15mM bicarbonate buffers: the impact of drug solubility and drug diffusion coefficient (drug pKa = 3)……..126

Table 4.6-2. Drug flux ratio in USP 50 mM phosphate and 15 mM bicarbonate buffers: the impact of drug solubility and drug diffusion coefficient (drug pKa = 5)……..126

Table 4.7-1. Drug flux ratio in USP 50 mM phosphate and 15 mM bicarbonate buffers: the impact of drug pKa and drug diffusion coefficient (drug solubility = 1×10^{-8} M)….127

Table 4.7-2. Drug flux ratio in USP 50mM phosphate and 15 mM bicarbonate buffers: the impact of drug pKa and drug diffusion coefficient (drug solubility = 1×10^{-3} M)…..127

Table 4.8. Phosphate buffer as an equivalent substitute for 15 mM bicarbonate buffer……128

Table 4.9. pKa values, maximum dose, and salt forms of some BCS II weak acids.....129

LIST OF FIGURES

Figure 1.1. The chemical structures of fenofibrate, ketoprofen and indomethacin……..20

Figure 2.1a. DSC thermograms of the jet-milled fenofibrate……..55

Figure 2.1b. DSC thermograms of fenofibrate "as received" from Sigma……..55

Figure 2.2. PXRD patterns of fenofibrate "as received" and jet-milled……...56

Figure 2.3. Particle size distribution of fenofibrate powders……...57

Figure 2.4. SEM picture of a typical fenofibrate powder (63-75μm)……..58

Figure 2.5. Dissolution profiles of various size fractions of fenofibrate powder at 50 rpm and 100 rpm. (Error bars represent the standard deviation of a mean of three experiments.)…….59

Figure 2.6. Bifunctional analysis of the dependence of diffusional layer thickness h_{app} on particle sizes under different hydrodynamics in a USP dissolution apparatus II (n = 3)…….60

Figure 2.7. Dependence of h_{app} on square root of particle sizes under different hydrodynamics in a USP dissolution apparatus II (n = 3)……61

Figure 2.8. Dimensionless analysis of the dependence of diffusional layer thickness h_{app} on particle sizes and hydrodynamics in a USP dissolution apparatus II (n = 3)…..62

Figure 3.1. Chemical Structure of ketoprofen……88

Figure 3.2. Total solubility as function of pH and SLS…….90

Figure 3.3. Intrinsic dissolution curves of ketoprofen at various SLS concentrations pH 4.0 buffers……..91

Figure 3.4. The intrinsic dissolution rate as function of pH and SLS……92

Figure 4.1. Dependence of drug flux ratio in the USP 50 mM phosphate buffer versus 15 mM bicarbonate buffer on drug pKa and solubility……130

ABSTRACT

TOWARD AN IN VITRO BIOEQUIVALENCE TEST

by

Jie Sheng

Chair: Gordon L. Amidon

Oral absorption of Biopharmaceutics Classification System (BCS) II drugs is limited by *in vivo* dissolution. The current pharmacopeial *in vitro* dissolution methodologies are designed for quality control, and do not reflect *in vivo* performance criteria. This project is an investigation into the key *in vitro* dissolution parameters: hydrodynamics, pH, surfactants/bile salts, and buffer species that are important to *in vivo* dissolution. Hydrodynamics, i.e., the convective contributor to dissolution, was examined through the stagnant diffusional layer thickness, h_{app}, of fenofibrate in a USP dissolution apparatus II. These results demonstrate that h_{app} has different functional dependences depending on particle sizes and the paddle speed. At 50 rpm, h_{app} is linear with square root of particle size ($R^2 = 0.98$) within the range of 6.8-106 μm. In contrast, at 100 rpm a transitional particle radius exists at 23.7 μm, above which the relationship becomes constant. Further, the effect of particle size and paddle speed on h_{app} can be combined using dimensional analysis.

In addition, key components of GI fluids such as pH, bile salts and buffer species were also investigated. The effects of pH and surfactants on ketoprofen (a BCS II weak acid) were investigated. The dramatic enhancement of *in vitro* solubility/dissolution attributable to an increase of pH and presence of SLS mimics the *in vivo* solubilization/dissolution behavior of ketoprofen, when the pH increases from 1 to 2 in the stomach to 5 to 6 in the duodenum. Further, even at the same pH and buffer concentration, the importance of buffer species was demonstrated by a) 50-200% faster intrinsic dissolution rates of ketoprofen and indomethacin in USP SIF, FaSSIF phosphates than in various concentrations of bicarbonates more reflective of *in vivo*; and b) the dependence of buffer differential on biopharmaceutical properties, e.g., drug pKa, solubility and diffusivity. Finally, simple phosphate buffers are recommended: at pH 6.5, ketoprofen and indomethacin require 13 -14 mM and 3-4 mM phosphate buffer to match 85% and 108% of the dissolution rates in 15 mM bicarbonate buffer, respectively.

In summary, this research demonstrates that to establish a meaningful *in vitro* bioequivalence method, both the hydrodynamics and the GI fluids composition should be carefully considered.

CHAPTER I.

INFLUENCE OF FASTED STATE GASTROENTEROLOGICAL FACTORS ON IN VIVO DISSOLUTION OF POORLY SOLUBLE DRUGS

Introduction

Orally administered drug products are the most dominant dosage forms. However, predicting oral drug absorption remains a challenge due to the variety of biopharmaceutical properties of the drug and drug products, as well as the complexity of gastrointestinal (GI) physiology.

Gastrointestinal tract presents a complex environment for orally administered drugs. In healthy humans at fasted state, there are two important physiological factors impacting on drug dissolution and the subsequent absorption: 1). the hydrodynamics of GI tract; and 2) the components of GI fluids. The hydrodynamics of GI tract is intimately related to GI motility, which emcompasses gastric emptying, migrating motility complex (MMC), and the frequency and intensity of small intestine movement, while the critical GI fluid components are pH, bile salts and buffer species, volume, enzymes, osmolarity and calcium contents may be also important. In addition, GI transit time and splanchnic blood flow may also play indirect roles in drug absorption. All of these GI physiological factors are dynamically interacting with each other, which is further complicated by high variability within and between individuals.

Biopharmaceutical properties of the active pharmaceutical ingredient (API) are the inherent nature of a drug molecule, which determines the rate of drug dissolution and extent of drug absorption. The biopharmaceutical classification system (BCS) proposed by Amidon et. al. has established the foundation for correlating the biopharmaceutical properties of an API with its *in vivo* performance. The four BCS classes, based on drug solubility and permeability [1], are listed in Table 1.1. BCS II drugs exhibit high permeability and low solubility, and their oral absorption is rate-limited by *in vivo* dissolution. In light of the reality that more and more BCS II drugs are being discovered, investigating the correlation of *in vitro* dissolution of BCS II drugs with their *in vivo* performance, and gaining a mechanistic understanding of IVIVC warrants more research efforts.

The objective of this project is to investigate the *in vitro* dissolution factors reflecting the *in vivo* dissolution GI physiological factors such as motility, pH, surfactants and buffer species under fasted state, focusing on BCS II drugs. These four aforementioned GI physiological determinants, and their impact on dissolution of BCS II drugs, are reviewed in the following sections.

Gastrointestinal factors

Motility

The GI hydrodynamic conditions are highly dependant on food intake and highly variable among individuals [2-4]. The gastrointestinal motility that impacts on drug dissolution and absorption includes gastric emptying [2,5], and the mixing, segmental contractions and propulsive movement in the small intestine [6-8]. The gastric emptying is

affected by a number of factors, including the intake volume, calories, viscosity, particle size, pH, osmolarity and temperature [2,3,5,9]. Generally, the emptying time is shorter for content with characteristics of large volume (≥ 200 mL), low calorie, iso-osmotic, low viscosity and higher pH, compared to content with small volume (≤ 50 mL), high calorie, hyper- or hypotonic, high viscosity and low pH [2,10]. It was also demonstrated that young normal premenopausal women have slower gastric emptying rate relative to age-matched men, which is due to a decreased antral contractility as supported by both dynamic antral scintigraphy and antroduodenal manometry [11]. The gastric emptying is further complicated by the fasted-state migrating motility complexes (MMC). MMCs exist and cycle through three phases, which are motor quiescent period (Phase I, no contraction), intermittent contractions (Phase II, slow waves and low intensity) and strong contractions (Phase III, house keeping wave) [2,12,13]. The MMC phase III begins in the stomach, and propagates to the pylorus, and then increases slowly down through the small intestine at fasting state [6].

The hydrodynamics of the small intestine is more consistent compared to the stomach in terms of movement pattern and flow rates. The dominant motility patterns in the small intestine are the circumferential and longitudinal contractions. The circumferential movement mixes the GI contents in radical direction, and the longitudinal movement moves the GI contents in the distal direction. The segmental amplitude oscillates between a minimal mean of 9.7 mm to a maximum mean of 20.5 mm for the cross section diameter[14]. Intestinal motility is regulated by neurological, endocrinological and gastrointestinal mechanisms, in addition to food intake [15-17]. In fasted state, the flow rate stays mostly between 0 and 2.0 mL/min, with a net average of

0.73 mL/min in the jejunum and 0.43 mL/min in the ileum [18]. In the fed states, the flow rate increases to a range of 0 - 7.0 mL/min, with an average of 3.0 mL/min and 2.0 mL/min, respectively [18].

pH

In fasted state, the gastric pH is highly variable with a range of pH 1.2 – 8.38 [4,19-21]. It was reported that young Caucasians have gastric pH below 3 under 90% of the fasted state, and 25-75% of them within pH range 1.4 to 2.1 [22]. In comparison, about 10-20% of the same ethnic groups over the age of 65 years have a gastric pH value of 6 or higher, and the percentage seems to be even higher for Japanese subjects [23].

In general, the pH values in the small intestine are higher than in the stomach [24]. While the pH value in the small intestine is more consistent and much less dependent on fasted and fed states, there is an upward pH gradient from the duodenum towards the ileum, covering a range of 6.0 - 7.5 [25], as shown in Table 1.2. This pH range is consistent with the recent findings from duodenal aspirates. For example, the median duodenum pH value was reported to be 6.2 from twenty healthy human duodenal aspirates [19], and in another paper the pH value from twelve pooled human intestinal fluid collected at the fourth part of the duodenum at fasted state was found to be 6.7 [26]. In jejunum, the pH shifts to higher values. It has been reported that the average jejunum pH values are 6.8 [27], 7.1 [21]and 7.5 [28], at fasted state.

Bile Salts

A detailed review of the physical chemistry of bile as it pertains to the physiology of GI tract has been published in 1980s [29]. The dominant bile salts are cholate, deoxycholate, chenodeoxycholate, and their corresponding tauro- and glycol-conjugated

forms [27,30]. The total concentration of bile salts in fasted state stomach is generally low. In radiolabeled pool sample, the average bile salts is 80 μM [31]. Gastric fluids collected from 36 healthy volunteers showed a range of 0.0 – 2.5 mM, an average value of 0.2 mM, with a standard derivation of 0.5 mM [21]. Other researchers reported an average value of 0.275 mM, while 50% of their samples were not detected with bile salt concentration [32]. In a most recent study, it was reported that the gastric bile salts concentration at fasted state is below the quantification limit, i.e., less than 0.5 mM [19]. These results indicate that large variability exists for the gastric bile salt concentrations, partially due to variable duodenal reflux among individuals.

In upper small intestine, the bile salt concentration is generally higher than that in stomach. For example, in earlier studies the average bile salt concentration at fasted state was reported to be 4.5-6.4 mM in duodenum, and 5-6 mM in jejunum [33-35]. Later, Lindahl et. al. reported a slightly lower average bile salt concentration in jejunal fluids was 2.9 mM, with a standard derivation of 2.9 mM [21]. This value is consistent with recent studies, such as 2.00 ± 1.92 mM [36], 2.0 ± 0.2 mM [28], 2.6 mM [19], 3.5 ± 1.6 mM [27], and 2.82 mM [26], in fasting jejunal fluids. The literature data indicates that bile concentration along the GI tract is generally low at the fasting state.

An indirect indication of the bile salt contents is surface tension. The surface tension is significantly lower than that of water, i.e., in the range of 33 – 46 mNm^{-1} in fasting stomach, and 28 – 33.6 mNm^{-1} in upper small intestine [4,19,27,28]. It should be noted that a total bile salt concentration of 10 mM may present variation in surface tension measurement because of the various compositions of di- or trihydroxy- species in the bile salts [37].

Buffer Species

The dominant buffer species in human body fluids, including the gastrointestinal fluids, are bicarbonates. Gastroduodenal bicarbonate has long been known as the main buffer system to create a pH gradient along the gastrointestinal lumen [38-41]. It was also known that endogenous bicarbonate is mainly transported into the lumen by Na-HCO_3 cotransporters (NBC) through cystic fibrosis transmembrane regulator (CFTR) pathway, and partially by paracellular migration depending on intestinal transmucosal hydrostatic pressure and motility. The secretion of bicarbonate into mucus gel provides a near-neutral pH at the epithelial surfaces in the stomach and duodenum, neutralizing luminal acids [42-44]. Bicarbonate concentrations in human GI fluids have been reported to be within a dynamic range, depending on the fasted and fed states as well as local regions along the GI tract [39,45-47]. For example, as early as 1935, the bicarbonate concentration was measured directly from the fasted human duodenum using titration method, and the values were reported in the range of 4-21 mM [38,40], with an average of 15 mM [47]. More recently, the P_{CO_2} in the human duodenum was measured using P_{CO_2} electrode in situ with perfusion of 154 mM NaCl at 2 mL/min, and then the HCO_3^- concentration was calculated to be mean value of 6.7 ± 0.34 mM at pH 7.22 using the Henderson-Hasselbalch equation [48]. In the literature of pharmaceutical field, the bicarbonate concentration has been expressed indirectly using buffer capacity. For example, Person et. al. [28] showed that the mean value of the buffer capacity of human jejunum at fasted state is 2.4-2.8 $mmolL^{-1}pH^{-1}$, which corresponds to 18.1 mM of bicarbonate concentration at pH 7.5 assuming that the buffer capacity is solely attributed by the bicarbonate buffer species. Recently, Kalantizi et al.[19] reported the range of buffer

capacity for distal duodenum of fasted human, which is equivalent to 4.35 – 21.6 mM of HCO_3^- at pH 6.2. It should be noted that the buffer capacity of the fasting intestinal fluids is contributed by not only bicarbonates, but also a very small amount of phosphates (0.4 – 1.8 mM from 4 volunteers) [49] as well as endogenous enzymes and amino acids. Nonetheless, even though bicarbonate buffer is the obvious choice, it has been rarely employed in drug dissolution testing.

Other Gastrointestinal Factors

In addition to GI motility, pH, bile salts and buffer species, the transit time along small intestine [50-53], the fluid volume [54-56] and splanchnic blood flow [57-59], also impact on drug dissolution and/or drug absorption process. These factors are frequently further complicated by liquid or solid intake.

Effects of GI Factors on BCS II Drugs

BCS II class drugs exhibit characteristics of high permeability and low solubility, and their drug solubility or dissolution rate is the rate limiting step in drug absorption. This class of drugs includes non-ionizable compounds such as carbamazepine, fenofibrate and griseofulvin, and ionizable compounds such as ibuprofen (acid) and diazepam (base).

For non-ionizable compounds, the pH changes along the GI tract would not have an impact on drug solubilization or dissolution, whereas the contents of bile salts would significantly increase the solubilization thus enhancing its dissolution rate. Examples are griseofulvin [60] and fenofibrate [61]. In the case of griseofulvin, its solubility increased 107-fold, 31-fold, fourfold, and threefold in the presence of SDS, CTAB, Tween 80, and

Cremophor EL. Dissolution into SDS and CTAB were markedly enhanced as well, with about one-third as much as solubility enhancement [60]. The less significantly increased dissolution rate relative to solubility is due to a smaller diffusion coefficient of the drug-loaded micelles [60]. For fenofibrate, its solubility was enhanced approximately 2000-fold, and intrinsic dissolution rate was improved about 500-fold, in a pH 6.8 buffer containing 2% (w/v) sodium lauryl sulfate compared to that in buffer alone [61]. At fasted state, the concentrations of bile salts are low, in the range of 2.0-6.0 mM, reported by many researchers. Thus, compared with the fed state, the impact of bile salts on poorly soluble non-ionizable drugs is far less significant in fasted state.

For BCS II weak bases such as dipyridamole (pKa: 5.7-6.4) [62,63] and ketoconazole (pKa: 2.94 and 6.51) [64,65], their *in vivo* solubility and dissolution are more complex compared with the weak acids. BCS II weak bases, with pKb values that could lead to ionizing greatly in the gastric acidic environment, would dissolve quickly in stomach. Once they enter the duodenum, the extent of ionization is significantly reduced due to elevated pH [26,66]. It is very likely that the ionized base form would precipitate at the upper small intestine. The rate and extent of precipitation, and the size and the polymorphic form of the precipitates, are controlled by a number of factors such as the extent of supersatuartion and solid form of the weak base, and the pH, fluid volume, viscosity and bile salts concentration of the duodenum. The gastric pH appeared to be a primary determinant in dipyridamole absorption in the elderly [67]. In 11 healthy subjects, the low fasting gastric group was pretreated with or without 40 mg of famotidine, and the high fasting gastric group (pH > 5) was pretreated with or without 1360 mg of glutamic acid hydrochloride. In both groups, an elevated gastric pH is responsible for not only a

decreased absorption in terms of Cmax and AUC, but also a slower Tmax, in dipyridamole [67]. In a recent study, the *in vitro* dissolution rate and *in vivo* dog absorption of two weak bases, i.e., ketoconazole and dipyridamole, were demonstrated to be pH-dependant [68]. Particularly, the AUC increased significantly when the gastric pH is lowered by pentagastrin pH of 2-3, whereas AUC decreased markedly with an elevated gastric pH to 5-7.5 by famotidine treatment. For ketoconozloe, a 30-fold difference was observed between the pengastrin and famotidine groups, and for dipyridamole the difference was 9-fold [68].

For very weak acids with high pKa values such as phenytoin (pKa: 8.06) [69], its ionization would be very limited in the stomach as well as along the small intestine, thus resulting in the unionized free acid as the dominant form in the GI tract. For BCS II weak acids such as ibuprofen and ketoprofen, with respective pKa values of 4.2 and 4.5, which are in the GI physiological range, extensive ionization of these compounds at upper small intestine is expected. This is because the average pH in upper small intestine is around 5.8 - 6.5, which is at least 1 unit higher than the drug pKa, increasing the apparent solubility of the weak acid by 10 - 100 fold. Thus, their *in vivo* solubility and subsequent dissolution would be high, presumably behaving more likely as a BCS I compound. However, the combined effects of pH and surfactants on the solubilization and dissolution of weak acid drugs has received little attention, especially in view of reflecting an *in vivo* change of pH and surfactant along the gastrointestinal tract using an *in vitro* model. Therefore, it is important to investigate the effects of pH combined with surfactant on the solubility and dissolution of BCS II water-poorly soluble weak acids in an *in vitro* environment.

In addition to pH and bile salts, the buffer species, namely, the bicarbonate, is a critical factor that significantly impact on dissolution of ionizble drugs, but has been overlooked in the past. As stated previously, bicarbonate is the dominant physiological buffer species along the GI tract. Further, buffer concentration and species have been shown to impact on the dissolution of ionizable drugs such as naproxefen. The intrinsic dissolution rate of naproxen increase with the escalation of buffer concentration, which was demonstrated consistently in three buffers including phosphate, citrate and acetate [70]. More interestingly, the work also showed that naproxen demonstrated a decreased dissolution rate in the following buffer species: phosphate > citrate > acetate, despite all the buffers were maintained at the same buffer concentration and same pH value [70]. Therefore, it is important to investigate the impact of bicarbonate species, and to evaluate the difference between bicarbonate and pharmaceutically commonly used buffer such as phosphate, on ionizable drug dissolution.

It should be noted that the same active species could be synthesized as different salt forms, or crystallized as different crystal forms (polymorphs), solvates (pseudo-polymorphs) and amorphous form. All of these chemical and physical transformations of same active species could have an impact on drug dissolution and absorption, particularly for the BCS II drugs. However, in pharmaceutical industries their development is more likely due to the need of creating feasible processes for bulk and formulation manufacturing, fulfilling regulatory requirements and extending exclusive marketing right via patent. The API should be distinguished from its drug products. In the content of immediate-release dosage forms, the drug dissolution can still be modified significantly by the excipients and/or manufacturing conditions during the formulation

processes. To name a few, manufacturing variables could have an impact on dissolution because they could induce changes in crystal forms, surface characteristics, particle size, porosity of API and /or drug products [71-74]. For example, particle size reduction is frequently used in processing API as well as intermediate drug products to enhance drug dissolution/absorption and/or manufacturing feasibility. It has been reported that the diffusional layer thickness is a function of drug particle sizes, which subsequently would impact on the drug dissolution rate [74-76]. The dependence of diffusional layer thickness on the hydrodynamic conditions that is pharmaceutically relevant such as in a USP device or under normal GI motility, however, has been largely ignored. Furthermore, the combined effects of particle size and fluid velocity on diffusional layer thickness have yet to be addressed.

Selection of Model Compounds

The model compounds employed in this thesis are fenofibrate, ketoprofen and indomethacin. The chemical structures and the biopharmaceutical properties of these three compounds are showed in Figure 1.1 and Table 1.3, respectively.

Fenofibrate was selected to investigate the combined effects of particle size and fluid velocity on diffusional layer thickness for its non-ionizable and poorly soluble nature, and its existence as a single polymorph. Ketoprofen was chosen to investigate the combined effects of pH and surfactants simulating upper small intestine for its pKa value within GI physiological range and its poor solubility. Ketoprofen and indomethacin were employed to investigate the effects of buffer species, i.e., bicarbonates versus phosphates, owing to their pKa value within GI physiological range and its poor solubility.

Implications of GI Factors in Establishing a Bioequivalence Dissolution Methodology

The purposes of developing a dissolution methodology are to serve quality control (QC) or bioequivalence (BE) evaluation [77-79]. The routinely used dissolution testing aimed for QC is to ensure that the drug products meet dissolution specifications, comply with regulatory requirements, and detect manufacture reproducibility. The focus of a BE dissolution testing is shifted to provide the *in vivo* performance of a drug product. Its primary goal is to predict *in vivo* dissolution, and potentially *in vivo* absorption for highly permeable drugs [80]. Therefore, the design of these two dissolution testing are quite different. Ideally, the QC dissolution should be the same or very similar to the BE dissolution testing, thus the *in vitro* dissolution would reflect the *in vivo* situation, because assuring the *in vivo* quality is the ultimate goal of a drug product.

Most of the dissolution related literature addresses the needs of QC, and only limited research has been invested to design BE dissolution methods. In establishing a meaningful BE dissolution methodology, two very important aspects must be considered: the hydrodynamic conditions along the GI tract and the complex contents of the GI fluids. The interplay between the GI hydrodynamics and GI fluids present the most challenging environment in designing a biorelevant dissolution test.

The dynamic and heterogeneous fluid velocity of the GI tract induced by GI motility remains an obstacle for an accurate simulation of *in vivo* hydrodynamic conditions, despite of several attempts [81-83]. Meanwhile, investigation of the pharmacopeial type of dissolution apparatus demonstrates the complexity of fluid

velocity profiles in either basket or paddle device [84-87]. Further, a comparison of these two results clearly reveals a remarkable gap between the pharmacopeial apparatus hydrodynamics and the *in vivo* physiological hydrodynamics. The geometric, kinematic and dynamic factors in the pharmacopeial apparatus are very different from those along the *in vivo* GI tract. Therefore, the USP apparatus such as the type II paddle apparatus is suitable for QC purpose monitoring the mass transport of API from the dosage forms. However, it is much less relevant in assessing the *in vivo* performance of a drug product. Even though the USP dissolution apparatus II has been most widely employed in checking the release profiles of drug products, fundamental understanding of how the drug particles and fluid velocities are combined to impact on drug dissolution has yet to be explored. For example, in the original Noyes-Whitney equation $\frac{dM}{dt} = -\frac{D}{h} A(C_s - C_t)$, the dependence of h on drug particle size and paddle speeds have never been investigated quantitatively in a USP dissolution apparatus II. Many dissolution models assume h to be a constant, or comparable with particle radius. This simple assumption is convenient; however, it has not been supported by any direct experimental data. In addition, such an assumption is contradictory to a basic fluid dynamic principle, i.e., the apparent diffusional layer thickness is altered by hydrodynamics. Even though a USP dissolution apparatus II is well-defined, the fluid velocity is clearly changing with the paddle speeds. Thus, a changing apparent h with paddle speeds is foreseeable and an alternation of h therefore reciprocally affects the dissolution rate.

The equally important consideration in designing a BE dissolution test is the selection of appropriate dissolution medium. Dissolution media mimicking the *in vivo* GI

fluids has attracted numerous interests and achieved significant progress in the past decade. The earliest proposal is found in the paper discussing pH-partition hypothesis to estimate drug absorption by Dressman et al. in 1985 [88]. Later, the historical paper by Amidon et al. enabled further enhancement of biorelevant media under the frame of Biopharmaceutics Classification System (BCS) [1]. In 1997 characterization of fluids from stomach and upper jejunum in healthy fasted-state volunteers was conducted [21]. In 1998 based on human GI physiology, the milestone paper by Dressman et al. provided the insightful and comprehensive initiatives in designing dissolution medium mimicking *in vivo* GI fluids [4]. More recently, solubility and dissolution of neutral and ionizable weak acids and bases were investigated in human, canine, and simulated fluids. The major aim of these studies is to investigate how drugs with various properties would dissolve under normal GI conditions, in human, dog and simulated biorelevant media [19,26-28,36,89]. Almost all these studies focused on pH, osmolality and bile acids. However, the intuitively physiological buffer, i.e., bicarbonate buffer, as well as its impact on drug dissolution, has been rarely investigated [90]. Gastroduodenal bicarbonate has long been known as the main buffer system maintaining a pH gradient along the gastrointestinal lumen [41]. As a predominant buffer in human gastrointestinal physiology, bicarbonate has been overlooked in drug dissolution testing. Most published studies use phosphate or acetate buffers instead, creating a disconnect between the physiological buffer species and the buffer species used in *in vitro* dissolution studies, including the simulated GI fluids. To this date, there has been few experimental data or theoretical derivation pertaining to bicarbonate buffer as a dissolution medium. In literature, it has been reported that the concentration and buffer species significantly impact on dissolution

rates of ionizable drugs even at the same pH value [70,91,92]. Thus there is a need to characterize the dissolution properties of bicarbonate buffer and compare them with those of the more often–used buffer systems. In order to mimic the *in vivo* source of bicarbonate, an external supply of CO_2 is necessary to maintain the bicarbonate in the *in vitro* dissolution media. For example, this can be achieved using purging CO_2 gas into the dissolution media sustaining a partial CO_2 pressure through the testing.

Summary

In summary, the two essential aspects that must be considered in order to mimic *in vivo* situation and to design meaningful BE dissolution, are the GI hydrodynamics and GI fluid contents. The GI motility determines how fast the drug is entering the duodenum and jejunum, how long the drug is staying in the small intestine, and how dynamic a drug particle is interacting with the GI fluids. Chapter 2 of this thesis deals with the combined effects of drug particle size and paddle speed on diffusional layer thickness of a poorly soluble drug, fenofibrate, in a USP dissolution apparatus II. The GI fluid contents not only determine the drug solubility but also the drug dissolution rate along the GI tract. Among various GI fluid factors, chapter 3 focuses on the combined effects of pH and surfactants on a poorly soluble and ionizable weak acid, ketoprofen, under normal conditions in the upper small intestine. Further, chapter 4 examines the impact of buffer species, particularly the physiological bicarbonates versus pharmaceutical phosphates, on weak BCS II acids such as ketoprofen and indomethacin.

Specific Aims: (1). To determine the combined effects of particle size and fluid hydrodynamics on diffusional layer thickness of a poorly soluble drug, fenofibrate. (2). To investigate the solubilization and dissolution of a poorly soluble and weakly acid, ketoprofen, under the conditions mimicing the pH and surfactants along small intestine. (3). To compare the pharmaceutical phosphate buffers with physiological bicarbonates in dissolution of BCS II weak acids, ketoprofen and indomethacin.

Table 1.1. Biopharmaceutical Classification System (BCS).

BCS class I: High solubility High Permeability	**BCS class II:** Low solubility High Permeability
BCS class III: High solubility Low Permeability	**BCS class IV:** Low solubility Low Permeability

Table 1.2. pH in the small intestine in healthy humans in the fasted state[a].

Location	Fasted state pH
Mid distal duodenum	4.9
	6.1
	6.3
	6.4
Jejunum	4.4-6.5
	6.6
Ileum	6.5
	6.8-8.0
	7.4

[a]: Reproduced from Ref. (Dressman 1998)

Table 1.3. Biopharmaceutical properties of fenofibrate, ketoprofen and indomethacin.

Biopharmaceutical properties	Fenofibrate	Ketoprofen	Indomethacin
Intrinsic solubility in water at 37°C	< 0.3 μg/mL	0.253 mg/mL	2.43 μg/mL
Permeability (cm/s)	ClogP: 3.86	[a]8.7×10^{-4}	[b]3.4×10^{-4}
Diffusivity (cm^2/s)	7.15×10^{-6}	9.3×10^{-6}	8.0×10^{-6}
pKa	Non-ionizable	4.76	4.17
Maximum dose (mg)	200	75	50
Provisional BCS classification	BCS II	BCS II	BCS II
Therapeutic category	Lipid-regulating fibric	Nonsteroid anti-inflammatory acid	Nonsteroid anti-inflammatory acid

[a]: human jejunum permeability
[b]: calculated using ADMET Predictor 1.2.

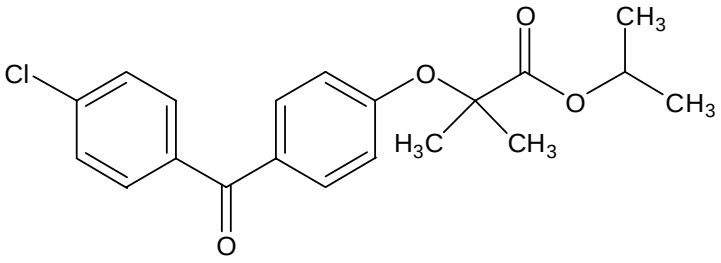

Fenofibrate

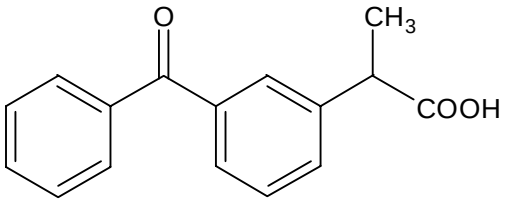

Ketoprofen

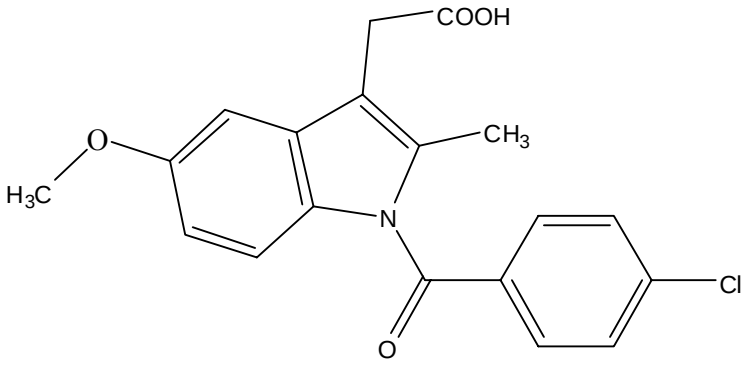

Indomethacin

Figure 1.1. The chemical structures of fenofibrate, ketoprofen and indomethacin.

References.

1. Amidon GL, Lennernas H, Shah VP, Crison JR. **1995**. A theoretical basis for a biopharmaceutic drug classification: The correlation of in vitro drug product dissolution and in vivo bioavailability. Pharm Res 12:413-420.
2. Oberle RL, Chen TS, Lloyd C, Barnett JL, Owyang C, Meyer J, Amidon GL. **1990**. The influence of the interdigestive migrating myoelectric complex on the gastric emptying of liquids. Gastroenterology 99:1275-1282.
3. Maughan RJ, Leiper JB. **1996**. Methods for the assessment of gastric emptying in humans: An overview. Diabet Med 13:S6-10.
4. Dressman JB, Amidon GL, Reppas C, Shah VP. **1998**. Dissolution testing as a prognostic tool for oral drug absorption: Immediate release dosage forms. Pharm Res 15:11-22.
5. Chaudhuri TK, Fink S. **1990**. Update: Pharmaceuticals and gastric emptying. Am J Gastroenterol 85:223-230.
6. Hansen MB. **2002**. Small intestinal manometry. Physiol Res 51:541-556.
7. Jones MP, Wessinger S. **2005**. Small intestinal motility. Curr Opin Gastroenterol 21:141-146.
8. Smout AJ. **2006**. Recent developments in gastrointestinal motility. Scand J Gastroenterol Suppl:25-31.
9. Medhus A, Sandstad O, Bredesen J, Husebye E. **1995**. The migrating motor complex modulates intestinal motility response and rate of gastric emptying of caloric meals. Neurogastroenterol Motil 7:1-8.
10. Hausken T, Mundt M, Samsom M. **2002**. Low antroduodenal pressure gradients are responsible for gastric emptying of a low-caloric liquid meal in humans. Neurogastroenterol Motil 14:97-105.
11. Knight LC, Parkman HP, Brown KL, Miller MA, Trate DM, Maurer AH, Fisher RS. **1997**. Delayed gastric emptying and decreased antral contractility in normal premenopausal women compared with men. Am J Gastroenterol 92:968-975.
12. Coupe AJ, Davis SS, Evans DF, Wilding IR. **1991**. Correlation of the gastric emptying of nondisintegrating tablets with gastrointestinal motility. Pharm Res 8:1281-1285.
13. Luiking YC, van der Reijden AC, van Berge Henegouwen GP, Akkermans LM. **1998**. Migrating motor complex cycle duration is determined by gastric or duodenal origin of phase iii. Am J Physiol 275:G1246-1251.
14. Froehlich JM, Patak MA, von Weymarn C, Juli CF, Zollikofer CL, Wentz KU. **2005**. Small bowel motility assessment with magnetic resonance imaging. J Magn Reson Imaging 21:370-375.
15. Kerlin P, Phillips S. **1982**. Variability of motility of the ileum and jejunum in healthy humans. Gastroenterology 82:694-700.
16. Husebye E. **1999**. The patterns of small bowel motility: Physiology and implications in organic disease and functional disorders. Neurogastroenterol Motil 11:141-161.
17. Thomson AB, Keelan M, Thiesen A, Clandinin MT, Ropeleski M, Wild GE. **2001**. Small bowel review: Normal physiology part 2. Dig Dis Sci 46:2588-2607.
18. Kerlin P, Zinsmeister A, Phillips S. **1982**. Relationship of motility to flow of contents in the human small intestine. Gastroenterology 82:701-706.

19. Kalantzi L, Goumas K, Kalioras V, Abrahamsson B, Dressman JB, Reppas C. **2006**. Characterization of the human upper gastrointestinal contents under conditions simulating bioavailability/bioequivalence studies. Pharm Res 23:165-176.
20. Altman PL, Katz DD. **1961**. Blood and other body fluids. Biological handbooks, ed., Washington: Federation of American Societies for Experimental Biology. p xvii, 540 p.
21. Lindahl A, Ungell AL, Knutson L, Lennernas H. **1997**. Characterization of fluids from the stomach and proximal jejunum in men and women. Pharm Res 14:497-502.
22. Dressman JB, Berardi RR, Dermentzoglou LC, Russell TL, Schmaltz SP, Barnett JL, Jarvenpaa KM. **1990**. Upper gastrointestinal (gi) ph in young, healthy men and women. Pharm Res 7:756-761.
23. Ogata H, Aoyagi N, Kaniwa N, Ejima A, Suzuki K, Ishioka T, Morishita M, Ohta K, Takagishi Y, Doi Y, et al. **1984**. Development and evaluation of a new peroral test agent ga-test for assessment of gastric acidity. J Pharmacobiodyn 7:656-664.
24. Davis SS, Hardy JG, Fara JW. **1986**. Transit of pharmaceutical dosage forms through the small intestine. Gut 27:886-892.
25. Coupe AJ, Davis SS, Wilding IR. **1991**. Variation in gastrointestinal transit of pharmaceutical dosage forms in healthy subjects. Pharm Res 8:360-364.
26. Kalantzi L, Persson E, Polentarutti B, Abrahamsson B, Goumas K, Dressman JB, Reppas C. **2006**. Canine intestinal contents vs. Simulated media for the assessment of solubility of two weak bases in the human small intestinal contents. Pharm Res 23:1373-1381.
27. Perez de la Cruz Moreno M, Oth M, Deferme S, Lammert F, Tack J, Dressman J, Augustijns P. **2006**. Characterization of fasted-state human intestinal fluids collected from duodenum and jejunum. J Pharm Pharmacol 58:1079-1089.
28. Persson EM, Gustafsson AS, Carlsson AS, Nilsson RG, Knutson L, Forsell P, Hanisch G, Lennernas H, Abrahamsson B. **2005**. The effects of food on the dissolution of poorly soluble drugs in human and in model small intestinal fluids. Pharm Res 22:2141-2151.
29. Schultz SG, Rauner BB, Wood JD, American Physiological Society (1887-). **1989**. The gastrointestinal system. ed., Bethesda, Md.: American Physiological Society. p v.621-661.
30. Wiedmann TS, Kamel L. **2002**. Examination of the solubilization of drugs by bile salt micelles. J Pharm Sci 91:1743-1764.
31. Rhodes J, Barnardo DE, Phillips SF, Rovelstad RA, Hofmann AF. **1969**. Increased reflux of bile into the stomach in patients with gastric ulcer. Gastroenterology 57:241-252.
32. Efentakis M, Dressman JB. **1998**. Gastric juice as a dissolution medium: Surface tension and ph. Eur J Drug Metab Pharmacokinet 23:97-102.
33. van Berge Henegouwen GP, Hofmann AF. **1978**. Nocturnal gallbladder storage and emptying in gallstone patients and healthy subjects. Gastroenterology 75:879-885.
34. Tangerman A, van Schaik A, van der Hoek EW. **1986**. Analysis of conjugated and unconjugated bile acids in serum and jejunal fluid of normal subjects. Clin Chim Acta 159:123-132.

35. Marzio L, Neri M, Capone F, Di Felice F, De Angelis C, Mezzetti A, Cuccurullo F. **1988**. Gallbladder contraction and its relationship to interdigestive duodenal motor activity in normal human subjects. Dig Dis Sci 33:540-544.
36. Pedersen BL, Brondsted H, Lennernas H, Christensen FN, Mullertz A, Kristensen HG. **2000**. Dissolution of hydrocortisone in human and simulated intestinal fluids. Pharm Res 17:183-189.
37. Luner PE. **2000**. Wetting properties of bile salt solutions and dissolution media. J Pharm Sci 89:382-395.
38. Karr WG, Abbott WO, Sample AB. **1935**. Intubation studies of the human small intestine. Iv. Chemical characteristics of the intestinal contents in the fasting state and as influenced by the administration of acids, of alkalies and of water. J Clin Invest 14:893-900.
39. Rees WD, Botham D, Turnberg LA. **1982**. A demonstration of bicarbonate production by the normal human stomach in vivo. Dig Dis Sci 27:961-966.
40. Tietz NW. **1995**. Clinical guide to laboratory tests. 3rd ed., Philadelphia: W.B. Saunders Co. p xxxix, 1064 p.
41. Allen A, Flemstrom G. **2005**. Gastroduodenal mucus bicarbonate barrier: Protection against acid and pepsin. Am J Physiol Cell Physiol 288:C1-19.
42. Johnson LR. **1994**. Physiology of the gastrointestinal tract. 3rd ed., New York: Raven Press.
43. Konturek PC, Konturek SJ, Ochmanski W. **2004**. Neuroendocrinology of gastric h+ and duodenal hco3- secretion: The role of brain-gut axis. Eur J Pharmacol 499:15-27.
44. Konturek SJ, Konturek PC, Pawlik T, Sliwowski Z, Ochmanski W, Hahn EG. **2004**. Duodenal mucosal protection by bicarbonate secretion and its mechanisms. J Physiol Pharmacol 55 Suppl 2:5-17.
45. Rune SJ. **1972**. Acid-base parameters of duodenal contents in man. Gastroenterology 62:533-539.
46. Kristensen M. **1975**. Titration curves for gastric secretion. A study on duodenal ulcer and gastric ulcer with particular reference to the effect of glycopyrronium. Scand J Gastroenterol Suppl 32:11-144.
47. Goodman LS, Hardman JG, Limbird LE, Gilman AG. **2001**. Goodman and gilman's the pharmacological basis of therapeutics. 10th ed., New York: McGraw-Hill, Medical Publishing Division. p xxvii, 2148 p. [2141] leaf of fold. plates.
48. Repishti M, Hogan DL, Pratha V, Davydova L, Donowitz M, Tse CM, Isenberg JI. **2001**. Human duodenal mucosal brush border na(+)/h(+) exchangers nhe2 and nhe3 alter net bicarbonate movement. Am J Physiol Gastrointest Liver Physiol 281:G159-163.
49. Brouwers J, Augustijns P. GPEN 2006, Lawrence, Kansas, **2006**.
50. Amidon GL, DeBrincat GA, Najib N. **1991**. Effects of gravity on gastric emptying, intestinal transit, and drug absorption. J Clin Pharmacol 31:968-973.
51. Moes AJ. **1993**. Gastroretentive dosage forms. Crit Rev Ther Drug Carrier Syst 10:143-195.
52. Kimura T, Higaki K. **2002**. Gastrointestinal transit and drug absorption. Biol Pharm Bull 25:149-164.
53. Soffer EE. **2000**. Small bowel motility: Ready for prime time? Curr Gastroenterol Rep 2:364-369.

54. Gisolfi CV, Summers RW, Lambert GP, Xia T. **1998**. Effect of beverage osmolality on intestinal fluid absorption during exercise. J Appl Physiol 85:1941-1948.
55. Ryan AJ, Lambert GP, Shi X, Chang RT, Summers RW, Gisolfi CV. **1998**. Effect of hypohydration on gastric emptying and intestinal absorption during exercise. J Appl Physiol 84:1581-1588.
56. Schneeman BO. **2002**. Gastrointestinal physiology and functions. Br J Nutr 88 Suppl 2:S159-163.
57. Sieber C, Beglinger C, Jager K, Stalder GA. **1992**. Intestinal phase of superior mesenteric artery blood flow in man. Gut 33:497-501.
58. Oosterhuis B, Jonkman JH. **1993**. Pharmacokinetic studies in healthy volunteers in the context of in vitro/in vivo correlations. Eur J Drug Metab Pharmacokinet 18:19-30.
59. Matheson PJ, Wilson MA, Garrison RN. **2000**. Regulation of intestinal blood flow. J Surg Res 93:182-196.
60. Balakrishnan A, Rege BD, Amidon GL, Polli JE. **2004**. Surfactant-mediated dissolution: Contributions of solubility enhancement and relatively low micelle diffusivity. J Pharm Sci 93:2064-2075.
61. Granero GE, Ramachandran C, Amidon GL. **2005**. Dissolution and solubility behavior of fenofibrate in sodium lauryl sulfate solutions. Drug Dev Ind Pharm 31:917-922.
62. Gu CH, Rao D, Gandhi RB, Hilden J, Raghavan K. **2005**. Using a novel multicompartment dissolution system to predict the effect of gastric ph on the oral absorption of weak bases with poor intrinsic solubility. J Pharm Sci 94:199-208.
63. Tabak M, Borisevitch IE. **1992**. Interaction of dipyridamole with micelles of lysophosphatidylcholine and with bovine serum albumin: Fluorescence studies. Biochim Biophys Acta 1116:241-249.
64. Carlson JA, Mann HJ, Canafax DM. **1983**. Effect of ph on disintegration and dissolution of ketoconazole tablets. Am J Hosp Pharm 40:1334-1336.
65. Hoeschele JD, Roy AK, Pecoraro VL, Carver PL. **1994**. In vitro analysis of the interaction between sucralfate and ketoconazole. Antimicrob Agents Chemother 38:319-325.
66. Galia E, Nicolaides E, Horter D, Lobenberg R, Reppas C, Dressman JB. **1998**. Evaluation of various dissolution media for predicting in vivo performance of class i and ii drugs. Pharm Res 15:698-705.
67. Russell TL, Berardi RR, Barnett JL, O'Sullivan TL, Wagner JG, Dressman JB. **1994**. Ph-related changes in the absorption of dipyridamole in the elderly. Pharm Res 11:136-143.
68. Zhou R, Moench P, Heran C, Lu X, Mathias N, Faria TN, Wall DA, Hussain MA, Smith RL, Sun D. **2005**. Ph-dependent dissolution in vitro and absorption in vivo of weakly basic drugs: Development of a canine model. Pharm Res 22:188-192.
69. Schwartz PA, Rhodes CT, Cooper JW, Jr. **1977**. Solubility and ionization characteristics of phenytoin. J Pharm Sci 66:994-997.
70. McNamara DP, Amidon GL. **1988**. Reaction plane approach for estimating the effects of buffers on the dissolution rate of acidic drugs. J Pharm Sci 77:511-517.
71. Airaksinen S, Luukkonen P, Jorgensen A, Karjalainen M, Rantanen J, Yliruusi J. **2003**. Effects of excipients on hydrate formation in wet masses containing theophylline. J Pharm Sci 92:516-528.

72. Santos H, Veiga F, Pina ME, Sousa JJ. **2004**. Compaction, compression and drug release characteristics of xanthan gum pellets of different compositions. Eur J Pharm Sci 21:271-281.
73. Crowley MM, Schroeder B, Fredersdorf A, Obara S, Talarico M, Kucera S, McGinity JW. **2004**. Physicochemical properties and mechanism of drug release from ethyl cellulose matrix tablets prepared by direct compression and hot-melt extrusion. INT J PHARM 269:509-522.
74. Jinno J, Kamada N, Miyake M, Yamada K, Mukai T, Odomi M, Toguchi H, Liversidge GG, Higaki K, Kimura T. **2006**. Effect of particle size reduction on dissolution and oral absorption of a poorly water-soluble drug, cilostazol, in beagle dogs. J Control Release 111:56-64.
75. Bisrat M, Nystrom C. **1988**. Physicochemical aspects of drug release.8. The relation between particle-size and surface specific dissolution rate in agitated suspensions. Int J Pharm 47:223-231.
76. deAlmeida LP, Simoes S, Brito P, Portugal A, Figueiredo M. **1997**. Modeling dissolution of sparingly soluble multisized powders. J Pharm Sci 86:726-732.
77. Dokoumetzidis A, Macheras P. **2006**. A century of dissolution research: From noyes and whitney to the biopharmaceutics classification system. INT J PHARM 321:1-11.
78. Graffner C. **2006**. Regulatory aspects of drug dissolution from a european perspective. Eur J Pharm Sci 29:288-293.
79. Azarmi S, Roa W, Lobenberg R. **2007**. Current perspectives in dissolution testing of conventional and novel dosage forms. INT J PHARM 328:12-21.
80. Dressman J. **2004**. Future directions for academic research in dissolution testing. Dissolution Technology 11:8-9.
81. Pal A, Indireshkumar K, Schwizer W, Abrahamsson B, Fried M, Brasseur JG. **2004**. Gastric flow and mixing studied using computer simulation. Proc Biol Sci 271:2587-2594.
82. Kwiatek MA, Steingoetter A, Pal A, Menne D, Brasseur JG, Hebbard GS, Boesiger P, Thumshirn M, Fried M, Schwizer W. **2006**. Quantification of distal antral contractile motility in healthy human stomach with magnetic resonance imaging. J Magn Reson Imaging 24:1101-1109.
83. Pal A, Brasseur JG, Abrahamsson B. **2007**. A stomach road or "magenstrasse" for gastric emptying. J Biomech 40:1202-1210.
84. Healy AM, McCarthy LG, Gallagher KM, Corrigan OI. **2002**. Sensitivity of dissolution rate to location in the paddle dissolution apparatus. J Pharm Pharmacol 54:441-444.
85. Kukura J, Arratia PE, Szalai ES, Muzzio FJ. **2003**. Engineering tools for understanding the hydrodynamics of dissolution tests. Drug Dev Ind Pharm 29:231-239.
86. McCarthy LG, Bradley G, Sexton JC, Corrigan OI, Healy AM. **2004**. Computational fluid dynamics modeling of the paddle dissolution apparatus: Agitation rate, mixing patterns, and fluid velocities. AAPS Pharm Sci Tech 5:e31.
87. McCarthy LG, Kosiol C, Healy AM, Bradley G, Sexton JC, Corrigan OI. **2003**. Simulating the hydrodynamic conditions in the united states pharmacopeia paddle dissolution apparatus. AAPS Pharm Sci Tech 4:E22.

88. Dressman JB, Amidon GL, Fleisher D. **1985**. Absorption potential: Estimating the fraction absorbed for orally administered compounds. J Pharm Sci 74:588-589.
89. Vertzoni M, Fotaki N, Kostewicz E, Stippler E, Leuner C, Nicolaides E, Dressman J, Reppas C. **2004**. Dissolution media simulating the intralumenal composition of the small intestine: Physiological issues and practical aspects. J Pharm Pharmacol 56:453-462.
90. McNamara DP, Whitney KM, Goss SL. **2003**. Use of a physiologic bicarbonate buffer system for dissolution characterization of ionizable drugs. Pharm Res 20:1641-1646.
91. Mooney KG, Mintun MA, Himmelstein KJ, Stella VJ. **1981**. Dissolution kinetics of carboxylic acids i: Effect of ph under unbuffered conditions. J Pharm Sci 70:13-22.
92. Mooney KG, Mintun MA, Himmelstein KJ, Stella VJ. **1981**. Dissolution kinetics of carboxylic acids ii: Effect of buffers. J Pharm Sci 70:22-32.

CHAPTER II

PARTICLE DIFFUSIONAL LAYER THICKNESS IN A USP DISSOLUTION APPARATUS II: A COMBINED FUNCTION OF PARTICLE SIZE AND PADDLE SPEED

Abstract

This work was to investigate the effects of particle size and paddle speed on the particle diffuisonal layer thickness h_{app} in a USP dissolution apparatus II. After the determination of the powder dissolution rates of five size fractions of fenofibrate, including < 20, 20-32, 32-45, 63-75 and 90-106 μm, the present work shows that the dependence of h_{app} on particle size follows different functions in accordance with the paddle speed. At 50 rpm, the function of h_{app} is best described by a linear plot of $h_{app} = 9.91\sqrt{d} - 23.31$ ($R^2 = 0.98$) throughout the particle size range of 6.8-106 μm. In contrast, at 100 rpm a transitional particle radius of 23.7 μm exists, under which linear relationship $h_{app} = 1.59r$ ($R^2 = 0.98$) occurs, but above which h_{app} becomes a constant of 43.5 μm. Thus, h_{app} changes not only with particle size, but also with the hydrodynamics under standard USP configurations, which has been overlooked in the past. Further, the effect of particle size and paddle speed on h_{app} was combined using dimensionless analysis. Within certain fluid velocity/particle regime, linear correlation of $\frac{h_{app}}{d}$ with the

square-root of Reynolds number $(\frac{d\varpi}{\upsilon})^{1/2}$, i.e., $\frac{h_{app}}{d} = 1.5207 - 9.25\times10^{-4}(\frac{d\varpi}{\nu})^{1/2}$ ($R^2 = 0.9875$), was observed.

Introduction

The Biopharmaceutics Classification System (BCS) categorizes drugs into four classes according to their solubility and permeability.[1] The BCS II class of compounds exhibits high permeability and low solubility relative to the administered dose. For a BCS II drug formulated into an immediate release (IR) dosage form, the combination of high drug permeability and adequate GI transit time will lead to a rate and extent of oral absorption that is controlled by the *in vivo* process of drug dissolution.[1,2]

Mechanistically, one of the fundamental issues in modeling and understanding dissolution is to determine the relationship between the diffusional layer thickness (h_{app}) and particle size under a defined set of hydrodynamic conditions. In the past, the Noyes-Whitney equation $\frac{dM}{dt} = -\frac{D}{h}A(C_s - C_t)$ has been widely used to describe drug particle dissolution,[3] where h is a thin static liquid layer at the solid surface under steady state conditions. For the past half century, the Noyes-Whitney equation has served as the theoretical basis for many classical dissolution models that assumed various relationships between the drug particle size and h_{app}. For example, h_{app} was assumed to be a constant by Hixson and Crowell,[4] while Higuchi and Hiestand[5-7] proposed that it was approximately equal to the radius of the particle, and Niebergall et al.[8] determined it to be equal to the square root of the particle radius. All of these assumptions imply that the correlation between h_{app} and particle size is applicable to all particle size ranges. In

recent years, this correlation has been advanced by hypothesizing the existence of a transitional particle size, above and below which h_{app} behaves differently depending on the magnitude of the drug particle radius. For example, using intrinsic dissolution studies from rotating disks, Hintz and Johnson[9] proposed that 30 μm was the critical particle radius. Specifically, their model stipulates that the value of h is a constant 30 microns for particles with radii larger than 30 microns, while for particles less than 30 microns h functions as a thickness equal to the particle radius. However, this assumption is based on a rotating disk hydrodynamic system, uses a compressed tablet, and powder size plays no role. Thus, this assumption needs to be verified with powder dissolution testing using various particle sizes. Further, such an assumption is contradictory to a basic fluid dynamic principle, i.e., the apparent diffusional layer thickness is often altered by hydrodynamics. Recently, Nystrom and colleagues used a Coulter Counter to directly measure particle size and concluded that a critical diameter of 15 μm existed for griseofulvin and oxazepam, below which the h_{app} decreased substantially with decreasing particle size. The effect of particle size on h_{app} became less significant when particles diameters were above 15 μm.[10] More recently, employing the same particle size measuring technique, Figueiredo et al. concluded that the critical particle size should be 22 μm for ibuprofen, where the value of h was linearly proportional to particle diameter (kd) when the diameter was less than 22 μm but was a constant (kd_{cri}) when the particle diameter was above 22 μm.[11]

In the previously reported studies, even though the dependence of h_{app} on particle size has been mathematically described, its dependence on the dissolution hydrodynamics has received very little consideration. Therefore, a complete examination of h_{app} as a

function of particle size and pharmaceutically relevant hydrodynamics is theoretically and practically significant. In this paper, we employed Equation 1 to do so.

$$\frac{h_{app}}{d} = a + b(\frac{dv^0}{\upsilon})^{1/2} \qquad (1)$$

where d is the drug particle diameter, v^0 is the linear velocity of fluid in cm/s, υ is the kinematic viscosity (cm^2/sec) of the fluid, a and b are parameters that can be estimated through experimental data. Mathematically, Eq 1 is similar to Equation 2,

$$\frac{kd}{D} = 2.0 + 0.6 \times (\frac{dv^0}{\upsilon})^{1/2}(\frac{\upsilon}{D})^{1/3} \qquad (2)$$

where k is mass transfer rate cm/s, and D is the diffusion coefficient of the drug molecule cm^2/s. As early as 1952, Eq 2 was theoretically derived and experimentally validated by Ranz & Marshall to describe the rate of evaporation of pure liquid drops and water drops containing dissolved and suspended solids, such as in spray-drying operations.[12,13] In a subsequent article published in the same year, Ranz extrapolated his theory to mass transfer of single particles and packed beads.[14] In 1954, F.H. Garner and his colleagues applied this theory to dissolution from a fixed solid sphere in fluid flow.[15] Specifically, they found that the dissolution of benzoic acid in a stream of water was correlated with another equation of similar functional form to the Ranz-Marshall equation (Eq 2), $\frac{kd}{D} = 44 + 0.48(\frac{dv^0}{\upsilon})^{1/2}(\frac{\upsilon}{D})^{1/3}$. In 1960, Bird elaborated the Ranz-Marshall equation to describe simultaneous heat and mass transfer of a liquid or solid sphere under forced convection.[16] In 1962, Harriott applied Eq 2 for depicting mass transfer of benzoic acid, boric acid, zinc and lead sulfate particles suspended in agitated and baffled tanks.[17] More recently, Fogler et al. employed Eq 2 to study the dissolution of poly-

dispersed particles.[18] Drug powders dissolved in a USP dissolution apparatus II would encounter a similar hydrodynamic environment to that investigated in Harriott and Fogler's studies: that is, mass transfer from solid spheres under forced convection.

In this paper, fenofibrate was selected to serve as a model BCS II drug. Selection of USP II conditions is pharmaceutically relevant and of particular importance from a regulatory perspective. Moreover, five size fractions were utilized in the current study to further characterize and understand the impact of particle size on h_{app}. The focus of this work is to: 1) determine the diffusion layer thickness h_{app} for a BCS II model drug, fenofibrate, in a USP dissolution apparatus II; and 2) illustrate the dependence of h_{app} on particle size and hydrodynamics using function form $\frac{h_{app}}{d} = a + b(\frac{dv^0}{\upsilon})^{1/2}$.

Theoretical Section

Calculation of Diffusional Layer Thickness h_{app}

The diffusion layer thickness h_{app} of drug particles in a USP dissolution apparatus II can be calculated based on their dissolution rates. At dissolution time zero, the initial weight of a single drug particle is $M_0 = \frac{4\pi}{3}\rho r_{0,v}^3$. At any time t afterwards, the particle weight is $M_t = \frac{4\pi}{3}\rho r_{t,v}^3$, where $r_{0,v}$ and $r_{t,v}$ are the volume particle radius at time zero and t, respectively. M_0 and M_t can be brought together by the mass balance of the drug particle, namely,

$$M_0 - M_t = \frac{(C_t)V}{N} \qquad (3)$$

where N is the total number of particles, C_t is the drug concentration at time t, and V is the dissolution volume. In addition, the Noyes-Whitney equation was originally derived

in the slab coordinate. When it is applied to a spherical particle using spherical coordinate, it can be rewritten as [19,20]:

$$-\frac{dM}{dt} = DA(C_S - C_t)(\frac{1}{r} + \frac{1}{h_{app}}) \quad (4)$$

Eq 4 can be simplified to the following:

$$-\frac{dr_t}{dt} = \frac{D(C_S - C_t)}{\rho}(\frac{1}{r_t} + \frac{1}{h_{app}}) \quad (5)$$

where ρ is the density of drug particles, C_S is the drug solubility in the dissolution medium, and h_{app} is the apparent diffusion layer thickness. Thus, with known parameters including C_S , C_t , ρ , V , D and N , the relationship between r_t and t can be established, the derivative of which is connected to h_{app} through Eq 5.

For a system that is approximately spherical, Eq 4 is still valid. However, in the case of non-spherical shape, the particle mass M should be related to the particle volume radius r_v , and the particle surface area A should be related to the particle surface radius r_s . The volume radius r_v can be measured directly by Coulter Counter method. The surface particle radius is calculated using equation $A = 4\pi r_s^2$, where the surface area A is determined by BET methodology. Therefore, Eq 4 can now be written as follows:

$$-\frac{\rho 4\pi r_{t,v}^2 dr_{t,v}}{dt} = D4\pi r_{t,s}^2 (C_S - C_t)(\frac{1}{r_{t,s}} + \frac{1}{h_{app}}) \quad (6)$$

Further, if the ratio of $\frac{r_s}{r_v}$ is assumed to be constant, then equation (6) can be simplified in the following:

$$-\frac{dr_{t,v}}{dt} = [(\frac{r_s}{r_v})\frac{1}{h_{app}} + \frac{1}{r_{t,v}}]\frac{D}{\rho}(\frac{r_s}{r_v})(C_S - C_t) \quad (7)$$

The ratio between the surface radius and volume radius, i.e. $\frac{r_s}{r_v}$, is defined as the shape factor. This ratio is a fundamental property related to the particle dissolution rate in addition to drug solubility and diffusivity that are the essential factors dictating the diffusion and convection within the solid-liquid interface. The dissolution of an individual particle presumably proceeds in an isometric manner at the initial stage of the dissolution test. Therefore, the shape factor could be assumed as a constant in calculating the h_{app} values. Eqs 3 and 7 are employed in calculating h_{app}.

Dependence of h_{app} on Particle Size and Fluid Velocity

The diffusion layer thickness h_{app} for drug particles in a particular geometry is a function of drug properties including particle diameter d and diffusivity D, and fluid properties of fluid velocity v^0 and kinematic viscosity υ.[21]

$$h_{app} = f(d, D; v^0, \upsilon) \quad (8)$$

Therefore we have $n = 5$ variables for h_{app} of drug particle dissolution in a USP vessel. These $n = 5$ variables are built up from $k = 2$ independent dimensions that are: length *L* (cm) and time *T* (s). According to the π-theorem, the variables $n = 5$ can be reduced to 3 independent dimensionless numbers, which are defined as $\frac{h_{app}}{d}$, Reynolds number $\mathrm{Re} = \frac{dv^0}{\upsilon}$ and Schmidt number $S_{Ch} = \frac{\upsilon}{D}$. Then, Eq 8 can be expressed as:

$$\frac{h_{app}}{d} = f(\mathrm{Re}, S_{Ch}) \qquad (9)$$

Most of previous work, both theoretical and practical,[12-15,17,18,22] suggested the form of:

$$\frac{h_{app}}{d} = \mathrm{a} + \mathrm{b} \times (\mathrm{Re})^{1/2} (S_{Ch})^{1/3} \qquad (10)$$

In the current case, the kinematic viscosity of dissolution medium υ and drug diffusivity of fenofibrate D are constant, thus equation 1 arrives.

$$\frac{h_{app}}{d} = \mathrm{a}+\mathrm{b} \times (\mathrm{Re})^{1/2} = a + b(\frac{dv^0}{\upsilon})^{1/2} \qquad (1)$$

where a and b are constants and can be determined using regression analysis of the experimental data such as h_{app} and d.

Experimental Section

Materials and Preparation

Fenofibrate (> 99% purity), sodium lauryl sulfate and all other chemicals were of analytical grade and were purchased from Sigma Chemical Company (St. Louis, MO). Distilled, deionized and filtered water was prepared in house and used for all experiments. Fenofibrate "as received" from Sigma had a broad size distribution, with which four size fractions, i.e., 20-32, 32-45, 63-75 and 90-106 μm were obtained by sieving. In brief, the bulk material was initially dry sieved through the USA standard test sieves (Newark Wire Cloth Company, Clifton, NJ). Then, 300 mg of the dry sieved fractions were well suspended into 60 mL of 0.9% NaCl solution containing 0.05% SLS,

and the suspensions were wet sieved through the same standard sieves. The wet sieved fractions on the sieve were rinsed with 0.9% NaCl solution containing 0.05% SLS and subsequently with water, and then they were dried overnight in a vacuum oven at 30°C. The < 20 μm size fraction was achieved by jet-milling the bulk material as received from Sigma. About 100 g of fenofibrate bulk material was jet-milled through a lab scale size fluid energy grinder (Sturtevant Inc., Hanover, MA) that was operated using compressed nitrogen, with an approximate yield of 95%. The milling air setting was 60 – 70 PSIG, and the feed air pressure was operated between 90 – 100 PSIG. The crystal form of the jet-milled fenofibrate was also characterized using powder X-ray diffraction (PXRD) and differential scanning calorimetry (DSC) to confirm the absence of amorphous material and process induced changes in crystal form. All the five fractions of particles were fully characterized with regards to their specific surface area, particle volume diameter, number diameter, and density. The USP pH 6.8 50 mM phosphate buffer without pancreatin was prepared following standard procedures.[23] Piecewise regression analysis and parameter estimations were performed using Sigmaplot 10.0 (SPSS Inc., Chicago, IL).

Powder X-ray Diffraction (PXRD)

Powder diffraction patterns of jet-milled and "as received" fenofibrate were recorded with a Scintag X-ray diffractometer (Franklin, MA) using CuKα radiation (λ = 1.54 Å), tube voltage of 40 kV, and tube current of 20 mA. The intensities were measured at 2-theta values from 5° to 40° at a continuous scan rate of 5° /min.

Differential Scanning Calorimetry (DSC)

The thermal behavior of jet-milled and "as received" fenofibrate were studied using a TA Instruments 2920 modulated DSC (TA Instruments, New Castle, DE) with refrigerated cooling system (RCS) in standard mode. Approximately 5-10 mg samples were weighed into aluminum DSC pans, crimped, equilibrated to -80°C and then heated up to 100°C at speed of 5.0°C/min, with nitrogen purge at 110 mL/min.

Particle Size Determination

The mean volume particle size diameters for all size fractions were determined using the Coulter Counter (non-laser light scattering) method. The jet-milled material was first suspended in the 0.9% NaCl solution containing 0.25% SLS, saturated with fenofibrate. Then the suspension was quickly transferred into the 0.9% NaCl solution containing 0.1% SLS and saturated with fenofibrate, which served as the suspending medium and testing electrolyte for all samples during particle size measurement. It should be emphasized that the diameter given by the Coulter is a volume equivalent diameter, namely, $d_v = (6v/\pi)^{1/3}$, where v is the particle volume directly measured by the Coulter.

Specific Surface Area Measurement

The specific surface area of fenofibrate powders was determined at liquid nitrogen temperature using BET methodology employing nitrogen as the adsorbate. The surface area was used to calculate the particle surface radius by equation $A = 4\pi r_s^2$.[24]

Solubility Measurement

The aqueous solubility of fenofibrate was measured at 37ºC in 0.25% SLS pH 6.8 phosphate buffer, instead of water. Since SLS has a CMC of 0.25% (w/v) in water, it serves as a reasonable surrogate of the *in vivo* surfactant properties provided by bile salts

and provides the necessary enhancement in solubility and dissolution rate for fenofibrate that is practically insoluble in water with a solubility of < 0.3 μg/mL. Fenofibrate solubility was determined by suspending excess fenofibrate powder in 5 mL buffer in a screw-capped vial. The suspension was equilibrated by shaking in an orbital shaker water bath (LABLINE Instruments, Inc., Melrose Park, IL). At suitable time intervals, 1.0 mL of aliquots were drawn and filtered through 0.45-μm membrane, and then diluted with an appropriate amount of phosphate buffer prior to the spectrophotometric assay at λ = 292 nm using a UV spectrophotometer (Beckman Coulter DU 650, Fullerton, CA). The equilibrium solubility of fenofibrate was established when the difference between three consecutive measurements is within 1%, a process that may take up to 7 days.

Dissolution Profiles in USP Dissolution Apparatus II

The dissolution profiles of various size fractions of fenofibrate were measured in a USP dissolution apparatus II at 37°C using pH 6.8 phosphate buffer containing 0.25% SLS. For the jet-milled fenobibrate, 50 mg powder was weighted into a 1.0 mL of eppendorf tube, then 0.5 mL of the dissolution medium were added, and then the suspension was sonicated at low power for 5 seconds. The well dispersed jet-milled suspension was then immediately transferred into the prepared dissolution vessel, and rinsed with the dissolution medium three times 5 mL each. The four bigger size fractions of fenofibrate powders (50 mg) were directly dropped into the 37ºC 500 mL dissolution medium that was previously degassed. For the Dissolution experiments were conducted in triplicate at both 50 rpm and 100 rpm for each particle size. Aliquots were drawn at 0.33 – 1 min intervals, filtered through 0.45-μm membrane and diluted if necessary prior to UV spectroscopic analysis at λ = 292 nm (BeckmanCoulter DU 650, Fullerton, CA).

Results

Characterization of Fenofibrate Particles

As evident from the DSC traces of the jet-milled and "as received" fenofibrate (Figures 2.1a and 2.1b), a negligible glass transition occurs around -45°C with a very small enthalpy of -0.0015 w/g, followed by the melting point around 79.5°C with an enthalpy of fusion of approximate 95 J/g. This DSC result indicates that no significant changes in crystal forms or amorphous content were introduced through the jet-milling process. These results are further confirmed by PXRD (Figure 2.2) where the slightly decreased peak intensities are consistent with a reduction in particle size.

The volume particle size distribution of each size fraction is shown in Figure 2.3, and the surface area equivalent particle radius, shape factor and density for each size fraction are summarized in Table 2.1. Visual observation via SEM shows the irregular and multi-sided morphology of fenofibrate particles (Figure 2.4), suggesting that fenofibrate particles would dissolve in a relatively isometric manner.

The diffusivity of fenofibrate was calculated as 7.4×10^{-6} cm^2/s using the ADMET Predictor™ 1.2.1 (Simulation Plus Co., Lancaster, CA), which used the Hayduk-Laudie formula $D = \frac{13.26\times10^{-5}}{\eta_{water}^{1.4} V^{0.589}}$.[25] This value is consistent with the literature reported experimental value of 7.15×10^{-6} cm^2/s using the rotating disk method.[26]

Dissolution Profiles of Fenofibrate

The solubility of fenofibrate was determined to be 150.4 ± 1.4 μg/mL in 0.25% SLS 50 mM pH 6.8 phosphate buffer. The dissolution profiles of fenofibrate particles at 50 rpm and 100 rpm are shown in Figure 2.5. Several elements can be drawn from these

dissolution profiles. First, as expected, the dissolution rates increase with decreasing particle sizes in the following order: jet-milled material (< 20 micron) > 20-32 > 32-45 > 63-75 > 90-106 μm size fractions. This observation is consistent with the larger surface area per unit weight of the smaller particles. Secondly, the dissolution rates of the jet-milled material are similar at the 50 rpm and 100 rpm. Finally, the four larger size fractions of fenofibrate dissolve faster at a paddle speed of 100 rpm than at 50 rpm, presumably due to the higher fluid velocities at 100 rpm that lead to thinning of h_{app} and subsequently more efficient mass transfer.

Dependence of Diffusional Layer Thickness on Hydrodynamics and Particle Sizes

The dependence of h_{app} on particle size and hydrodynamics/fluid velocity were examined and illustrated in the two following ways. The first approach is bifunctional analysis demonstrating h_{app} as a function of r under different paddle speeds, as shown in Figure 2.6. This approach determined the transitional particle size through which the value of h_{app} exhibits a different correlation with particle radius. Determination of transitional particle size has been employed previously in the literature.[9-11] The second approach is dimensionless analysis using Eq 1, investigating the combined effects of particle sizes and paddle speeds on h_{app}.

Bifunctional analysis: The transitional particle size for fenofibrate in a USP dissolution apparatus II is fluid velocity dependant. Using piecewise regression, the transitional particle sizes are 37.7 ± 5.4 μm ($R^2 = 0.9972$) and 23.7 ± 0.6 μm ($R^2 = 0.9998$), under 50 and 100 rpm, respectively (Figure 2.6). For drug particles smaller than the transitional sizes, the h_{app} displays a linear relationship with the drug

particle radius. The linear slopes vary with paddle speeds, and the values are 1.71 (R^2 = 0.9872) and 1.59 (R^2 = 0.9828), at 50 rpm and 100 rpm, respectively. In comparison, for drug particles larger than the transitional sizes, at 100 rpm a constant h_{app} was observed with an approximate value of 43.5 μm for any particles with radius larger than 23.7 μm; and at 50 rpm the h_{app} value continues to increase with particle size but at a slower rate. The bifunctional analysis also leads to the plot of h_{app} versus $\sqrt{d}$, as shown in Figure 2.7. Evidently, at 50 rpm h_{app} demonstrates a linear correlation with $\sqrt{d}$, i.e., $h_{app} = 9.91\sqrt{d} - 23.31, R^2 = 0.9769$, throughout the tested particle size range 6.8-106 μm in this work. Whether this linear relationship applies to particles in near-micron or sub-micron range needs further research, partially due to the complex microfluid dynamics surrounding these very small particles. In comparison, at 100 rpm the linear relationship transforms into plateau for larger particles. This dependence of h_{app} on $\sqrt{d}$ was then further exploited in dimensional analysis.

Dimensionless analysis: According to Eq 1 $\frac{h_{app}}{d} = a + b(\frac{dv^0}{\upsilon})^{1/2}$, the Re number $(\frac{dv^0}{\upsilon})$ was calculated using drug particle diameter d (cm), linear fluid velocity v^0 (cm/sec), and kinematic viscosity υ of dissolution medium ($0.758 \times 10^{-2} cm^2/s$) at 37ºC.[27] The linear velocity of fluid/dissolution medium in an agitated USP vessel depends on the rotational speeds of paddle and the location in the vessel. In addition, the use of the linear velocity of the fluid is not convenient in practice, and the rotational speed of the paddle ϖ is readily available and can be easily adjusted to the linear

velocity through paddle diameter d_{ϖ}, i.e., $v^0 = \varpi \times d_{\varpi}$. It therefore lends to the calculation of the Reynolds number using ϖ, i.e., $d_{\varpi} \times \frac{d\varpi}{\upsilon}$. The relationship between $\frac{h_{app}}{d}$ and $\frac{d\varpi}{\upsilon}$ is proposed in equation 11:

$$\frac{h_{app}}{d} = a + \text{constant}(d_{\varpi} \times \frac{d\varpi}{\upsilon})^{1/2} = a + b(\frac{d\varpi}{\upsilon})^{1/2} \qquad (11)$$

where R_e is calculated based on the following: d is the particle diameter in μm, ϖ is the rotational speed of paddle in rpm, υ is the kinematic viscosity of dissolution medium in cm^2/sec, and the diameter of the USP paddle (d_{ϖ}) is included in the parameter b (Eq 11). Figure 2.8 demonstrates that the h_{app} of suspended drug particles in the USP vessel can be successfully described with the semi-theoretical equation (Eq 11). Here, $\frac{h_{app}}{d}$ exhibits a two-regional dependence on particle Re, i.e., $(\frac{d\varpi}{\upsilon})^{1/2}$. One region is linear, where the particle Re is ≥ 592, and is described by $\frac{h_{app}}{d} = 1.5207 - 9.25 \times 10^{-4}(\frac{d\varpi}{\upsilon})^{1/2}$. Assuming the drug diffusivity is $7.15 \times 10^{-6} cm^2/s$,[26] this regression corresponds to an $R^2 = 0.9875$ ($P < 0.0001$), and estimates the values of a = 1.5207 ± 0.0417 and b = -9.25×10^{-4} ± 4.66×10^{-5}. The other region describes the relation for particles with smaller Re number (either smaller particle size and/or slower paddle speeds), the relationship between $\frac{h_{app}}{d}$ and Re may be more complex.

Discussion

Calculation of Diffusion Layer Thickness h_{app}

Due to its mathematical simplicity, a spherical shape is the best contour to select to experimentally determine the value of h_{app}, an approach that was elaborated by Wang and Flanagan.[19,20] Numerous attempts to prepare spherical and crystalline fenofibrate particles for this study were unsuccessful because fenofibrate either forms amorphous spheres or crystalline needles following recrystallization processes as confirmed by polarized microscopy. Therefore, irregular shapes of fenofibrate particles were employed here with consideration given to their shape factor; that is, the ratio of particle surface radius to volume radius. Here, it is assumed that drug particles would dissolve in an approximately isotropic manner, implying that the shape factor would remain unchanged. This assumption has been used widely in the past, when the shape factors were considered constant, as in the initial stages of the dissolution testing. Even in the case of dissolving crystals with a high degree of non-isometricity sharp edges such as needles and plates, the shape factor has been reported to change insignificantly until considerable dissolution occurs.[28,29] In addition to the shape factor, the quantity of amorphous content, may also contribute to non-isometric dissolution. PXRD and DSC results confirmed the absence of detectable amorphous form for the jet-milled material.

The thickness of a hydrodynamic boundary layer is often defined as the distance from the surface of the solid to the point where the tangential velocity attains a value of 90% of the main stream.[21] In general, this layer thickness is not easily evaluated from experimental work except under well-defined hydrodynamic conditions as in the case of the rotating-disk.[21] In this work, the h_{app} is calculated using Eq 7 to describe the distance over which the diffusion process dominates the mass transfer. As such, it reveals the

drug dissolution in terms of how resistance to mass transfer may occur in the solid-liquid interface in a simple model. In addition, the diffusional thickness can often be used to predict changes in mass transfer caused by factors such as chemical reactions.[30,31] It is important to note that the h_{app} determined in a USP dissolution apparatus is an apparent averaged value from all particles under specific hydrodynamic conditions, because the local environment of fluid dynamics surrounding each individual drug particle is not the same throughout the USP dissolution apparatus II vessel.[32-36]

Dependence of h_{app} on Hydrodynamics and Particle Sizes

Bifunctional analysis with transitional particle sizes

Dissolution phenomena have been studied in a quantitative manner for more than a century, during which various relationships between h_{app} and particle size have been proposed.[5,8-11] Bifunctional analysis of fenofibrate dissolution data suggests that Higuchi-Hiestand's assumption[5,6] and Hintz-Johnson's hypothesis[9] appear to be valid, only if the powder dissolution occurs under specific hydrodynamic conditions.

Higuchi-Hiestand assumed that h_{app} was equal to or greater than the particle radius, and conducted their experiments with 2.2 mg of micronized methylprednisolone (≤ 25 μm) in 100 mL of water in bottles that were rotated at 6 rpm at 25°C.[5-7] In comparison with their work (Table 2.2), the current study experimentally demonstrates that in a USP dissolution apparatus II h_{app} may be equal to or greater than particle radius r, only if the specific hydrodynamic conditions are provided. The first observation is based on the data that at paddle speed of 100 rpm, the particle radius r 44.6 ± 0.4 μm is not significantly different from the corresponding h_{app} value of 43.5 ± 11.2 μm. The second point was observed at both paddle speeds. For example, at 50 rpm h_{app} is equal to $1.71r$, and the

value of h_{app} decreases to $1.59r$ at a higher paddle speed of 100 rpm, both suggesting that h_{app} could be greater than particle radius.

The description of h_{app} as a function of particle size under both paddle speeds was compared with Hintz's work as well, as shown in Table 2.2. Both sets of data consistently demonstrate the existence of a transitional particle size C_r in the 30 μm size range, and a linear relationship between h_{app} and r when particle size is below C_r. When particle size is above C_r, a constant h_{app} value, however, was observed at 100 rpm. Further, despite the similar observations, it is evident that distinct differences exist between the Hintz-Johnson's assumption and our work in the following specific aspects: 1) the value of C_r; 2) the linear slope value between the h_{app} and r; and 3) the value of constant h_{app}. This difference is attributed to the differences in hydrodynamic conditions under which the dissolution studies are conducted. In Hinz-Johnson work, the $h_{app} = r$ assumption was suggested based on a rotating disk system, where a planar constant surface area pertains rather than a powder dissolution of spherical geometry where more complex hydrodynamics pertains. For example, based on Levich's equation $h = 1.61(\frac{D}{\upsilon})^{1/3}(\frac{\upsilon}{\varpi})^{1/2}$ [21], a diffusivity of fenofibrate as 7.15 $\times 10^{-6}$ cm^2/s and kinematic viscosity of the dissolution medium as 7.58 $\times 10^{-3}$ cm^2/s at 37°C, for fenofibrate, a rotational speed of 21 rpm would give a h equals to 30 μm. Clearly, the dissolution hydrodynamics in these two systems are very different.

Dimensionless analysis

The key dissolution variables employed in Eq 1, particle size and Reynolds number that is an indicator of the fluid dynamics, were compared to the previous utilization of the

Ranz-Marshall equation (Eq 2) as shown in Table 2.3, and the similarities and differences are discussed as follows. In Ranz's original work on mass transfer of single particles and packed beds,[14] the theory was applied to particle sizes in the range of 0.06 cm to 1.1 cm and R_e number ranging from 2 to as high as 10^5. In later studies, the particle size varied from 15 to 1270 μm, and the R_e number ranged from 1 to 10^5 (Table 2.3). Comparably, the R_e number under standard USP dissolution conditions such as 50 and 100 rpm is within the R_e range tested in the original Ranz theory[12-14] and other work.[15,17,18,22,37] The R_e number in a USP dissolution apparatus II encompass a considerable range from a value of zero at the vessel wall to the highest value at the paddle tip. Using equation $R_e = \frac{\varpi\, d_\varpi^2}{\upsilon}$, the maximum R_e numbers can be determined as 2.9×10^4 and 5.8×10^4 at 50 rpm and 100 rpm, respectively,[33] where ϖ is the rotational speed of the paddle, d_ϖ is the diameter of the paddle, and ν is the kinematic viscosity of the fluid. Although the mean particle size in this work, 32 - 106 μm, is generally smaller than that utilized by Ranz's and others, our results have shown that the theoretical diffusion layer thickness $\frac{h_{app}}{d} = a + b(\frac{dv^0}{\upsilon})^{1/2}$ could be extrapolated with remarkable accuracy to the particle size range beyond the Ranz's.

Industrial Significance of h_{app}

Dependence of h_{app} on paddle speeds and particle size

Dimensionless analysis demonstrated a bipartite behavior of the dependence of h_{app} on paddle speeds and particle size, which may be contributed by several factors. First,

crystal defects and roughness on the particle surface represent a larger percentage of the crystal weight after milling, since the surface area to volume ratio is increased. These effects were observed to have a significant impact on dissolution rate for particles with diameters in the micron range. Second, at small particle sizes, turbulence in the form of microeddies begins to play a more important role in the hydrodynamics near to the dissolving surface, in other words a microenvironment different from the bulk hydrodynamics is created.[38-40] It is also thought that the effective eddy diffusivity of drug molecule in the turbulent fluid may be very different from that in bulk fluid.[41] Surface roughness, crystal defects and microeddies would lead to a faster dissolution rate than expected using surface area and the bulk fluid velocity. This region of small Re number merits further research.

Eq 11, $\frac{h_{app}}{d} = a + b(\frac{d\varpi}{\upsilon})^{1/2}$, was also applied to *in vitro* dissolution behavior of other drugs including digoxin and oxazepam independently reported by Nyström et al.[10,42] In their studies, dissolution rates were measured with two different particle sizes under three rotational speeds, i.e. 350, 500 and 800 rpm. Dissolution rate data for digoxin fit the following the relationship:

$\frac{h_{app}}{d} = 22.17 - 0.012(\frac{d\varpi}{\upsilon})^{1/2}$ with the $R_{sq} = 0.9403$ $(P = 0.0052)$

For oxazepam, h_{app} conforms to the following equation:

$\frac{h_{app}}{d} = 3.05 - 0.016(\frac{d\varpi}{\upsilon})^{1/2}$ with the $R_{sq} = 0.9472$ $(P = 0.0063)$.

The successful fitting of digoxin and oxazepam dissolution data into the function form of Eq 11 further supports the linear correlation between $\frac{h_{app}}{d}$ and $(\frac{d\varpi}{\upsilon})^{1/2}$ and its use to

estimate h_{app} values for drug particles in the standard USP dissolution II apparatus, based on the measured particle size d and the rotational paddle speed ϖ.

h_{app} for poorly soluble drugs

Recent estimates suggest that the percentage of BCS II drugs in the top US 200 oral IR products is greater than 25%.[43] Probably as a result of the widespread application of combinatorial chemistry and high-throughout screening activities during the drug discovery process,[44,45] this percentage will probably continue increase. To ensure satisfactory oral absorption, particle size reduction has been widely used to increase the surface to volume ratio and thus improve the dissolution rate of poorly soluble drugs. The current work clearly reveals that the h_{app} values generally decrease with decreasing particle size (Figure 2.6). Therefore, an increase in the dissolution rate resulting from a particle size reduction process is attributed not only to an increase in the surface area to volume ratio, but also to a decrease in h_{app}, an important contribution that is rarely addressed in the literature.

In addition, since the layer thickness h_{app} depends on the drug diffusivity D, the corresponding h_{app} for two drug substances with different D values would be expected to be different. However, it is likely that the h_{app} would only change slightly because: 1) according to the Levich theory[21], h_{app} is only dependent to the one-third power on D i.e. $h = 1.61(\frac{D}{\upsilon})^{1/3}(\frac{\upsilon}{\varpi})^{1/2}$ and 2) drug diffusivity of most small drug molecules is low and in the range of 10^{-6}-10^{-5} cm^2/s.

Furthermore, the results in this paper suggest the following: 1). for drug particles with radius in the range of 3.4- 23.7 μm, h_{app} is approximately 1.5-fold of particle radius (Figure 2.6). 2). under the paddle speed of 50 rpm, the diffusional h_{app} exhibits a linear relationship with the square root of particle diameter, across the studied particle size range (Figure 2.7).

Finally, Figure 2.6 suggests that for small drug particles, h_{app} is not significantly different under 50 and 100 rpm. The exact size range for the small particles, where h_{app} is independent of paddle speeds in a USP dissolution apparatus II, is yet to be determined. In this work, the jet-milled fenofibrate with a mean r_v of 3.4 μm, demonstrates that its h_{app} is independent of fluid velocity. In the case of cilostazol, the size limit could be in the low micron range, i.e., 13 μm. Cilostazol is a poorly soluble compound with a water solubility of 6.25 μg/mL at 37°C. Three size fractions with mean particle sizes of 13, 2.4 and 0.22 μm were prepared using techniques hammer-mill, jet-mill and spray-drying, respectively. *In vitro* powder dissolution profiles of 5 mg of these cilostazol samples, in 900 mL of water, FaSSIF and FeSSIF at 37°C in USP apparatus II, were equivalent at the paddle speeds of 50 and 200 rpm[46]. This result indicates that the h_{app} is independent of paddle speeds when the cilostazol particles are smaller than 13 μm. Both results suggest that the hydrodynamic considerations are important for large particles, and very small particles in micron range are less influenced by hydrodynamics.

Relevance to *In Vivo* Conditions

The unique result, namely, h_{app} is independent of fluid velocity for the very small particles, suggests that the highly variable GI fluid velocity varying with GI motility

phases may not impact on the h_{app} of low micron range particles in *in vivo*. The micronized powder of felodipine, with a median particle size of 8 μm, may be an example of such a drug. Felodipine is a poorly soluble, neutral and lipophilic drug, and its oral absorption that is indicated by AUC does not appear to be affected by the *in vivo* hydrodynamics in dog studies.[47,48] The independence of h_{app} on GI motility, for small particles such as jet-milled material, imply that the *in vivo* variability would be significantly reduced within subjects and between subjects. Therefore, reducing particle size not only improves the dissolution rate and absorption fraction for poorly soluble drugs, but also potentially minimizes the *in vivo* variability.

However, it should be emphasized here that establishing *in vitro* dissolution methodology reflecting *in vivo* scenario requires considerations in many aspects. For example, pH and surfactants are critical in selecting an appropriate dissolution medium. Additionally important factors include the fluid velocity and device geometry, which combine to determine the dissolution hydrodynamics. One disparity between dissolution testing and the *in vivo* situation is that the paddle speed remains unchanged during a given dissolution test. By contrast, the GI tract regularly transitions through migrating motility cycles and fasted or fed states. Hence, the GI fluid velocity varies considerably along various regions of small intestine,[49-52] which can lead to large inter- and intra-subject variations in *in vivo* h_{app}. To mimic the wide range of *in vivo* h_{app}, it may be more appropriate to vary the *in vitro* hydrodynamic conditions during a test e.g. paddle speed (Type II tester), dip rate (Type III) and flow rates (Type IV). It is unrealistic to assume that use of a single USP dissolution setting such as 50 rpm can reflect the complete hydrodynamics of a full GI motility cycle. However, a single paddle speed

might be used to represent one certain GI motility-fluid flow and particle size combination.

Revision of the test apparatus design to better reflect the geometry of the intestinal tract and its flow patterns should be considered. One particularly important aspect to consider is the representation of oscillating flow, corresponding to the segmental mixing in the fed state, which is unique in its effects on *in vivo* h_{app}. Applying dimensional principle, the *in vivo* h_{app} is a function of: $\frac{h_{app}}{d} = f(\mathrm{Re}, S_{ch}, St)$, where Re and S_{ch} are defined as previously, and St is the Strouhal number describing oscillatory fluid. St number is calculated as $St = \frac{fl}{v^0}$, where f is vortex shedding, l is the characteristic length (hydraulic diameter), and v^0 is the linear velocity of GI fluid.

Potentially, a dimensionless analysis of the *in vitro* hydrodynamics and the *in vivo* GI motility using the rule of $\frac{h_{app}}{d} = f(\mathrm{Re}, S_{ch}, St)$ would be useful in improving accuracy of predicting *in vivo* dissolution and absorption of drug products, enhancing correlation between *in vitro* dissolution and *in vivo* response and developing *in vitro* bioequivalence methods.

Conclusions

The diffusional layer thickness h_{app} was determined through fenofibrate powder dissolution testing in a USP apparatus II with various particle sizes and paddle speeds. The dependence of h_{app} on drug particle size and dissolution hydrodynamics, reveals that at 100rpm the h_{app} is approximate 1.5-fold of the particle radius or a constant, which

occurs below and above a transitional size of 23.7 μm, respectively. Further, the result at 50 rpm suggests that a diffusional h_{app} being linearly proportional to square root of particle diameter is an overall better functional form. Further, dimensionless analysis supports a linear correlation of $\frac{h_{app}}{d}$ with particle Re within specific particle-hydrodynamic regime. However, the extrapolation of *in vitro* results to the *in vivo* situation requires further investigation due to the *in vivo* hydrodynamics varying with various GI motility phases.

Table 2.1. Physical characteristics of various size fractions of fenofibrate powder.

Particle fractions (μm)	Number radius[a] (mean ± SD) (μm)	Surface radius[b] (mean ± SD) (μm)	Volume radius[c] (mean ± SD) (μm)	Specific surface area (mean ± SD) (m^2/g)	Tapped density (g/mL)	Shape factor[d]
< 20 μm (jet-milled)	1.2 ± 0.5	2.7 ± 0.5	3.4 ± 0.9	1.575 ± 0.058	0.36 ± 0.03	0.79
20-32 μm	13.8 ± 6.2	16.2 ± 5.2	16.1 ± 0.6	0.296 ± 0.031	0.64 ± 0.02	1.01
32-45 μm	19.7 ± 4.8	28.4 ± 3.0	26.3 ± 1.2	0.181 ± 0.002	0.76 ± 0.01	1.09
63-75 μm	34.4 ± 4.4	44.6 ± 11.2	37.1 ± 1.0	0.154 ± 0.001	0.76 ± 0.02	1.25
90-106 μm	51.1 ± 18.9	56.3 ± 14.5	53.0 ± 0.5	0.083 ± 0.006	0.77 ± 0.02	1.06

[a]: number radius was measured using scanning electronic microscopy (SEM).
[b]: surface radius was converted through the surface area that was measured by BET methodology.
[c]: volume radius was directly measured using Coulter Counter method.
[d]: shape factor was defined as the ratio of the surface equivalent radius to the volume equivalent radius, i.e., r_s / r_v.

Table 2.2. Comparison of the relationship between h_{app} and r in: Higuchi-Hiestand's work, Hintz-Johnson's work and the current work in a USP dissolution apparatus II.

Conditions	Below c_r : h_{app} as a function of r	Critical particle size: the value of c_r (μm)	Above c_r : h_{app} as a function of r
Higuchi-Hiestand[5,6]	h_{app} is comparable to, or greater than the particle radius r		
Hintz-Johnson[9]	$h_{app} = r$ $(r < 30 \mu m)$	30	Constant, 30 μm
USP dissolution apparatus II, at 100 rpm	$h_{app} = 1.59r$ $(r < 23.7 \mu m)$	23.7	Constant, approximate 43.5 μm
USP dissolution apparatus II, at 50 rpm	$h_{app} = 1.71r$ $(r < 37.7 \mu m)$	37.7	h_{app} increases with r slowly

Table 2.3. Particle sizes and Re: comparison of fenofibrate powder dissolution in a USP dissolution apparatus II and previous studies using the function form of Eq 2.

System	Particle diameter range (μm)	Reynolds numbers of fluids
[a]USP dissolution apparatus II	2 – 106	$0 < R_e < 5.8\times10^4$
Mass transfer from single particles and packed beds[12-14]	600 -1100	$1 < R_e < 7\times10^5$
[b]Mass transfer from a fixed solid sphere in fluid flow[15]	1270	$20 < R_e < 10^3$
[c]Mass transfer of solid particles suspended in agitated tanks[17]	15 - 600	$325 < R_e < 1.08\times10^5$
[d]Estimate the k value of polydisperse solid particles[18]	Not defined.	Not defined in the paper.
Mass transfer of a single particle in creeping-flow[22]	Not defined.	The correlation is [e]very good as of: $1< R_e < 10^3$ Reasonable as of: $10^3< R_e < 10^4$

[a]: The unit for rotational speed ϖ is rpm, for particle size d is cm.
[b]: Overall mass transfer for the fixed sphere.
[c]: The fluid velocity was estimated using slip velocity presented in Harriott's paper.
[d]: k is the mass transfer coefficient and equals to $\frac{D}{h_{app}}$.
[e]: The experimental value is within 30% of the theoretical predicted values.

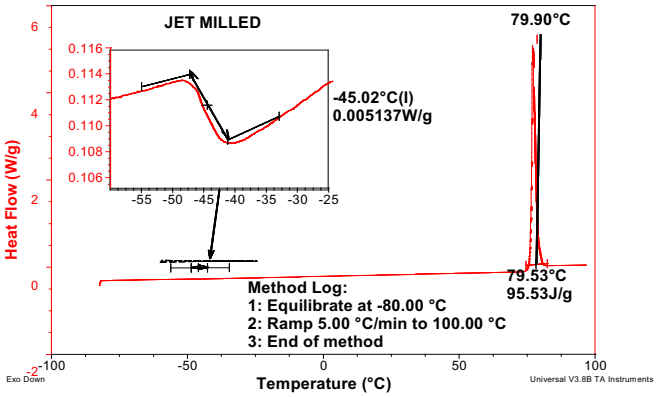

Figure 2.1a. DSC thermograms of the jet-milled fenofibrate.

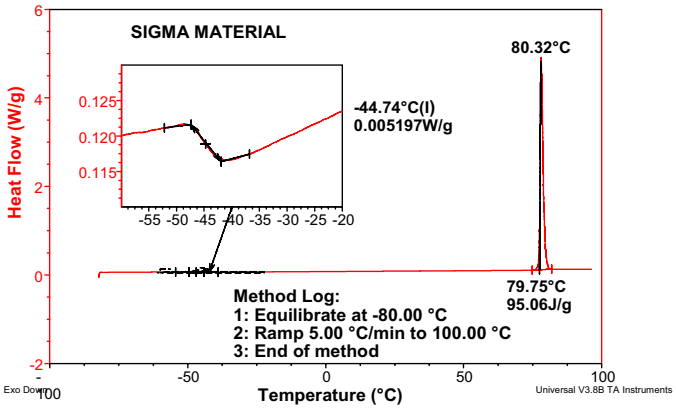

Figure 2.1b. DSC thermograms of fenofibrate "as received" from Sigma.

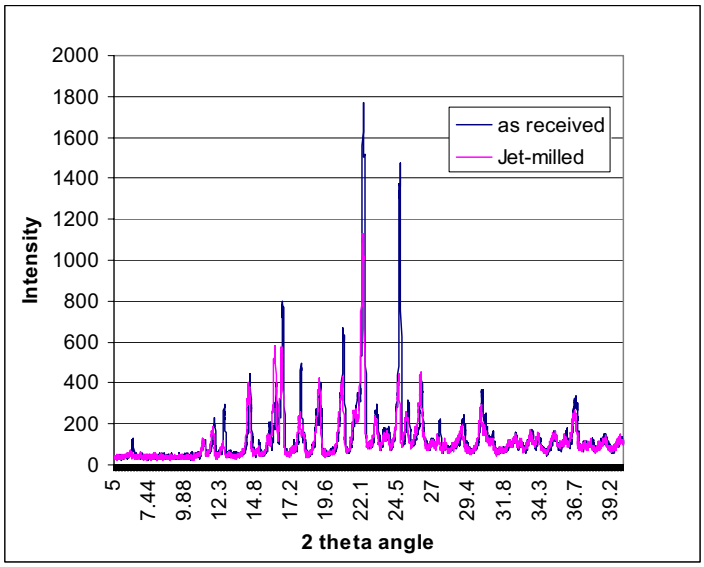

Figure 2.2. PXRD patterns of fenofibrate "as received" and jet-milled.

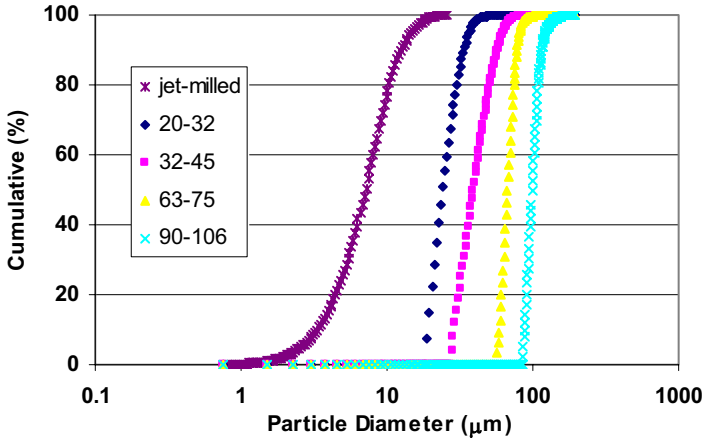

Figure 2.3. Particle size distribution of fenofibrate powders.

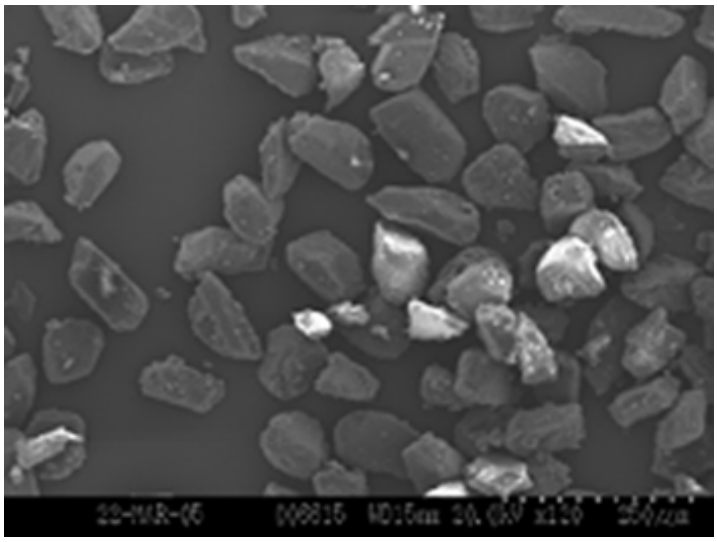

Figure 2.4. SEM picture of a typical fenofibrate powder (63-75µm).

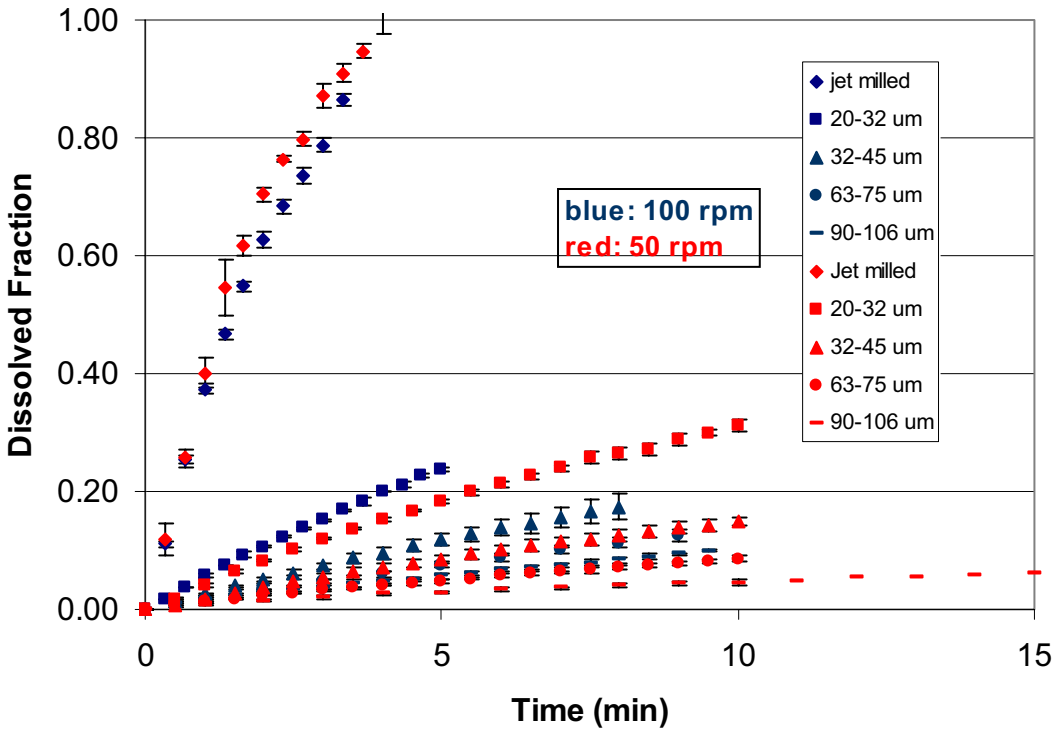

Figure 2.5. Dissolution profiles of various size fractions of fenofibrate powder at 50 rpm and 100 rpm. (Error bars represent the standard deviation of a mean of three experiments.)

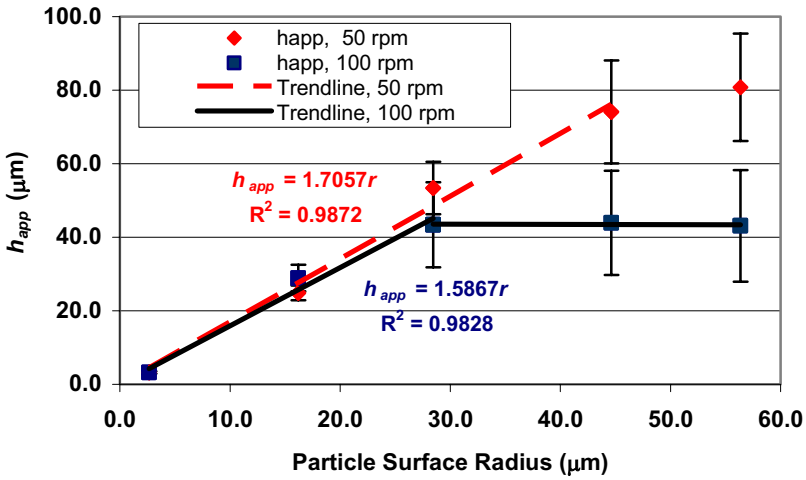

Figure 2.6. Bifunctional analysis of the dependence of diffusional layer thickness h_{app} on particle sizes under different hydrodynamics in a USP dissolution apparatus II (n = 3).

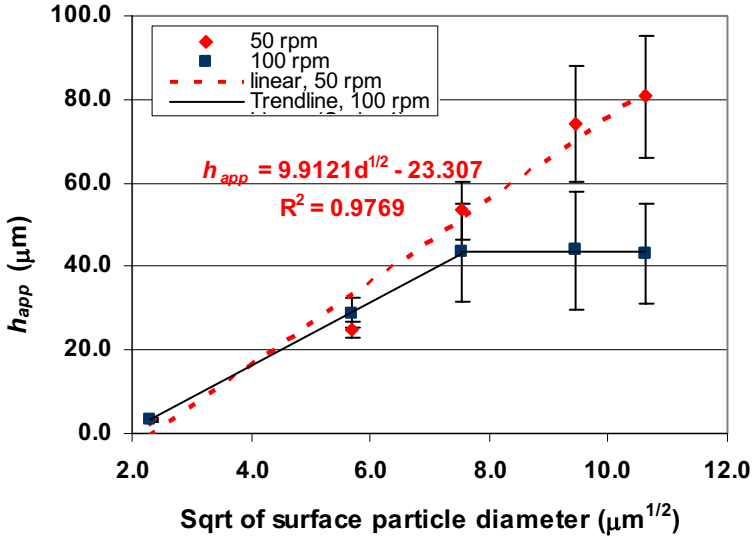

Figure 2.7. Dependence of h_{app} on square root of particle sizes under different hydrodynamics in a USP dissolution apparatus II (n = 3).

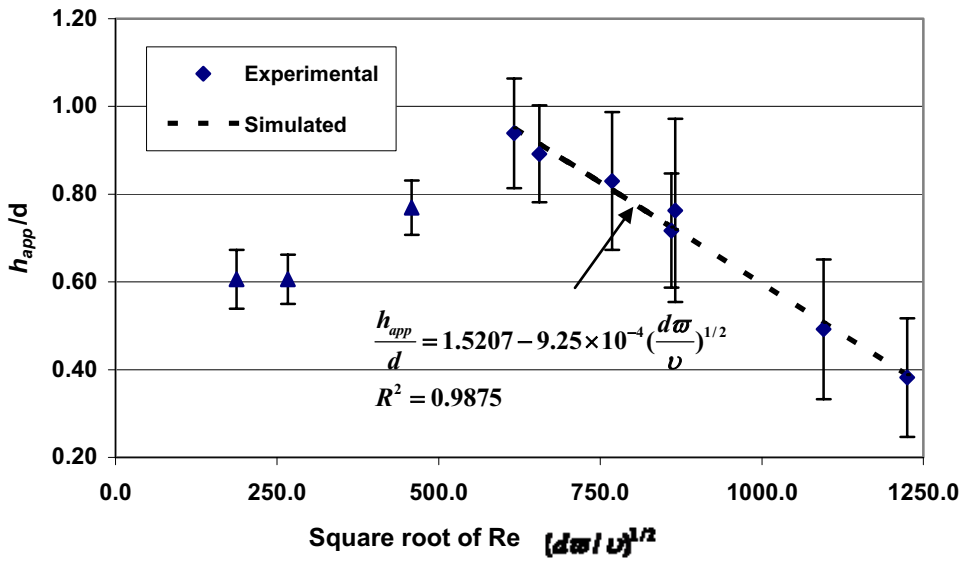

Figure 2.8. Dimensionless analysis of the dependence of diffusional layer thickness h_{app} on particle sizes and hydrodynamics in a USP dissolution apparatus II (n = 3).

References.

1. Amidon GL, Lennernas H, Shah VP, Crison JR. **1995**. A theoretical basis for a biopharmaceutic drug classification: The correlation of in vitro drug product dissolution and in vivo bioavailability. Pharm Res 12:413-420.
2. Lennernas H, Abrahamsson B. **2005**. The use of biopharmaceutic classification of drugs in drug discovery and development: Current status and future extension. J Pharm Pharmacol 57:273-285.
3. Noyes AA, Whitney WR. **1897**. J Am Chem Soc 19:930-934.
4. Martin AN, Bustamante P. **1993**. Physical pharmacy: Physical chemical principles in the pharmaceutical sciences. 4th ed., Philadelphia: Lea & Febiger. p 333-334.
5. Higuchi WI, Hiestand EN. **1963**. Dissolution rates of finely divided drug powders. I. Effect of a distribution of particle sizes in a diffusion-controlled process. J Pharm Sci 52:67-71.
6. Higuchi WI, Hiestand EN, Rowe EL. **1963**. Dissolution rates of finely divided drug powders. 2. Micronized methylprednisolone. J Pharm Sci 52:162-164.
7. Higuchi WI. **1967**. Diffusional models useful in biopharmaceutics - drug release rate processes. J Pharm Sci 56:315-324.
8. Niebergall PJ, Milosovich G, Goyan JE. **1963**. Dissolution rate studies. Ii. Dissolution of particles under conditions of rapid agitation. J Pharm Sci 52:236-241.
9. Hintz RJ, Johnson KC. **1989**. The effect of particle-size distribution on dissolution rate and oral absorption. Int J Pharm 51:9-17.
10. Bistrat M, Anderberg EK, Barnett MI, Nystrom C. **1992**. Physicochemical aspects of drug release.15. Investigation of diffusional transport in dissolution of suspended, sparingly soluble drugs. Int J Pharm 80:191-201.
11. deAlmeida LP, Simoes S, Brito P, Portugal A, Figueiredo M. **1997**. Modeling dissolution of sparingly soluble multisized powders. J Pharm Sci 86:726-732.
12. Ranz WE, Marshall WR. **1952**. Evaporation from drops.1. Chem Eng Pro 48:141-146.
13. Ranz WE, Marshall WR. **1952**. Evaporation from drops.2. Chem Eng Pro 48:173-180.
14. Ranz WE. **1952**. Friction and transfer coefficients for single particles and packed beds. Chem Eng Pro 48:247-253.
15. Garner FH, Grafton RW. **1954**. Mass transfer in fluid flow from a solid sphere. Proc R Soc Lond A 224:64-81.
16. Bird RB. **1960**. Transport phenomena. ed., New York: Wiley. p p. 409 & 647.
17. Harriott P. **1962**. Mass transfer to particles.1. Suspended in agitated tanks. AICHE J 8:93-101.
18. Leblanc SE, Fogler HS. **1987**. Population balance modeling of the dissolution of polydisperse solids - rate limiting regimes. AICHE J 33:54-63.
19. Wang J, Flanagan DR. **1999**. General solution for diffusion-controlled dissolution of spherical particles. 1. Theory. J Pharm Sci 88:731-738.
20. Wang J, Flanagan DR. **2002**. General solution for diffusion-controlled dissolution of spherical particles. 2. Evaluation of experimental data. J Pharm Sci 91:534-542.
21. Levich VG. **1962**. Physicochemical hydrodynamics. ed., Englewood Cliffs, N.J.: Prentice-Hall. p 700.

22. Agarwal PK. **1988**. Transport phenomena in multi-particle systems.2. Particle-fluid heat and mass-transfer. Chem Eng Sci 43:2501-2510.
23. USP. **2000**. The united states pharmacopeia usp 24, the national formulary nf19. ed., Rockville, Maryland: United States Pharmacopeial Convention, Inc. p 2236.
24. Allen T. **1997**. Particle size measurement. 5th ed., London; New York: Chapman & Hall. p 2 v.
25. Hayduk W, Laudie H. **1974**. Prediction of diffusion-coefficients for nonelectrolytes in dilute aqueous-solutions. AICHE J 20:611-615.
26. Granero GE, Ramachandran C, Amidon GL. **2005**. Dissolution and solubility behavior of fenofibrate in sodium lauryl sulfate solutions. Drug Dev Ind Pharm 31:917-922.
27. Dean JA, Lange NA. **1999**. Lange's handbook of chemistry. 15th ed., New York: McGraw-Hill. p 5.134.
28. Dali MV, Carstensen JT. **1996**. Effect of change in shape factor of a single crystal on its dissolution behavior. Pharm Res 13:155-162.
29. Lai TYF, Carstensen JT. **1978**. Effect of shape factor on cube root dissolution behavior. Int J Pharm 1:33-40.
30. Mooney KG, Mintun MA, Himmelstein KJ, Stella VJ. **1981**. Dissolution kinetics of carboxylic acids i: Effect of ph under unbuffered conditions. J Pharm Sci 70:13-22.
31. Mooney KG, Mintun MA, Himmelstein KJ, Stella VJ. **1981**. Dissolution kinetics of carboxylic acids ii: Effect of buffers. J Pharm Sci 70:22-32.
32. Healy AM, McCarthy LG, Gallagher KM, Corrigan OI. **2002**. Sensitivity of dissolution rate to location in the paddle dissolution apparatus. J Pharm Pharmacol 54:441-444.
33. Kukura J, Arratia PE, Szalai ES, Muzzio FJ. **2003**. Engineering tools for understanding the hydrodynamics of dissolution tests. Drug Dev Ind Pharm 29:231-239.
34. McCarthy LG, Bradley G, Sexton JC, Corrigan OI, Healy AM. **2004**. Computational fluid dynamics modeling of the paddle dissolution apparatus: Agitation rate, mixing patterns, and fluid velocities. AAPS Pharm Sci Tech 5:e31.
35. McCarthy LG, Kosiol C, Healy AM, Bradley G, Sexton JC, Corrigan OI. **2003**. Simulating the hydrodynamic conditions in the united states pharmacopeia paddle dissolution apparatus. AAPS Pharm Sci Tech 4:E22.
36. Baxter JL, Kukura J, Muzzio FJ. **2005**. Shear-induced variability in the united states pharmacopeia apparatus 2: Modifications to the existing system. AAPS J 7:E857-864.
37. Devotta I, Ambeskar VD, Mandhare AB, Mashelkar RA. **1994**. The life time of a dissolving polymeric particle. Chem Eng Sci 49:645-654.
38. Brian PLT, Hales HB, Sherwood TK. **1969**. Transport of heat and mass between liquids and spherical particles in an agitated tank. AICHE J 15:727-732.
39. Sherwood TK, Pigford RL, Wilke CR. **1975**. Mass transfer. ed., New York: McGraw-Hill. p ix, 677.
40. Diebold SM. **2000**. Hydrodynamik und lösungsgeschwindigkeit: Untersuchungen zum einfluss der hydrodynamik auf die lösungsgeschwindigkeit schwer wasserlöslicher arzneistoffe. Institute for Pharmaceutical Technology, ed., Frankfurt: Johann Wolfgang Goethe University.

41. Bird RB, Stewart WE, Lightfoot EN. **2002**. Transport phenomena. 2nd ed., New York: J. Wiley. p xii, 895.
42. Bisrat M, Nystrom C. **1988**. Physicochemical aspects of drug release.8. The relation between particle-size and surface specific dissolution rate in agitated suspensions. Int J Pharm 47:223-231.
43. Takagi T, Chandrasekharan, R., Bermejo, M., Yamashita, S., Amidon, G.L. **In preparation**. Provisional biopharmaceutical classification of the top united states, european and japanese drugs.
44. Lipinski CA, Lombardo F, Dominy BW, Feeney PJ. **1997**. Experimental and computational approaches to estimate solubility and permeability in drug discovery and development settings. Adv Drug Deliver Rev 23:3-25.
45. Lipinski CA. **2000**. Drug-like properties and the causes of poor solubility and poor permeability. J Pharmacol Toxicol Methods 44:235-249.
46. Jinno J, Kamada N, Miyake M, Yamada K, Mukai T, Odomi M, Toguchi H, Liversidge GG, Higaki K, Kimura T. **2006**. Effect of particle size reduction on dissolution and oral absorption of a poorly water-soluble drug, cilostazol, in beagle dogs. J Control Release 111:56-64.
47. Scholz A, Kostewicz E, Abrahamsson B, Dressman JB. **2003**. Can the usp paddle method be used to represent in-vivo hydrodynamics? J Pharm Pharmacol 55:443-451.
48. Scholz A, Abrahamsson B, Diebold SM, Kostewicz E, Polentarutti BI, Ungell AL, Dressman JB. **2002**. Influence of hydrodynamics and particle size on the absorption of felodipine in labradors. Pharm Res 19:42-46.
49. Meyer JH, Dressman J, Amidon G. **1985**. Hydrodynamic aspects of gastrointestinal (gi) transit. Nippon Heikatsukin Gakkai Zasshi 21 Suppl:99-100.
50. Meyer JH, Doty JE. **1988**. Gi transit and absorption of solid food: Multiple effects of guar. Am J Clin Nutr 48:267-273.
51. Oberle RL, Chen TS, Lloyd C, Barnett JL, Owyang C, Meyer J, Amidon GL. **1990**. The influence of the interdigestive migrating myoelectric complex on the gastric emptying of liquids. Gastroenterology 99:1275-1282.
52. Sirois PJ, Amidon GL, Meyer JH, Doty J, Dressman JB. **1990**. Gastric emptying of nondigestible solids in dogs: A hydrodynamic correlation. Am J Physiol 258:G65-72.

CHAPTER III

SOLUBILIZATION AND DISSOLUTION OF INSOLUBLE WEAK ACID, KETOPROFEN: EFFECTS OF PH COMBINED WITH SURFACTANT

Abstract

This study investigated the combined effect of pH and surfactant on the solubility and dissolution of ketoprofen (KP), a highly permeable and an ionizable and water-poorly soluble drug in gastrointestinal tract. The equilibrium solubility of KP was determined in buffers at the pH range from 4.0 to 6.8 and sodium lauryl sulfate (SLS) concentrations from 0% to 2.0%. Its intrinsic dissolution rate was measured in the same media using a rotating disk apparatus. A simple additive model accounting for the free unionized KP and ionized KP^- forms, and their corresponding micellar forms was employed to study the *in-vitro* solubility and dissolution behavior. Nonlinear regression analysis showed that the proposed model agreed well with the experimental data, with $Rsq = 0.96$ ($P < 0.0001$) for the solubility study, and $Rsq = 0.98$ ($P < 0.0001$) for the intrinsic dissolution rate measurement. The pK_a and c_{KP} values are estimated as 4.76 ± 0.00 and 0.253 ± 0.05 mg/mL, respectively, in good agreement with literature reports. The micellar solubilization coefficient $k*$ for the unionized $[KP]_{micelle}$ is 757 ± 165 L/mol, whereas the value $k**$ for the ionized $[KP^-]_{micelle}$ is 9.88 ± 6.70 L/mol. The diffusion

coefficients of various species: KP, KP^-, $[KP]_{micelle}$, and $[KP^-]_{micelle}$, are 7.68 × 10^{-6}, 1.54 × 10^{-6}, 2.32 × 10^{-7}, and 2.13 × 10^{-20} cm^2/s, respectively. The maximum enhancement of solubilization is approximately 232-fold, while the maximum dissolution amplification is only 54-fold because of the smaller diffusivity of micellar species. The dramatic enhancement of *in-vitro* solubility/dissolution attributable to an increase of pH and presence of SLS mimics the *in-vivo* solubilization/dissolution behavior of *KP* along the gastrointestinal tract, when the pH increases from 1-2 in the stomach to 5-6 in the duodenum. The results suggest that the KP dissolves very rapidly in small intestine, implying that its absorption will be predominantly controlled by gastric emptying, and only minimally limited by the subsequent dissolution processes. This behavior is very similar to BCS I drugs, thus KP may be considered for possible waivers of bioequivalence.

Introduction

The Biopharmaceutics Classification System (BCS) categorizes drugs into four classes according to their solubility and permeability [1]. BCS I compounds can be waived of the *in-vivo* bioequivalence study because of its high solubility and high permeability. Whereas, the BCS II class of compounds exhibit high permeability and low solubility relative to the administered dose. Solubility, one of the key parameters in BCS, as well as dissolution rate are the most essential factors controlling the rate and extent of drug absorption. The *in-vivo* drug solubilization and dissolution processes are complicated by a number of physiological processes and factors in the gastroenterological tract, such as gastrointestinal motility [2,3], pH, bile salts, buffer capacity, ionic strength, food intake and

viscosity [4]. Among them, pH and surfactant reflect the gastrointestinal pH change and the presence of bile salts. They are also the major physiochemical determinants of drug dissolution. Both surfactant and pH effects are important when considering ionizable drugs, particularly those with the pKa values in the gastrointestinal pH range.

The individual effect of pH and surfactants on the solubility and dissolution of drugs has been studied previously. As early as 1960's, Olander proposed both the film theory and the surface-renewal theory of simple mass transfer in conjunction with various equilibrium reactions [5]. Monney et al applied the film model to studying the pH effect on drug dissolution [6,7]. Other researchers studied the effect of surfactant on solubilization and dissolution of drugs. For example, Rippie et al investigated the solubilization effect of polysorbate 80 on weakly acidic and basic drugs [8]; and Elworthy et al analyzed the effect of four different nonionic surfactants on the dissolution of poorly soluble drug, griseofulvin [9]. During the late 1970's and early 1980's, research on the effects of pH [10,11] and surfactant [12,13] on drug solubilization and dissolution focused on disintegration and dissolution of traditional tablets. Later, the dissolution theory was further advanced with the establishment of the convective diffusion model. This model was first developed by McNamara and Amidon [14] and followed by others [15,16] to describe the effects of ionization at the solid-liquid surface and irreversible reaction of the dissolved species in the hydrodynamic boundary layer. In the last decade, drug solubilization/dissolution research has evolved to the stage of investigating the pH or surfactant effects on controlled-release dosage forms [17] in polymeric matrix, studying their combination effects with food uptake [18], and working with poorly water-soluble drugs [19,20].

However, the combined effects of pH and surfactants on the solubilization and dissolution of weak acid drugs has received little attention, especially in view of

reflecting an *in-vivo* change of pH and surfactant along the gastrointestinal tract using an *in-vitro* model. The purpose of this paper is to investigate the effects of pH combined with surfactant on the solubility and dissolution of BCS II water-poorly soluble weak acids in an *in-vitro* environment. In this paper ketoprofen is selected as a model compound for its desirable biopharmaceutical properties, including an approximate pKa of 4.6 which is in physiological range and high permeability of 8.7×10^{-6} cm/s in human jejunum.

Methods

Theoretical Basis

Solubilization by pH combined with Surfactant – an Equilibrium Model

The equilibrium model, as shown in Scheme 1, was established by Jinno et al [21]. It is employed here to describe the effects of pH and surfactant on the equilibria of KP in aqueous solutions. In the scheme, the pH effect is associated with an ionization equilibrium and the surfactant effect includes two solubilization equilibria.

The pH effect is described as an ionization process, shown as the following:

$$K_a = (c_{KP^-})[H^+]/c_{KP} \quad (1)$$

where $[H^+]$ is hydrogen ion concentration, K_a is the dissociation constant of ketoprofen, and c_{KP} and c_{KP^-} are the concentrations of unionized and ionized ketoprofen, respectively. The surfactant effect exerts its micellar impact not only on the unionized drug molecules but also on the ionized drug molecules. These effects are expressed in the following equations:

$$k^* = (c_{[KP]})(c_m)/c_{[KP]micelle} \quad (2)$$

$$k^{**} = (c_{[KP^-]})(c_m) / c_{[KP^-]micelle} \quad (3)$$

$$c_m = c_{\text{surfactant}} - cmc \quad (4)$$

where k* and k** are the equilibrium constants for micellar solubilization of unionized drug and ionized drug, whereas $c_{[KP]micelle}$ and $c_{[KP^-]micelle}$ are the concentrations of unionized and ionized drugs in the micelle, and c_m is the concentration of micellar surfactant. The value of c_m is determined using eq 4, and the critical micelle concentration (CMC) of sodium lauryl sulfate is taken from literature [22,23] as 0.008 M that is equivalent to 0.25% (w/v).

Total Solubility

The total solubility of a weak acid or a weak base in surfactant-containing buffers was discussed previously in literature [8,24]. For ketoprofen, its total solubility c_{total} can be expressed as a sum of the solubility values of individual KP relevant species:

$$c_{total} = c_{KP} + c_{KP^-} + c_{[KP]micelle} + c_{[KP^-]micelle} \quad (5)$$

Substituting c_{KP^-}, $c_{[KP]_{micelle}}$, $c_{[KP^-]_{micelle}}$ in eq 5 with eqs 1, 2 and 3 gives eq 6:

$$c_{total} = [1 + \frac{K_a}{[H^+]} + (k^* + k^{**}\frac{K_a}{[H^+]})c_m]c_{KP} \quad (6)$$

It is noticed that the value of c_{KP}, namely the intrinsic solubility of ketoprofen, is constant for all tested experiments due to the existence of excess amount of KP_{solid} in the system. Therefore, a dimensionless solubility number, c_{SP} (equal to c_{total} / c_{KP}), is introduced to illustrate the extent of solubilization power.

Furthermore, eq 6 can be transformed into eqs 7 and 8 that clearly reveal how c_{total} changes according to the pH and surfactant, respectively. Eq 7 consists of two components, each of which comprises both the free solute form and the micelle-solubilized form, and respectively represents the solubility of unionized drug in the $(1+k*c_m)$ term and that of ionized drug in $(1+k**c_m)\frac{K_a}{[H^+]}$. The solubility of the ionized drug rather than the unionized drug is the component influenced by the pH effect. For a given surfactant concentration c_m, eq 7 suggests that the total solubility of KP increases reciprocally with $[H^+]$ concentration and thus exhibits a positive log-linear relationship with pH. In addition, eq 7 also suggests that higher values of c_m would lead to greater sensitivity of the total solubility relative to pH changes. This is primarily due to the contribution of the micelle solubilized ionized-drug, which is expressed in expression of $\Delta c_{total} = c_{KP}(1+k**c_m)K_a[\Delta(\frac{1}{[H^+]})]$. For a given $[H^+]$ concentration or pH, eq 8 shows that c_{SP} would increase linearly with the micellar concentration c_m. Certainly, this linear relationship is well described using a constant intercept of $(1+\frac{K_a}{[H^+]})$ and a fixed slope of $(k*+k**\frac{K_a}{[H^+]})$. The value of the intercept is determined by the pH of the solution. In comparison, the slope is determined not only by the pH but also by the drug-micelle association constants. For a weak acid drug, a higher value of pH would lead to a decreased $[H^+]$, and consequently increase the solubilization power c_{SP}.

$$c_{SP} = \frac{c_{total}}{c_{KP}} = (1+k*c_m) + \frac{K_a}{[H^+]}(1+k**c_m) \qquad (7)$$

$$c_{SP} = \frac{c_{total}}{c_{KP}} = (1 + \frac{K_a}{[H^+]}) + (k* + k** \frac{K_a}{[H^+]})c_m \quad (8)$$

Total Dissolution

The general equation describing one-dimensional mass transport in a fluid [25] is composed of the diffusive, convective, and reactive contributions and is shown as follows:

$$c_i / \ t = D_i d^2 c_i / dz^2 - \upsilon_Z dc_i / dz + R_i \quad (9)$$

where D_i, c_i and R_i are the diffusion coefficient, the molar concentration, and the rate of reaction per volume of species i, v is the fluid velocity, and t is the time. Assuming an instantaneously irreversible reaction at the solid-liquid surface, mass transfer in the rotating disk system at steady state can be simplified to

$$c_i / \ t = D_i d^2 c_i / dz^2 - \upsilon_Z dc_i / dz = 0 \quad (10)$$

where v_Z is the axial velocity of fluid toward the disk. Levich solved the equation to derive the flux of the solute from the rotating disk as

$$J = 0.62 D_i^{2/3} v^{-1/6} \omega^{1/2} c_{i0} \quad (11)$$

where J is the flux, v is the kinematic viscosity, D_i is the diffusivity of species i, C_{i0} is the concentration of species i at the disk surface, and ω is the angular velocity of the disk. Eq 11 is applicable for the micelle-facilitating dissolution of KP from a rotating disk and gives:

$$J_{total} = 0.62 v^{-1/6} \omega^{1/2} \Sigma (D_i^{2/3} c_{i0}) \quad (12)$$

where J_{total} is the total flux of the drug, which is a sum flux of four KP related species and expressed as

$$J_{total} = J_{KP} + J_{KP^-} + J_{[KP]micelle} + J_{[KP^-]micelle} \quad (13)$$

The dissolution rates of individual species are as follows:

$$J_{KP} = 0.62\nu^{-1/6}\omega^{1/2}D_{KP}{}^{2/3}c_{KP0} \quad (14)$$

$$J_{KP^-} = 0.62\nu^{-1/6}\omega^{1/2}D_{KP^-}{}^{2/3}c_{KP^-0} \quad (15)$$

$$J_{[KP]micelle} = 0.62\nu^{-1/6}\omega^{1/2}D_{[KP]micelle}{}^{2/3}c_{[KP0]micelle} \quad (16)$$

$$J_{[KP^-]micelle} = 0.62\nu^{-1/6}\omega^{1/2}D_{[KP^-]micelle}{}^{2/3}c_{[KP^-0]micelle} \quad (17)$$

Substituting J_{KP}, J_{KP^-}, $J_{[KP]micelle}$, and $J_{[KP^-]micelle}$ in eq 13 using eqs 14-17 gives the total flux:

$$\begin{aligned} J_{total} &= 0.62\nu^{-1/6}\omega^{1/2}(D_{KP}{}^{2/3}c_{KP0} + D_{KP^-}{}^{2/3}c_{KP^-0} + D_{[KP]micelle}{}^{2/3}c_{[KP0]micelle} + D_{[KP^-]micelle}{}^{2/3}c_{[KP^-0]micelle}) \\ &= 0.62\nu^{-1/6}\omega^{1/2}c_{KP0}(D_{KP}{}^{2/3} + D_{KP^-}{}^{2/3}\frac{K_a}{[H^+]} + D_{[KP]micelle}{}^{2/3}k*c_m + D_{[KP^-]micelle}{}^{2/3}k**c_m\frac{K_a}{[H^+]}) \end{aligned} \quad (18)$$

Assuming that the diffusion coefficients of all species are constant under the tested experimental conditions, the pH and surfactant effects on the total dissolution rate can be simplified and discussed as following. First, the flux contributed from the unionized free drug is constant for all tested experiments due to the invariable values of $D_{KP}{}^{2/3}$ and c_{KP0}. Secondly in terms of the effect of pH on the total dissolution rate, eq 18 indicates that it exhibits only through ionized drug molecules, either in the free solute form or micelle-solubilized form. The corresponding mathematical expressions are $0.62\nu^{-1/6}\omega^{1/2}c_{KP0}(D_{KP^-}{}^{2/3}\frac{K_a}{[H^+]})$ and $0.62\nu^{-1/6}\omega^{1/2}c_{KP0}(D_{[KP^-]micelle}{}^{2/3}k**c_m\frac{K_a}{[H^+]})$ for the free solute and the micellar form, respectively. Thirdly in terms of the surfactant effect on the total dissolution rate, eq 18 demonstrates that it exists in both the unionized

and ionized form, whereas the unionized form may contribute more significantly. This premise is resulted mainly from some previous observations [21,26,27] that the micelle association constant for the unionized form is much larger than that of the ionized form.

Materials and Data Analysis

Ketoprofen (KP) and sodium lauryl sulfate (SLS, > 99% purity) were purchased from Sigma Chemical Company (St. Louis, MO). HPLC grade acetonitrile was purchased from Fisher Scientific Company (Fair Lawn, NJ). All other chemicals were of analytical grade from Sigma Chemical Company (St. Louis, MO). Distilled, deionized and filtered water was prepared in house and used for all experiments. Model fitting and parameter estimations were performed with nonlinear regression analysis by Sigmaplot 8.0 (SPSS Inc., Chicago, IL). The regression analysis for the dissolution data was weighted by reciprocal values of square of the standard deviation.

Media Preparation

A series of McIlvaine buffers were prepared at pH 4.0, 4.6, 6.0 and 6.8 by mixing appropriate volumes of 0.1M citric acid and 0.2 M disodium phosphate solutions. SLS was dissolved with the buffers at the concentrations of 0.5, 1.0, and 2.0% w/v. All media were deaerated by stirring under vacuum prior to use.

Solubility Determination

An excess amount of ketoprofen powder (5-1000 mg) was shaken in screw-capped vials containing 5 mL of tested buffers at 37ºC in an orbital shaker water bath (LABLINE Instruments, Inc., Melrose Park, IL). The final pH of the testing solutions were checked and adjusted to the original values by adding 0.5 M disodium phosphate solution. At suitable time intervals, 1.0 mL of samples were collected and filtered through 0.45 mm membrane, and then diluted with appropriate amount of buffers prior to the HPLC

analysis. The equilibrium solubility of ketoprofen in various buffers was established as the difference between three consecutive measurements is within 1%. The HPLC was equipped with a pump (Model 510, Waters Associates, Milford, MA) operated at 1 mL/min, a sample processor (WISP Model 712, Waters Associates, Milford, MA), a variable wavelength UV detector (Spectroflow 783 Absorbance detector, Kratos analytical Instruments, Ramsy, NJ) set at 254 nm and connected to an integrator (HP 3396 Series II, HP Company, Avondale, PA). The mobile phase consisted of water (pH 3.2): acetonitrile (35/65 v/v). The analytical column used was a LiChroCART® column (250 x 4 mm I.D.) packed with LiChroCART® 100 RP-18, 5µm particle size (EM Science, Gibbstown,NJ) preceded by a LiChroCART® guard column (4 x 4 mm) of the same packing material. The retention time of ketoprofen under these conditions was about 5 minutes.

Intrinsic Dissolution Measurements

The intrinsic dissolution rates of ketoprofen in various buffers were measured using rotating disk method. Ketorpofen powder (150 mg) was compressed to form a circular compact, with a radius of 0.55 cm, in the rotating disk die at 1,000 lbs for 1 minute using a hydraulic laboratory press (Fred Carver, Inc., Summit, NJ). The die containing the compact was mounted onto a Plexiglass shaft attached to an overhead synchronous motor (Cole-Parmer Scientific, Niles, IL). The die was rotated at 50, 100, and 200 rpm, which was calibrated with a digital tachometer (Cole-Parmer Scientific, Niles, IL). The single face of the compact was exposed to 150 mL of the dissolution media in a jacketed beaker maintained at 37°C ± 1°C through the circulating water heated with a water bath circulator (Isotemp Constant Temperature Circulator Model 8000, Fisher Scientific, Pittsburgh, PA). The dissolution medium was continuously circulated through ultraviolet

(UV) spectrophotometer flow cells at 8 mL/min using a peristaltic pump (Masterflex, Cole-Parmer Instrument Co., Chicago, IL). UV absorption at 258 nm was recorded at 0.25-1 min intervals using a UV spectrophotometer (Perkin-Elmer Lambda 3B UV/VIS Spectrophotometer, Oak Brook, IL). Dissolved amounts of ketoprofen was maintained at less than 10% of the solubility over the entire experiment ensuring sink condition.

Results and Discussion

Total Solubility

The equilibrium solubility of ketoprofen in various buffers containing 0-2% (w/v) SLS is shown in Table 3.1. Eq 6 was selected to fit the measured solubility values by nonlinear regression analysis. Figure 3.2 illustrates the 3D mesh plot with the observed values as functions of pH and SLS concentrations ($Rsq = 0.96, P < 0.0001$). The c_{KP} , pK_a , $k*$, and $k**$ values were estimated as 0.253 ± 0.05 mg/mL, 4.76 ± 0.00, 757 ± 165 L/mol, and 9.88 ± 6.70 L/mol, respectively. The estimated c_{KP} and pK_a values agree well with the reported data [28,29]. The smaller $k**$ value relative to $k*$ is suggestive that the micellar solubilization of ionized drug is fairly insignificant presumably as a result of the anionic nature of SLS.

Using the estimated c_{KP} number (i.e., 0.253 mg/mL), the corresponding solubilization power values were calculated based on eqs 7 and 8 are listed in Table 3.2. The results indicate that the total solubility c_{tatal} increases positively with pH for any given SLS concentration, as expected. In the absence of SLS, the maximal solubilization power is obtained at pH 6.8 with a value of 142. In the presence of SLS, the combined solubilization power of pH and surfactant is enhanced even further than just single pH

effect. At pH 6.8 with 2.0% SLS, in particular, an exceptionally high solubilization power value of approximately 205 is observed. This observation is consistent with eq 7. As previously discussed, eq 7 expects an increased solubilization of both the unionized drug and the ionized drug at a higher c_m, expressed as $(1 + k * c_m)$ and $\frac{K_a}{[H^+]}(1 + k ** c_m)$, respectively. In addition, the fractional solubility from the unionized drug and the corresponding micelles, or that from the ionized drug and its micelles, is pH dependant. This is resulted from the interplay of pH and SLS on the ionizable drugs. For instance, at pH << pK_a, the solubility contribution from the ionized drug and its micelles is small relative to that of the unionized drug mainly because the value of $k **$ is much smaller compared with the $k *$. On the other hand, at pH >> pK_a, the solubility contribution from the ionized drug and the micelles becomes more significant. Furthermore, it appears that KP solubility is more sensitive to pH change than to the SLS changes. This is can be simply derived from Table 3.2 that pH could be enhance solubility in the range of 4-160 fold, while SLS could only increase 2-50 fold within the conducted experimental conditions.

The solubility results also indicated that the total solubility increased proportionally with SLS concentration for any given pH value, as showed in Table 3.2 that all the corresponding linear regression analysis had Rsq > 0.98. This observation is indeed theoretically expected from eq 8 that demonstrates an intercept of $(1 + \frac{K_a}{[H^+]})$ and a slope of $(k * + k ** \frac{K_a}{[H^+]})$. Furthermore, eq 8 also suggests that at higher pH the total solubility c_{total} is more responsive to a c_m change because the contribution from micellar

ionized drug $(k^{**}\frac{K_a}{[H^+]})$ becomes greater. This contribution, however, is quite limited on account of the very small value of k^{**}.

Intrinsic Dissolution Rate

A typical intrinsic dissolution rate as a function of the square root of the rotational speed is illustrated in Figure 3.3. The intrinsic dissolution rates were normalized to $J/\omega^{1/2}$ with the unit of $\times 10^4\ mg/cm^2/s^{1/2}/rad^{1/2}$ by multiplying the volume of media (150 mL) divided by the surface area of the compact (0.95 cm^2) using linear regression assuming zero intercept. Similarly, the dissolution flux increases with pH and addition of SLS. The dissolution flux is found to be linear with SLS concentration at all pH values (Rsq: 0.93-0.99). The intrinsic dissolution rates of ketoprofen in various buffers containing 0-2% (w/v) SLS are presented in Table 3.3. Using the estimated values of c_{KP}, pK_a, k^*, and k^{**} obtained from the solubility study, the measured intrinsic dissolution rate data were fitted to eq 18 by nonlinear regression analysis. Figure 3.4 illustrates the dissolution rate result ($J/\omega^{1/2}$) of the fitted surface plot with the experimental data as functions of pH and SLS concentrations ($Rsq = 0.98, P < 0.0001$). The estimated diffusivity values for species KP, KP^-, $[KP]_{micelle}$, and $[KP^-]_{micelle}$ are 7.68 × 10^{-6}, 1.54 × 10^{-6}, 2.32 × 10^{-7}, and 2.13 × 10^{-20} cm^2/s, respectively. It is apparent that the diffusivity value of $[KP^-]_{micelle}$ is trivial. Thus, the flux contribution from the micellar form is negligible. Then, eq 18 can be simplified as the following:

$$J_{total} = 0.62\nu^{-1/6}\omega^{1/2}c_{KP0}(D_{KP}{}^{2/3} + D_{KP^-}{}^{2/3}\frac{K_a}{[H^+]} + D_{[KP]_{micelle}}{}^{2/3}k^*c_m) \quad (19)$$

In eq 19, it becomes evident that the flux is composed of three fractions. One fraction is the constant flux from the unionized drug KP. The second fraction is the pH-influenced flux from the ionized drug KP^-. And the third fraction is the surfactant-controlled flux from the unionized micelles $[KP]_{micelle}$. As a result, the most significant dissolution enhancement should be achieved at maximum pH and SLS concentration. In fact, the maximal dissolution enhancement is about 50-fold at pH 6.8 with 2.0% SLS.

Interestingly, the effect of pH and surfactant on the intrinsic dissolution rate are independent and additive, which are reflected respectively in the expressions of $0.62v^{-1/6}\omega^{1/2}c_{KP0}D_{KP^-}{}^{2/3}\frac{K_a}{[H^+]}$ and $0.62v^{-1/6}\omega^{1/2}c_{KP0}D_{[KP]micelle}{}^{2/3}k*c_m$. For example, if the pH value is low, especially when pH << pKa, the $D_{KP^-}{}^{2/3}\frac{K_a}{[H^+]}$ contribution would be small. Accordingly, the surfactant effect would appear to be more significant. On the other hand, if pH increases until it is much larger than pKa, the fractional input from $D_{KP^-}{}^{2/3}\frac{K_a}{[H^+]}$ becomes more substantial compared with $D_{[KP]micelle}{}^{2/3}k*c_m$. Hence, the effect of pH would be more dominant in the KP dissolution. This phenomenon was observed in the study as shown in Table 3.3. In particular, at pH 4.0, the enhancement of flux with 2.0% SLS is about 42.5-fold, whereas at pH 6.8, the corresponding flux enhancement is only about 1.2-fold.

The overall dissolution amplification is moderate in contrast to the solubility enhancement owing to the much smaller diffusivity of micellar species. In fact, the diffusivity of the micellar $[KP^-]_{micelle}$ is in essence zero. Additionally, the $D_{[KP]_{micelle}}$ value is about 33 times lower than the D_{KP} value presumably by reason of a much higher

molecular weight of the micelle form. This ratio is much higher than the ratio of 9.0 observed with the carbamazepine-SLS system [30] and the 1.7 observed with the piroxicam-SLS system [21]. The rather low diffusivity of $[KP^-]_{micelle}$ in turn may be on account of an inherent higher micellar solubilization equilibrium coefficient (k*) relative to the reported values of approximate 300 L/mol for carbamazepine [30] and 348 mol/L for piroxicam [21]. The absolute diffusivity values of free KP and the KP^- forms, however, are within the same numerical range as those of carbamazepine [30], piroxicam [21] and benzoic acid [31].

Regulatory significance: potential waiver of *in vivo* bioequivalence

Recently, a Guidance for Industry was published in the Federal Register that proposed a waiver of *in vivo* bioavailability and bioequivalence studies for immediate release solid oral dosage forms containing Class I active moieties/active ingredients of the biopharmaceutics classification system [32]. This guidance pertains to highly water-soluble and highly permeable drugs that satisfy the following major conditions:

a. the highest dose strength is soluble in 250 mL of water or less over the pH range 1-7.5;
b. the extent of absorption in humans is determined to be 90% or more of an administered dose based on mass balance or compared to an intravenous reference dose;
c. 85% or more of the labeled amount of drug substance dissolves within 30 minutes using USP apparatus I at 100 rpm or apparatus II at 50 rpm in a volume of 900 mL or less of the following media;

1) acidic media such as 0.1 N HCl or simulated gastric fluid USP without enzymes; 2) a pH 4.5 buffer; and 3) a pH 6.8 buffer or simulated intestinal fluid USP without enzymes.

Class II drugs in the biopharmaceutics classification system possess low water solubility but are highly permeable. Thus, these drugs would not satisfy all the Class I waiver requirements, in particular with the solubility and dissolution requirements. However, Class II weakly acidic drugs with pKa in GI physiological range such as ketoprofen that may be completely ionized and thus highly soluble and rapidly dissolving in an intestinal milieu with an average pH of ~6.5, may be considered for the possible waivers of *in vivo* bioequivalence**.**

"Highly soluble" requirement

Ketoprofen, like many other drugs, is mainly absorbed in the small intestinal region where an average pH of ~6.5 and containing total concentrations of bile salts and lecithin around 7 mM in the fasted state, or a pH of around 5-6 and a total bile salts and lecithin concentration of about 19 mM in the fed state [33-35]. As a carboxylic acid drug, it has been shown previously that increase of pH would enhance its solubility and consequently the dissolution rate, particularly at pH > pKa of the acid. In addition, the bile salts are present in the small intestine. Previous studies have demonstrated that bile salts improve the *in-vivo* solubilization of many drugs. Thus, their dissolution and absorption are enhanced accordingly. This seems to be working with ketoprofen, as shown by the present study that SLS could serve as a bile salt improving its solubility and intrinsic dissolution. As ketoprofen is taken orally, it would have minimal solubility/dissolution in the acidic stomach in consequence of the local low pH (1-2) environment. Immediately after the drug is emptied into the upper small intestine, the

solubility/dissolution of ketoprofen would increase very quickly. This is mainly due to two factors: the dramatic increase of pH and the presence of bile salts in small intestine. From the model in the present paper, KP would have the solubility of at least 0.7 mg/mL at pH 5-6, even in the absence of any bile salts or surfactants. Consider an example of KP product with the maximum dose of 75 mg (Orudis®, Wyeth-Ayerst Pharmaceuticals, PA), the required dissolving volume for complete solubilization of KP would be less than 110 mL. This volume is much smaller than the 250 mL dissolving volume, which is currently used by FDA [32] for defining "highly soluble" drugs to classify a BCS I compound. Therefore, results in this paper suggest that KP can be defined as "highly soluble" drug at pH > 5-6. Nonetheless, this "highly soluble" definition does not hold true over the entire pH 1.2-7.4 range, in particular for the low pH end. With the consideration of high permeability of KP, it leads to support the hypothesis that the absorption behavior of KP could exhibit very similarly to that of BCS I compound in the local absorption region in the intestine.

"Rapidly dissolving" requirement

In addition to the drug, it is of importance to consider the drug products that are formulated and manufactured in rapidly dissolving solid immediate release dosage forms. For any KP immediate release products that dissolve very rapidly, the absorption kinetics from GI tract would be governed by the gastric emptying, rather than by the dissolution rate. Therefore, the absorption rate will be essentially controlled by the gastric emptying rate and no correlation with the solubility or dissolution rate is expected. Thus, appropriate *in vitro* dissolution testing procedures may be established specifically for BCS II acidic drugs in the future for the assurance of a waiver of *in vivo* bioequivalence.

Conclusions

In conclusion, we suggest KP, which possesses highly permeability, and is a weakly acidic drug with pKa in GI physiological range and thus exhibits pH enhanced solubility and dissolution rate in the absorption region, as a candidate for waivers of *in vivo* bioequivalence. The significance of the present study may be applicable to other weakly acidic drugs with high permeability. For these drugs, their solubility measurement may be conducted around pH 5-6 with appropriate SLS and their dissolution testing under aforementioned conditions for KP, which represents more biopharmaceutically and physiologically relevant pH. Interestingly, it has been advocated by other researchers that the current FDA definition of "high solubility" may be too restrict for 15 acidic drugs [36], including ibuprofen, piroxicam, naproxen and indomethacin. These drugs are all weak acids exhibiting pK_a values ranging from 4.2-5.3 and log P (octanol-water) values between 1 (ketoprofen) to 3.8 (indomethacin) [29]. An example of a weak acid NSAID that does not conform to this general trend is mefenamic acid. It has been reported that the enhancement of mefenamic acid upon ionization, though substantial is not sufficient to satisfy dose volume requirement [37]. Hence, the absorption and bioavailability of mefenamic acid would be dissolution rate-limited. A more general conclusion, therefore, for Class II weakly acidic drugs should stipulate that a) the drug should be highly permeable (> 90% absorption in humans; $P_{eff} \sim 2.5\times10^{3}$ cm/s; absorption half-time ~ 1h); b) that it be substantially ionized at a pH of 6.5 and/or c) that it satisfy high solubility requirements at pH 6.5. Under these circumstances, such Class II drugs would be essentially similar to Class I drugs and could be considered for waivers of *in vivo* bioequivalence testing.

In summary, the solubility and intrinsic dissolution rate behavior of ketoprofen is well characterized by the additive model described in this paper. Even though the *in-vivo* case is complicated with gastric emptying and other physiological factors, the solubility/dissolution enhancement due to an increase of pH and the presence of SLS could reflect the *in-vivo* solubility/dissolution behavior along the gastrointestinal tract. The study supports the possibility for ketoprofen and other BCSII weak acids that dissolve rapidly and completely in small intestine, to be waived of *in vivo* bioequivalence.

Table 3.1. Equilibrium solubility (mg/mL ± S.D.) of ketoprofen at various pH and SLS concentrations.

	SLS concentration (%, w/v)			
pH	0.0 %	0.5 %	1.0 %	2.0 %
4.0	0.28 ± 0.01	2.23 ± 0.03	4.70 ± 0.04	13.09 ± 0.04
4.6	0.49 ± 0.00	2.62 ± 0.02	5.61 ± 0.11	14.90 ± 0.50
6.0	3.68 ± 0.13	6.11 ± 0.12	9.26 ± 0.13	19.73 ± 0.46
6.8	40.76 ± 0.01	44.25 ± 0.00	49.63 ± 0.01	58.80 ± 0.01

Table 3.2. Solubilization power (C_{SN}) of various pH and SLS concentrations on Ketoprofen.

	SLS concentration (%, w/v)					
pH	0.0 %	0.5 %	1.0 %	2.0 %	Slope[1]	Rsq[1]
4.0	1.24	8.82	18.58	51.76	822.84	0.990
4.6	2.17	10.36	22.18	58.92	927.04	0.992
6.0	16.33	24.16	36.62	78.02	1013.45	0.987
6.8	161.17	174.97	196.24	232.50	1151.86	0.996

[1]: indicate the linear regression of C_{total} vs SLS for a given pH.

Table 3.3. The intrinsic dissolution rate ($J/\omega^{1/2}$, $\times 10^4$ $mg/cm^2/s^{1/2}/rad^{1/2} \pm S.D.$) of ketoprofen at various pH and SLS concentrations.

	SLS concentration (%, w/v)			
pH	0.0 %	0.5 %	1.0 %	2.0 %
4.0	1.68 ± 0.03	4.15 ± 0.03	6.05 ± 0.09	9.20 ± 0.16
4.6	3.05 ± 0.04	6.18 ± 0.05	8.30 ± 0.16	11.35 ± 0.11
6.0	14.61 ± 0.15	17.38 ± 0.09	20.32 ± 0.13	21.90 ± 0.32
6.8	71.38 ± 4.41	75.36 ± 1.30	79.93 ± 6.49	84.69 ± 2.89

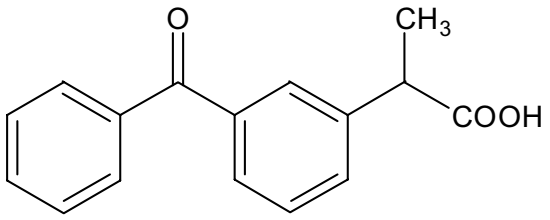

Figure 3.1. Chemical Structure of Ketoprofen.

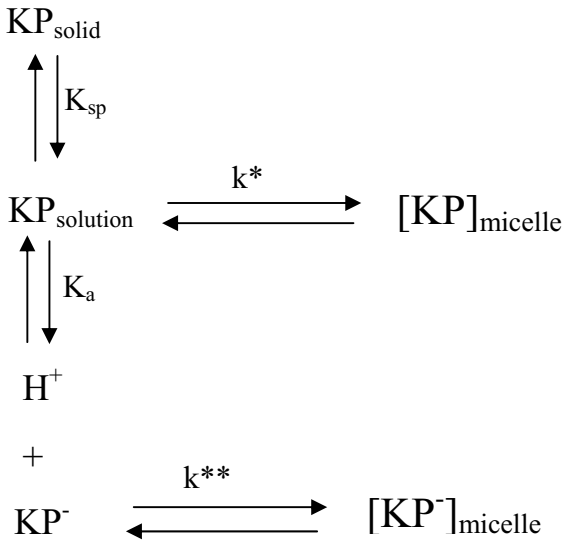

Scheme 3.1. Equilibrium model of ketoprofen in surfactant containing buffers. KP_{solid}: solid-state drug molecules; KP: dissolved and unionized free drug; KP^-: free ionized drug; $[KP]_{micelle}$: unionized drug micelles; and $[KP^-]_{micelle}$: ionized drug micelles.

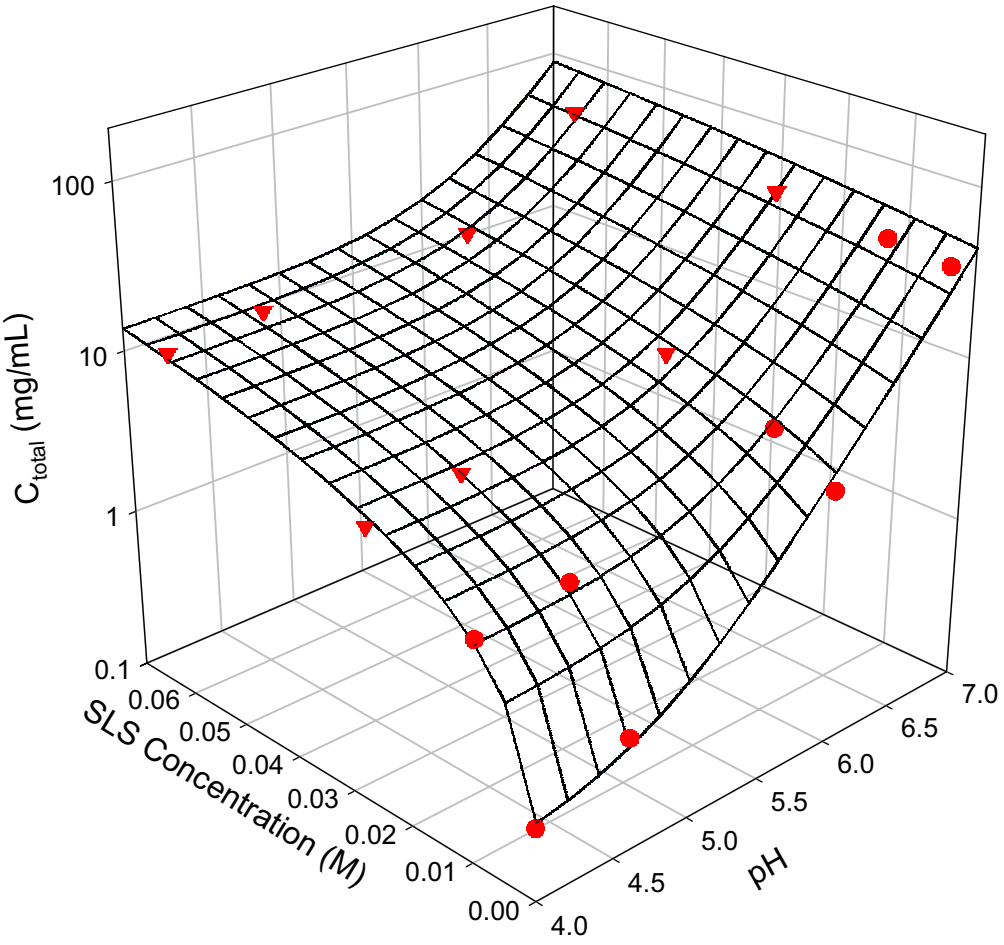

Figure 3.2. Total solubility as function of pH and SLS.

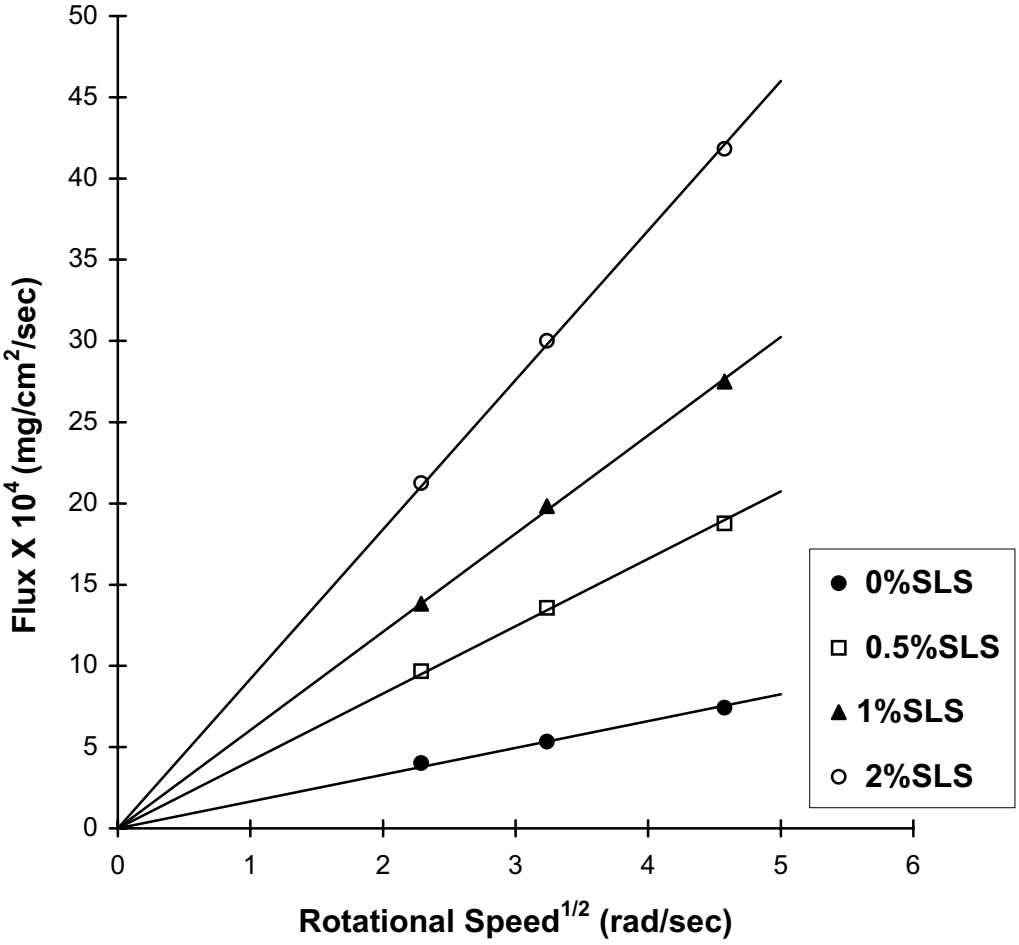

Figure 3.3. Intrinsic dissolution curves of ketoprofen at various SLS concentrations pH 4.0 buffers.

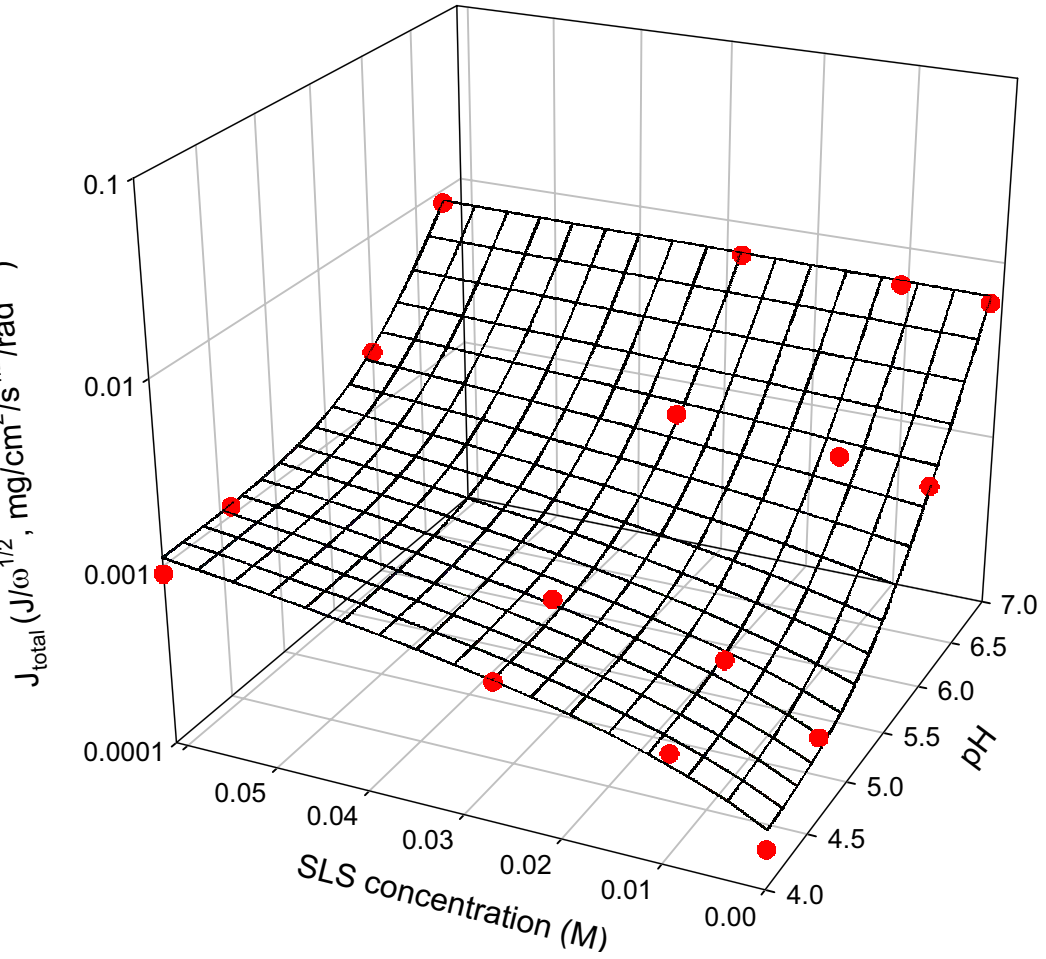

Figure 3.4. The intrinsic dissolution rate as function of pH and SLS.

References.

1. Amidon GL, Lennernas H, Shah VP, Crison JR. **1995**. A theoretical basis for a biopharmaceutic drug classification - the correlation of in-vitro drug product dissolution and in-vivo bioavailability. Pharmaceutical Research 12:413-420.
2. Tarling MM, Toner CC, Withington PS, Baxter MK, Whelpton R, Goldhill DR. **1997**. A model of gastric emptying using paracetamol absorption in intensive care patients. Intensive Care Med 23:256-260.
3. Macdonald IA. **1996**. Physiological regulation of gastric emptying and glucose absorption. Diabet Med 13:S11-15.
4. Li LY, Stewart BH, Fleisher D. **2000**. Oral delivery of hiv-protease inhibitors. Crit Rev Ther Drug Carrier Syst 17:73-99.
5. Olander DR. **1960**. Simultaneous mass transfer and equilibrium chemical reaction. Aiche Journal 6:233-239.
6. Mooney KG, Mintun MA, Himmelstein KJ, Stella VJ. **1981**. Dissolution kinetics of carboxylic acids i: Effect of ph under unbuffered conditions. J Pharm Sci 70:13-22.
7. Mooney KG, Mintun MA, Himmelstein KJ, Stella VJ. **1981**. Dissolution kinetics of carboxylic acids ii: Effect of buffers. J Pharm Sci 70:22-32.
8. Rippie EG, Lamb DJ, Romig PW. **1964**. Solubilization of weakly acidic and basic drugs by aqueous solutions of polysorbate 80. J Pharm Sci 53:1346-1348.
9. Elworthy P, Lipscomb F. **1968**. Effect of some nonionic surfactants and a polyoxyethylene glycol on the dissolution rate of griseofulvin. Journal of Pharmacy and Pharmacology 20:923-933.
10. Carlson JA, Mann HJ, Canafax DM. **1983**. Effect of ph on disintegration and dissolution of ketoconazole tablets. Am J Hosp Pharm 40:1334-1336.
11. Sakr A, Aboutaleb A, Kassem A, Khidr S. **1980**. Study on the dissolution and bioavailability of directly compressed salicylamide tablets. Pharmazeutische Industrie 42:412-415.
12. Schott H, Kwan LC, Feldman S. **1982**. The role of surfactants in the release of very slightly soluble drugs from tablets. J Pharm Sci 71:1038-1045.
13. Samaligy M, Szantmiklosi P. **1978**. Effect of surfactants on the release of a hydrophobic liquid drug from its tablet form. Pharmazeutische Industrie 40:274-277.
14. McNamara DP, Amidon GL. **1986**. Dissolution of acidic and basic compounds from the rotating disk: Influence of convective diffusion and reaction. J Pharm Sci 75:858-868.
15. Nelson KG, Shah AC. **1987**. Mass transport in dissolution kinetics. I: Convective diffusion to assess the role of fluid viscosity under forced flow conditions. J Pharm Sci 76:799-802.
16. Shah AC, Nelson KG. **1987**. Mass transport in dissolution kinetics. Ii: Convective diffusion to assess role of viscosity under conditions of gravitational flow. J Pharm Sci 76:910-913.
17. Holte O, Onsoyen E, Myrvold R, Karlsen J. **2003**. Sustained release of water-soluble drug from directly compressed alginate tablets. Eur J Pharm Sci 20:403-407.
18. Mu X, Tobyn MJ, Staniforth JN. **2003**. Development and evaluation of bio-dissolution systems capable of detecting the food effect on a polysaccharide-based matrix system. J Control Release 93:309-318.

19. Rodriguez-Hornedo N, Murphy D. **2004**. Surfactant-facilitated crystallization of dihydrate carbamazepine during dissolution of anhydrous polymorph. J Pharm Sci 93:449-460.
20. Abdoh AA, Zughul MB, Badwan AA. **2002**. Solubilization of terfenadine, riboflavin, and sudan iii by aqueous multi-basic organic acids. Journal of Dispersion Science and Technology 23:759-768.
21. Jinno J, Oh D, Crison JR, Amidon GL. **2000**. Dissolution of ionizable water-insoluble drugs: The combined effect of ph and surfactant. J Pharm Sci 89:268-274.
22. Amidon GE, Higuchi WI, Ho NF. **1982**. Theoretical and experimental studies of transport of micelle-solubilized solutes. J Pharm Sci 71:77-84.
23. Mukerjee P, Mysels KJ. Critical micelle concentrations of aqueous surfactant systems. ed.: U.S. Dept. of Commerce: NSRDSNBS. p 51.
24. Yalkowsky SH. **1999**. Solubility and solubilization in aqueous media. ed.: Oxford University Press: Cambridge. p 119, 261.
25. Cussler EL. **1997**. Diffusion: Mass transfer in fluid systems. ed., New York: Cambridge University Press. p 65-67.
26. Dyer DL. **1959**. The effect of ph on the solubilization of weak acids and bases. Journal of Colloid Science 14:640-645.
27. Collett JH, Koo L. **1975**. Interaction of substituted benzoic acids with polysorbate 20 micelles. J Pharm Sci 64:1253-1255.
28. He Y, Yalkowsky SH. **2003**. Handbook of aqueous solubility data. ed.: CRC press. p 1036.
29. Beetge E, du Plessis J, Muller DG, Goosen C, van Rensburg FJ. **2000**. The influence of the physicochemical characteristics and pharmacokinetic properties of selected nsaid's on their transdermal absorption. Int J Pharm 193:261-264.
30. Crison JR, Shah VP, Skelly JP, Amidon GL. **1996**. Drug dissolution into micellar solutions: Development of a convective diffusion model and comparison to the film equilibrium model with application to surfactant-facilitated dissolution of carbamazepine. J Pharm Sci 85:1005-1011.
31. Yang X, Matthews MA. **2000**. Diffusion coefficients of three organic solutes in aqueous sodium dodecyl sulfate solutions. J Colloid Interface Sci 229:53-61.
32. FDA. **2000**. Guidance for industry, waiver of in vivo bioavailability and bioequivalence studies for immediate release solid oral dosage forms based on a biopharmaceutics classification system. ed.: CDER/FDA.
33. Dressman JB, Amidon GL, Reppas C, Shah VP. **1998**. Dissolution testing as a prognostic tool for oral drug absorption: Immediate release dosage forms. Pharm Res 15:11-22.
34. Charman WN, Porter CJ, Mithani S, Dressman JB. **1997**. Physiochemical and physiological mechanisms for the effects of food on drug absorption: The role of lipids and ph. J Pharm Sci 86:269-282.
35. Horter D, Dressman JB. **2001**. Influence of physicochemical properties on dissolution of drugs in the gastrointestinal tract. Adv Drug Deliv Rev 46:75-87.
36. Yazdanian M, Briggs K, Jankovsky C, Hawi A. **2004**. The "high solubility" definition of the current fda guidance on biopharmaceutical classification system may be too strict for acidic drugs. Pharm Res 21:293-299.
37. TenHoor CN, Bakatselou V, Dressman J. **1991**. Solubility of mefenamic acid under simulated fed- and fasted-state conditions. Pharm Res 8:1203-1205.

CHAPTER IV

A COMPARISON OF PHOSPHATE AND BICARBONATE BUFFERS: RELEVANCE TO *IN VIVO* DISSOLUTION

Abstract

To evaluate the difference between the pharmaceutical phosphate buffers and the gastrointestinal bicarbonates in dissolution of ketoprofen and indomethacin, to illustrate the dependence of buffer differential on biopharmaceutical properties of BCS II weak acids, and to recommend phosphate buffers equivalent to bicarbonates. The intrinsic dissolution rates of, ketoprofen and indomethacin, were experimentally measured using rotating disk method at 37°C in USP SIF/FaSSIF and various concentrations of bicarbonates, and also theoretically forecasted using a reaction plane model that was improved in this work. Experimental results shows that the intrinsic dissolution rates of ketoprofen and indomethacin, in USP and FaSSIF phosphate buffers are 1.5-3.0 folds of that in the 15 mM bicarbonates, which is in good agreement with the theoretical analysis. Theoretical analysis demonstrates that the buffer differential is largely dependant on the drug pKa and solubility, and weakly dependant on the drug diffusivity. Further, in accordance with the drug pK, solubility and diffusivity, simple phosphate surrogate was proposed to match an average bicarbonate value (15 mM) at the upper gastrointestinal region. Specifically, surrogate phosphate buffer of 13-15 mM and 3-4 mM were recommended for ketoprofen and indomethacin, respectively, whose dissolution demonstrated high satisfaction with respective 85% and 104% equivalence in the 15 mM

bicarbonate buffer. This work highlights the substantial difference between pharmaceutical phosphates and physiological bicarbonates in determining the drug intrinsic dissolution rates of BCS II weak acids, such as ketoprofen and indomethacin. Based on both theoretical analysis and experimental confirmation, surrogate phosphates were recommended in order to closely reflect the *in vivo* dissolution of ketoprofen and indomethacin in gastrointestinal bicarbonates.

Introduction

Drug dissolution is the prerequisite to drug absorption and the subsequent clinical response for almost all drugs administered orally. For Biopharmaceutics Classification System (BCS) Class II drugs with high permeability and low solubility, their drug absorption is rate limited by *in vivo* drug dissolution. Thus, a correlation between an *in vitro* dissolution and *in vivo* performance is expected if the *in vitro* dissolution rate is similar to the *in vivo* dissolution rate [1]. To achieve this objective, the *in vitro* dissolution testing should be reflective of the *in vivo* situation. However, various components of the GI tract, such as transit time, hydrodynamics and fluid contents, present a complex nature of *in vivo* gastrointestinal fluids in upper small intestine [2-7]. Particularly, the dissolution media whose contents should mimic GI fluids, including pH, buffer species and concentration, bile salts, electrolytes, enzymes and a wide range of lipids, are important. In the past, developing biorelevant *in vitro* dissolution medium has attracted numerous interests [4,8-12], resulting in several widely used *in vitro* dissolution media. For example, the most dominant media include the USP simulated intestinal fluids (SIFs) [13] and fasted-state simulated small intestine fluids (FaSSIF) [4,8,14], as shown in Table 4.1. However,

their focus has been on simulating the gastrointestinal (GI) pH and bile salts. Further, the buffer species in these two media is phosphate. One seemingly very obvious choice, however, the GI buffer species, namely the bicarbonates, has been overlooked.

The principle physiological buffer along the human GI tract is not phosphate, rather the bicarbonate. Gastroduodenal bicarbonate has long been known as the main buffer system maintaining a pH gradient along the gastrointestinal lumen [15]. Bicarbonate is a ubiquitous component in human secreted fluids and is actively secreted by the pancreas to neutralize gastric secretion in the GI lumen. It has also been shown that epithelial cells of the duodenum secrete bicarbonate, which is an important mechanism to protect the duodenal epithelium against acid discharged from stomach [16-21]. Bicarbonate concentrations in human GI fluids have been reported to be within a dynamic range, depending on the fasted and fed states as well as local regions along the GI tract [17,19,22,23]. For example, as early as in 1935, the bicarbonate concentration was measured directly from the fasted human duodenum using titration method, and the values were reported in the range of 4-21 mM [24,25], with an average of 15 mM [23]. In 2001, Repishti et al. measured the pH and P_{CO_2} in human duodenum, and used the Henderson-Hasselbalch equation to calculate that the bicarbonate HCO_3^- in fasted-state duodenum has a mean value of 6.7 ± 0.34 mM at pH 7.22 [26]. Person et al. [5] showed that the mean value of the buffer capacity of human jejunum at fasted state is 2.4-2.8 $mmolL^{-1}pH^{-1}$, which corresponds to 18.1 mM of bicarbonate concentration at pH 7.5 assuming that the buffer capacity is solely attributed by the buffer species. Recently, Kalantizi et al.[6] reported the range of buffer capacity for distal duodenum of fasted human, which is equivalent to 4.35 – 21.6 mM of HCO_3^- at pH 6.2.

Bicarbonate is the prevailing buffer in human gastrointestinal GI tract, however, it has rarely been used [27] mainly due to the inconvenience of maintaining a constant pH and HCO_3^- concentration in the dissolution medium through continuous CO_2 gas purging. Almost all pharmaceutical dissolution studies rather use phosphate or acetate buffers, subsequently creating a disconnection with the buffer species between the *in vitro* and the physiological GI *in vivo* situation. This disconnect should be closely evaluated, because, not only buffer concentration but also buffer species can significantly impact dissolution rates of ionizable drugs, even if the pH of buffers is held constant [28-30]. It was shown that the intrinsic dissolution rates of naproxen increase with the escalation of buffer concentration, which was demonstrated consistently in three buffers including phosphate, citrate and acetate [30]. More interestingly, the work also showed that naproxen demonstrated a decreased dissolution rate in the following buffer species: phosphate > citrate > acetate, despite all the buffers were maintained at the same buffer concentration and same pH value [30]. Therefore, it is important to compare the bicarbonate buffer with the commonly used USP SIF/FaSSIF phosphate buffers, in the perspective of investigating their impact on dissolution rates of BCS II acidic drugs. This work is to focus on investigating the impact of GI buffer species and concentration on the dissolution of poorly soluble and ionizable acidic drugs.

Using model BCS II weak acids, such as ketoprofen and indomethacin, we not only demonstrated the dissolution difference between phosphates and bicarbonates experimentally, but also provided a mechanistic understanding of the buffer differential theoretically. In doing so, we illustrated the dependence of buffer differential on

biopharmaceutical properties of drugs, thus ultimately recommending simple phosphate buffer surrogate to be equivalent to *in vivo* bicarbonates.

Theoretical Section

Reaction plane model

The reaction plane model was initially developed for describing chemical reactions on a rotating disk [31], and it was extended to the pharmaceutical situations by Amidon et al. [30,32]. In the current paper, the reaction plane model was further improved to better predict the drug flux.

The general equation describing one-dimensional mass transport in a fluid [33] is composed of the diffusive, convective, and reactive contributions and is shown as the following:

$$\partial c_i / \partial t = D_i d^2 c_i / dz^2 - \upsilon_Z dc_i / dz + R_i \qquad (1)$$

where D_i, c_i and R_i are the diffusion coefficient, the molar concentration, and the rate of reaction per volume of species i ($mol/cm^3 \cdot s$), v is the fluid velocity (cm^2/s), and t is the time (s). The overall mass transport includes the acid-base reactions and convective diffusion, which is fast and slow process, respectively. The continuity Eq 1 can then be simplified by recognizing that slow processes control the overall mass transport.

Assuming instantaneous reactions at the solid-liquid surface, mass transport in a rotating disk system at steady state is simplified as:

$$\partial c_i / \partial t = D_i d^2 c_i / dz^2 - \upsilon_Z dc_i / dz = 0 \qquad (2)$$

Where v_z is the axial velocity of the fluid toward the disk. Litt and Serad [31] have shown that Eq 2 can be scaled by introducing the dimensionless distance variable, n, for the axial distance z , as:

$$n = (\Omega/\nu)^{1/2} z = 1.61(\frac{D}{\nu})^{1/3} \frac{z}{h} = 1.61(Sc)^{-1/3} \frac{z}{h}$$

$$C_{in}(n) = (c_{in} - c_{ib})/(c_{i0} - c_{ib}) \qquad (3)$$

$$V(n) = \upsilon_z /(\nu\Omega)^{1/2}$$

$$Sc_i = \nu / D_i$$

Where Ω is the angular velocity of the disk (rad/s), ν is the kinematic viscosity of the fluids (), c_{in} is the molar concentration of species at distance n, C_{in} is the dimensionless concentration of species i at position n, v_z is the axial velocity of the fluid as reported by Riddiford [34] $[-(\nu\Omega)^{1/2}(0.510n^2 - 0.333n^3 + ...)]$, $V(n)$ is the dimensionless velocity of the liquid, and Sc_i is the dimensionless Schmidt number of species i.

$$d^2C_i / dn^2 - VSc_i dC_i / dn = 0 \qquad (4)$$

Levich has shown that the molar flux of acid from the disk surface is:

$$N_{HA} = D_{HA}(\Omega/\nu)^{1/2} C_{HA_0} (Sc_{HA})^{1/3} /1.613 \text{ and} \qquad (5)$$

$$dC_i / dn = -(Sc_i)^{1/3} /1.613$$

At the solid surface, the following reactions exist:

$$
\begin{aligned}
&H_2O \rightleftharpoons H^+ + OH^- \\
&HA \rightleftharpoons H^+ + A^- \\
&HB \rightleftharpoons H^+ + B^- \\
&HA + B^- \rightleftharpoons HB + A^- \\
&HA + OH^- \rightleftharpoons H_2O + A^- \\
&HB + OH^- \rightleftharpoons H_2O + B^-
\end{aligned}
\qquad (6)
$$

After identifying various chemical reactions at the reaction plane, a set of mass balance equations accounting for all reacting species were established. When the flux of one species changes due to a chemical reaction at the reaction plane, it must be reflected by the flux of the corresponding reactants or products as defined in the aforementioned reactions (Eq 6). Therefore at steady state, the following flux condition must hold at the solid-liquid interface:

$$N_{H^+} + N_{HA} + N_{HB} = N_{OH^-} + N_{A^-} + N_{B^-} \qquad (7)$$

where N_{H^+}, N_{HA}, N_{HB}, N_{OH^-}, N_{A^-} and N_{B^-} individually denote the molar flux of H^+, HA, HB, OH^-, A^- and B^-. It should be noticed that the flux of species of A^- and B^- have different signs because they are supplied from opposite directions, i.e., from the solid surface or from the medium bulk to the reaction plane, respectively. Thus, the electrical neutrality is maintained in Eq 7.

Combined with equations 5 and 7, boundary conditions at the surface (n = 0):

$$
\begin{aligned}
&C_{HA} = 1 \\
&C_{A^-} = 1 \\
&C_{H^+} = 1 \\
&C_{HB} = 1
\end{aligned}
$$

and boundary conditions in the bulk solution (n = ∞):

$C_{HA} = 0$

$C_{A^-} = 0$

$C_{H^+} = 0$

$C_{HB} = 0$

the flux condition was rewritten explicitly in the following system equation (eq 8):

$$\left\{ \begin{array}{l} C_{H^+,0} \times C_{B^-,0} = K_a^{HB}(CT_{HB} - C_{B^-,0}) \\ D_{A^-}[HA]_0 K_a^{HA}(Sc_{A^-})^{1/3} / C_{H^+,0} + D_{B^-}(C_{B^-,0} - C_{B^-,b})(Sc_{B^-})^{1/3} + D_{OH^-}(\frac{K_a^w}{C_{H^+,0}} - \frac{K_a^w}{C_{H^+,b}})(Sc_{OH^-})^{1/3} \\ = D_{H^+}(C_{H^+,0} - C_{H^+,b})(Sc_{H^+})^{1/3} + D_{HB}(C_{HB,b} - C_{B^-,0})(Sc_{HB})^{1/3} + D_{HA}[HA]_0(Sc_{HA})^{1/3} \end{array} \right\} \quad (8)$$

where CT_{HB} is the total molar buffer concentration, $C_{B^-,0}$ is the molar concentration of the basic component at the solid-liquid interface, K_a^{HA} and K_a^{HB} are the ionization constant of the drug and buffer, respectively. The only unknown variables in system equation 8 are $C_{H^+,0}$ and $C_{B^-,0}$, which is readily solvable if the bulk pH, ionization constants of the acidic drug and the buffer, the total buffer concentration, the intrinsic solubility of the drug, and the diffusion coefficients of all species are available. Once $C_{H^+,0}$ is solved, the relative flux increase $\frac{N_{total}}{N_0}$ can be calculated with Eq 9:

$$\frac{N_{total}}{N_0} = 1 + \frac{K_a^{HA}}{C_{H^+,0}} \quad (9)$$

where N_{total} is the total drug flux at a specific pH and rotating speed, which includes the flux from both species HA and A^-; N_0 is the drug flux at the same rotating speed, but dominantly from species HA when the ionization or reaction of HA is negligible at low pH. Using the relative flux increase $\frac{N_{total}}{N_0}$, rather than the absolute total drug flux at

specific condition, made the buffer comparison straightforward, because of employing the N_0 as the common standard.

Film model

The film model was derived originally in 1960's [35] and applied to drug dissolution by Stella et al [28,36]. It is assumed in the film model that the dissolution of drug (HA) into the aqueous media occurs through a diffusion layer-controlled process [28,29,36]. This diffusion layer is calculated according to the Levich rotating-disk model, which is based on the diffusivity of the drug (D_{HA}) regardless of the presence of other species. Within this boundary layer, all concentration gradients of the reactants and products exist as a result of diffusion and instantaneous reactions between the dissolving drug, the buffers, hydroxyl ion and water. Unlike the reaction plane model, all reactions are reversible and homogenous, and they are concurrent with diffusion throughout the boundary layer. The final working equation was derived and detailed by Mooney et al. [28]. The only unknown variable in film model is $C_{H^+,0}$, i.e., the H^+ concentration at the solid-liquid interface, which is solvable by the Newton iterative method using Mathematica 5.1 (Wolfarm Research, Inc., Champaign, IL). Once $C_{H^+,0}$ is solved, the relative flux increase can be calculated using Eq 9.

Table 4.2 lists all the known parameters that were used in the reaction plane and film models, including the pKa values of model drugs and buffers, diffusivity values of all species, and the solubility of the model drugs. In both models, only the predominant ionization of phosphate or bicarbonate, under the working pH range of 6.5-6.8, was considered because other ionization is negligible. Specifically, for the phosphate buffer,

only the $pK_{a,2}$ of $H_2PO_4^-$ was utilized; and for the bicarbonate, the $pK_{a,1}$ of H_2CO_3 was considered.

Experimental Section

Materials and Dissolution Media Preparation

Ketoprofen, indomethacin (> 99% purity), carbonic anhydrase, and all other chemicals were of analytical grade and were purchased from Sigma (St. Louis, MO). Distilled, deionized and filtered water was prepared in house and used for all experiments. Dried and compressed 100% CO_2 was purchased from LifeGas (Ann Arbor, MI). All 3-D plots were generated using Sigmaplot 10.0 (SPSS Inc., Chicago, IL).

The USP SIF pH 6.8, 50 mM phosphate buffer without pancreatin [13] and fasted-state simulated intestinal fluid (FaSSIF, 29 mM pH 6.5 phosphate buffer) without bile salts [4] were prepared following standard procedures. Sodium phosphate was used instead of potassium phosphate because the principle cationic species in fasted small intestine is sodium [2,37,38]. Previous study conducted by Reppas et al. [4] has demonstrated that substituting sodium for potassium in standard USP and International Pharmacopeia buffer systems has no practical effects on the dissolution process of weak acids. The 15 mM bicarbonate buffer was established by initially preparing a 15 mM of sodium carbonate solution, and then the solution was continuously purged with CO_2 (g) until pH was reduced to 6.8 or 6.5. To ensure the bicarbonate buffer was equilibrating, both the pH and the total H_2CO_3 / HCO_3^- (aq) content in the bicarbonate buffer was monitored. The pH was continuously monitored with a standard pH meter and electrode (PHI™40,

Beckman Coulter, Inc., Fullerton, CA), and the H_2CO_3 / HCO_3^- (aq) content was checked periodically using methods described previously [39-41] with a standard CO_2 assay kit purchased from Sigma. After the CO_2 (aq) and the pH of the bicarbonate buffer reach an equilibrium, which takes 30-40 minutes at 37°C, only pH is followed through the intrinsic dissolution testing. To maintain a steady CO_2 (aq) concentration and pH in the bicarbonate buffer at 37°C, a continuous CO_2 (g) purge with a flow rate ~50 mL/min was generally required. Prior to dissolution testing, all buffers were adjusted to be isotonic to normal saline with NaCl.

Intrinsic Dissolution Measurement

The intrinsic dissolution rates of ketoprofen and indomethacin in various buffers were measured using a rotating disk system. Ketoprofen and indomethacin powder of 150 mg was compressed under 2000 LBs and 5000 LBs, respectively, for 60 seconds to form a circular compact with a radius of 0.45 cm using a hydraulic laboratory press (Fred Carver, Inc., Summit, NJ). The die containing the compact was mounted onto a Plexiglass shaft attached to an overhead synchronous motor (Cole-Parmer Scientific, Niles, IL). The die was rotated at 100 rpm, which was calibrated with a digital tachometer (Cole-Parmer Scientific, Niles, IL). The single face of the compact was exposed to 150 mL of the dissolution media in a jacketed beaker maintained at 37 ± 1°C through the circulating water heated with a water bath circulator (Isotemp Constant Temperature Circulator Model 8000, Fisher Scientific, Pittsburgh, PA). At pre-determined time points, 1.0 mL of dissolution sample was withdrawn and same amount of blank dissolution medium was refilled. The ketoprofen and indomethacin concentration in the dissolution media samples were measured using UV absorption at

258 nm and 265 nm, respectively, using a UV spectrophotometer (Beckman Coulter DU 650, Fullerton, CA). To ensure sink conditions, the concentrations of ketoprofen or indomethacin in the dissolution media were maintained less than 10% of their solubility for the entire experiment. Dissolution flux (mass/time/area) of ketoprofen and indomethacin were calculated as the multiplication of the slope of the concentration vs. time plot, volume of dissolution medium (150 mL), and area of the exposed disk (0.63585 cm^2). Individual dissolution experiments typically were carried out from 10 minutes for ketoprofen and up to several hours for indomethacin.

For comparative purposes, dissolution flux of ketoprofen and indomethacin in the following isotonic media were determined: pH 6.8 USP SIF 50 mM phosphate buffer without pancreatin, pH 6.5 FaSSIF containing 29 mM phosphate buffer without sodium taurocholate or lecithin, and pH 6.5 various concentrations of bicarbonate buffers that covers a normal range of bicarbonate concentrations along the fasted human duodenum. Buffers without any enzymes or bile salts were used to distinctively reveal the effects of buffer species. The final pH values of the dissolution media using phosphates were checked at the end of the dissolution experiments to assure that a constant pH has maintained throughout the dissolution testing.

Results

Dissolution of Ketoprofen and Indomethacin in Phosphate and Bicarbonate Buffers

The aim was to evaluate the dissolution difference of ketoprofen and indomethacin in bicarbonates and in the commonly used phosphate buffers. Table 4.3 lists the intrinsic

dissolution rates of ketoprofen in two phosphates (USP and FaSSIF), and three bicarbonate buffers with concentrations of 5, 15 and 20 mM, and Table 4.4 lists the flux ratio of indomethacin in phosphates versus in bicarbonates with concentrations of ranging 6.4 – 25.8 mM. As expected, the higher concentration of bicarbonate, the faster drug flux of indomethacin or ketoprofen to exhibit in the dissolution media. This is because a greater driving force for the reaction between the weakly acidic drug and species HCO_3^-, as shown in Eq 10, exists with the presence of higher bicarbonate concentration.

$$HA + HCO_3^- \rightarrow A^- + H_2CO_3(aq) \qquad (10)$$

More importantly, the intrinsic dissolution rates in the USP SIF buffer and in the FaSSIF are higher than in all bicarbonate buffers. For example, the respective dissolution rate of ketoprofen in the USP SIF and FaSSIF is at least 200% and 50% faster than that in the 15 mM bicarbonate, an average value in fasted duodenum. Again, the intrinsic dissolution rate of indomethacin in phosphate buffer is higher, showing about 30 - 150% of flux increase compared with that in various concentrations of bicarbonate buffers.

In Tables 4.3 and 4.4, the main differences between the phosphates and bicarbonates exhibit in pH (6.8 versus 6.5), buffer concentration and buffer species, which all could contribute to the observed dissolution rate difference. To distinctively reveal the effects of buffer species, intrinsic dissolution rates of ketoprofen were measured in phosphate and bicarbonate with the same pH, i.e., 6.8, and the same buffer concentration, i.e., 50 mM. The results in Table 4.5 showed the ketoprofen flux in this phosphate was still 2-fold of that in the bicarbonate. This experimental result supports the hypothesis that even if at the same pH and the same buffer concentration, in dissolution of ketoprofen, phosphate and bicarbonates are inherently distinctive from

each other. The distinction lie in the natural differences between phosphate and bicarbonate, namely, the pKa and the diffusion coefficient.

First of all, the pKa plays an important role in the driving force for the reaction between the acidic drug and the basic buffer species. At the solid-liquid interface, the essential chemical reaction driving the drug dissolution is the following:

$$HA + B^- \underset{k_r}{\overset{k_f}{\rightleftharpoons}} HB + A^-, \quad K = \frac{k_f}{k_r} = \frac{K_a^{HA}}{K_a^{HB}} \tag{11}$$

Eq 11 clearly indicates that a basic buffer with a higher pKa value translates into a smaller K_a^{HB}, which yields a larger equilibrium constant K for the reaction. Consistent with the experimental results, at 37°C phosphate buffer with an effective pKa of 6.533 provides greater driving force for the acidic drug–buffer reaction than that of bicarbonate with a pKa of 6.31 (shown in Table 4.2), thus leading to faster dissolution rate for ketoprofen and indomethacin.

Secondly, the pKa difference in these two buffer species also results in different buffer capacity at the solid-liquid interface. For a system the same pH and the same buffer concentration, phosphate buffer has about 23% higher buffer capacity relative to the bicarbonate, according to Eq 12.

$$\beta = 2.303C\frac{K_a^{HB}[H^+]}{(K_a^{HB} + [H^+])^2} \tag{12}$$

where β is the buffer capacity. In general, the $C_{H^+,0}$ concentration at the solid-liquid interface is lower than that in the bulk due to the ionization of acidic drug molecule. Within the boundary layer or at the solid-liquid interface, the buffer capacity is controlled not only by the extent of acidic drug disassociation but also the buffer capacity. The

higher buffer capacity of phosphate maintains the pH at the solid-liquid interface lower than, but closer, to the basic environment of the bulk, in relative to the bicarbonate system. Thus, a greater extent ionization of acidic drugs and the subsequent increase of drug dissolution in the phosphates are present.

Thirdly, the diffusion coefficient of buffer species may also have an indirect impact on drug dissolution rates through diffusional layer thickness. The Levich equation [42] indicates that the diffusional layer thickness $h = 1.612 D^{1/3} \upsilon^{1/6} \varpi^{-1/2}$ is accounted for one species, generally the drug molecule. In reality, there are a number of species involved in drug dissolution using the rotating disk. Therefore, it may be logical to consider the boundary layer thickness is an average value composed of all of the species involved in the dissolution. Thus, the species include not only the drug molecules but also the conjugate buffers HB and B^-, and OH^- and H^+. It is apparent that a smaller diffusion coefficient D would produce a thinner boundary layer thickness, which implies less resistant during mass transport. Specifically, the diffusivity for $H_2PO_4^- / HPO_4^{2-}$ is 11.5×10^{-6}cm^2/s, which implies a thinner diffusional layer thickness and a subsequent faster drug flux, in relative to H_2CO_3 and HCO_3^- with respective diffusivity values of 12.3×10^{-6}cm^2/s and 19.5×10^{-6} cm^2/s.

The relative drug flux increase of ketoprofen and indomethacin was forecasted using the reaction plane and film models, which was summarized in Tables 4.3 and 4.4. For ketoprofen, the reaction plane model excellently predicts its dissolution flux increase in phosphate buffer. For example, the reaction plane model predicts the relative drug flux increase in USP SIF buffer is 35-fold, which is very close to the experimental result of 35.8-fold. However, the reaction plane model appears to overestimate the ketoprofen

flux increase in the bicarbonate buffer, i.e., the model calculates a 16.5-fold, despite of an experimental value of 10.5-fold. In the case of indomethacin, both the reaction plane model and film model appear to underestimate the flux ratio of indomethacin in phosphates versus in bicarbonates (Table 4.4). Nevertheless, it should be recognized that even though neither of the models predicts the experimental results exactly, they both reasonably/quantitatively demonstrates the trend of drug flux increase depending on buffer concentration and species. The trend is that the dissolution rate of ketorpofen and indomethacin is up to 2-fold higher, in the studied phosphates, than that in the bicarbonates. Thus, both models are suitable for assessment of phosphate and bicarbonate buffer effects, at least semi-quantitatively.

Dependence of Buffer Differential on Biopharmaceutical Properties of Drugs

Experimentally, this work has showed that ketoprofen and indomethacin demonstrated up to 200% dissolution rate increase in USP SIF and FaSSIF phosphate than in the 15 mM bicarbonate buffer. Theoretically, the buffer differential can be forecasted reasonably well using reaction plane model and film model. The question is: for a given new drug entity, what is the magnitude of the buffer differential? To answer this question, three key parameters including drug pKa, solubility and diffusion coefficient, which are used in the theoretical analysis, are investigated to determine their importance on the buffer species effects.

The buffer differential effects were indicated by the drug flux ratio in the USP SIF to that in the 15 mM bicarbonate. Theoretical analysis indicated that drug pKa has a profound impact on buffer differential, as shown in Figure 4.1. For weak acids with pKa values of 7 or higher, the drug flux ratios in these two tested buffers were close to 1. This

result is reasonable because the ionization difference of these drugs in pH 6.8 USP SIF and pH 6.5 bicarbonate is limited. The observed drug flux is essentially contributed from the unionized form and thus determined by the intrinsic solubility of the unionized form, which should not differ appreciably in various buffers. In comparison, for weakly acidic drugs with pKa values of 6.5 or less, their intrinsic dissolution rates is about 50-200% higher in the USP SIF than that in the 15 mM bicarbonate buffer (Figure 4.1). Thus, the magnitude of buffer differential depends strongly on drug pKa whose value is in the regions of < 6.5, and very weakly in regions of drug pKa > 7.0. It should be noticed that this theoretical calculation underestimates the flux ratio in these two tested buffers. For example, the film model and reaction model predicted that the flux ratio of ketoprofen in these two buffers was 1.77 and 2.12, respectively, which was lower than the experimental ratio of 3.33. A similar result was seen with indomethacin, as shown in Table 4.4, i.e., the flux ratio forecasted theoretically was less than the experimental value.

It is also evident from Figure 4.1 that the buffer differential is more sensitive to the changes of drug pKa but less to the drug solubility. This high dependence of drug flux ratio on drug pKa is hypothesized by the following. It is the drug pKa, rather than the drug solubility, predominantly controls the extent of ionization of drug molecules at the solid-liquid interface. As a result, mainly depending on drug pKa, the amount of ionized drug species varies, as reacting with buffer components and thus demonstrating the buffer differential.

In addition to drug pKa, drug solubility also plays an important role in considering buffer effects in drug dissolution due to its self-buffering capability. Therefore, based on Eq 9 $\frac{N_{total}}{N_0} = 1 + \frac{K_a^{HA}}{C_{H^+,0}}$, acidic high-solubility drug increases the $C_{H^+,0}$ at the solid-liquid

interface, leading to an increase of absolute drug flux N_{total} but a decrease of the relative drug flux $\frac{N_{total}}{N_0}$. Further, the ratio of the relative drug flux in two buffers, i.e., the buffer differential, is much weakly dependant on drug solubility, due to a similar magnitude change of relative drug flux in two buffers. Tables 4.6-1 and 4.6-2 showed that the buffer differential vary insignificantly with drug solubility variation. In addition to drug pKa and solubility, drug diffusivity has a negligible impact on the buffer differential, as shown in Tables 4.7-1 and 4.7-2. In summary, the importance of drug properties on the magnitude of buffer differential decreases in the following order: drug pKa > drug solubility ~ drug diffusivity.

Surrogate Buffer Equivalent to the Bicarbonate

As demonstrated evidently in this work, ketoprofen and indomethacin show higher intrinsic dissolution rates in the commonly accepted USP SIF and FaSSIF phosphate buffer than in the physiological 15 mM bicarbonate buffer. Even though bicarbonate is the prevailing human physiological buffer, it is rarely used as an *in-vitro* dissolution media. The decision to not use bicarbonate is mainly due to its inconvenience because maintaining a stable bicarbonate buffer system requires an equilibrium between PCO_2 (g) and the dissolution media at a given pH, which is generally achieved by continuous purging CO_2 (g) into the media to compensate the fast loss of CO_2 to the atmosphere at 37ºC. Practical considerations lead to the alternative using a simple buffer such as phosphate buffer, as a surrogate for the bicarbonate. The ideal surrogate buffer should behave similarly to the physiological bicarbonates, exhibit almost the same dissolution rates for the same drug, and preferably be easily prepared and maintained. In this work, phosphate buffer surrogates for ketoprofen and indomethacin were initially forecasted

using both the reaction plane model and film model, and then were confirmed using intrinsic dissolution measurement. For ketoprofen, the reaction plane model and film model predicted that 12-14 mM phosphate buffer at pH 6.5 is equivalent to the 15 mM bicarbonate, and experimentally 13.0 mM phosphate was selected, as shown in Table 4.8. The intrinsic dissolution rate of ketoprofen in 13.0 mM phosphate buffer is 0.198 $mg/cm^2/min$, which is 85% of 0.231 $mg/cm^2/min$, the dissolution rate in the 15 mM bicarbonate. Similarly, for indomethacin, theoretical analysis predicted that ~3-4 mM phosphate buffer is suitable as the bicarbonate surrogate. Then, a 3.5 mM phosphate was used, in which the indomethacin intrinsic dissolution rate was 26.0 $\mu g/cm^2/min$. This drug flux is equivalent to 108% of the intrinsic dissolution rate in the bicarbonate. Here, theoretical analysis is useful to recommend a suitable phosphate concentration that is replaceable for the bicarbonate. Further, the theoretical approach is supported by the experimental results. It is also apparent in Table 4.8 that the surrogate phosphate buffer is not one single universal medium for all drug molecules, but rather it should be individualized according to the unique properties of drug molecules including pKa, solubility and diffusivity.

Discussion

Significance of Investigating Bicarbonate Buffer

Our work showed that even with FaSSIF, a phosphate buffer with much lower concentration of 29 mM at pH 6.5, the dissolution of ketoprofen and indomethacin still demonstrated higher rate in the FaSSIF than in the bicarbonate. Thus, an *in-vitro* dissolution testing in either USP SIF or FaSSIF is generally overestimating the true

dissolution rates of ketoprofen and indomethacin *in vivo*. This overestimation, suggested by theoretical analysis, is extrapolated to other BCS II weak acids particularly for those with pKa values less than 6.5. Therefore, although the pH value of USP SIF buffer and FaSSIF may mimic small intestine fluids, the buffer composition and concentration also have significant impacts on weakly acidic BCS II drugs. It is concluded here that not only the pH, but also perhaps more importantly, the buffer species and concentrations should be considered in composing the *in-vitro* dissolution media to closely reflect the *in vivo* dissolution fluids.

To constitute an ideal *in vitro* dissolution medium, buffer species and concentration, pH, bile salts and viscosity of the GI fluids should all be considered. This work was to seek the significance of physiological buffer species and concentration, without inclusion of any bile salts, in dissolution of BCS II acidic drugs. The rationale is the following. Firstly, studying a buffer system without including any other variables such as bile salts would distinctively reveal the buffer effects. Secondly, bile salts at fasting stage may not be important, due to its low concentration rage of 3-5 mM, with an average value of 4.3 mM [8]. A more recent study reported that the bile salt level in fasted human intestinal fluids was 2 ± 0.2 mM [5]. Thirdly, even though bile salts contribute significantly on solubilization and dissolution of low-solubility drugs, their effects on ionizable drugs become minimal if pH change is present. This is particularly true for drugs with pKa values within the pH range of proximal small intestine. Here, the two model compounds ketoprofen and indomethacin have pKa values of 4.76 and 4.18, respectively. If the pH in proximal small intestine is around 6.5, their solubility would be increased approximately 100-fold. In comparison, their solubility enhancement from a low

concentration of 2-5 mM bile salt would be negligible. Our previous studies have demonstrated that buffer/pH effects appear to be more important than surfactant effects in the case of BCS II acids such as piroxicam [11] and ketoprofen [43].

For neutral drugs such as fenofibrate, the difference between the USP SIF and FaSSIF phosphate buffer, from bicarbonates, is significant because no ionization of drug molecules would occur at the solid-liquid interface. The neutral drug would not react with the ionic species from the bulk buffer, and the drug dissolution is essentially controlled by the intrinsic solubility of the drug. Thus, buffer species or concentration has no impact on the drug dissolution rate. For BCS II weakly basic drugs, the buffer differential between the phosphate and bicarbonate should depend on the drug pKa. For a weak base with pKa values close to or higher than the pH range in the small intestine, its significant ionization is expected. As a result, the ionized form and the free base form react with the buffer components, and the buffer differential effects will be observed. In comparison, for weak bases with pKa lower than the pH range, and subsequently with negligible disassociation, in upper small intestine, a difference between the phosphate and bicarbonate is trivial. Dipyridamole is an example of such drug. Dipyridamole is a weak base with pKa value of 6.05 - 6.10, with low solubility of 5.8 µg/mL at 25°C. At pH 6.8, dipyridamole intrinsic flux is independent of the buffer species or concentration, where USP SIF, FaSSIF and bicarbonate buffer were employed [27].

Marketed BCS II Weak Acids

Evidently, the magnitude of the buffer effects depends on the biopharmaceutical properties of the drug molecule. Table 4.9 lists almost all BCS II weak acidic drugs currently on the market in US and foreign countries. All of the listed drugs have pKa

values less than 5.5. As demonstrated in this work, significant buffer differetnial between USP SIF and FaSSIF, and the bicarbonates, should be expected for any BCS II weak acids with a pKa less than 5.5. Specifically, only considering the effect of buffer species, the dissolution rates of these weak acids in the USP SIF and FaSSIF are very likely to be overestimated 50-200% fold of the true values *in vivo*.

Table 4.9 listed that several BCS II weak acids are marketed as sodium, potassium and calcium salts. In general, the salt forms would have a faster dissolution rate than the corresponding acid in the upper small intestine. We hypothesized that the salt forms, if they belong to BCS II class, should also demonstrate differential dissolution rates in USP SIF and FaSSIF relative to the bicarbonate buffers. This is because at upper small intestine the salt form of weak acids generally disassociate to a greater extent than the weak acids, and then the ionized acidic component behave similarly to the weak acid form. Even with very low-solubility salt form such as atorvastatin calcium, which is insoluble in aqueous solution at pH equal or below 4.0, and is very slightly soluble in distilled water at 37°C [44], the impacts of buffer differential may be similar to the case of indomethacin. The extent of buffer differential, however, on the salt forms requires further research.

Surrogates for Bicarbonate Buffer

It is evident that the bicarbonates are the best buffer system representing the *in vivo* GI situation. Practical considerations, however, lead to the use of easily prepared buffer systems, such as phosphate buffers to surrogate the bicarbonates. Further, the concentrations of surrogate phosphate vary significantly depending on the drug pKa and solubility. For drugs with high pKa values such as above pH 7.0, the drug dissolution

rate is only weakly influenced by buffer species and concentration. In this scenario, the commonly used USP SIF or FaSSIF behaves similarly to the bicarbonates. In contrast, BCS II weak acids with pKa values lower than 5.5, which prevails the current market, would show a drug flux in USP SIF that is about 50-200% fold of that in the bicarbonates (Figure 4.1). To minimize the discrepancy between USP SIF and bicarbonates, a lower concentration of phosphate is required to match the drug flux in the bicarbonates at pH 6.5, as suggested experimentally as well as theoretically in our work. Furthermore, this work showed that a low-solubility drug may require a lower phosphate buffer to mimic the bicarbonates than a relative high-solubility drug with similar pKa. For example, ketorpfen with an intrinsic solubility of 9.95×10^{-4} M requires 13-15 mM of phosphate to mimic the bicarbonates, whereas 3-4 mM of phosphate appears to be sufficient for a lower solubility drug such as indomethacin with solubility of 9.58×10^{-6} M. The effect of drug solubility on the surrogate phosphate concentration may result from the self-buffering effect of drug molecules at the solid-liquid interface. As the drug molecules dissolve and then disassociate into the ionized acid-base pairs, which maintains the microenvironmental pH within the boundary layer and functions as self-buffering species in contact with the incoming bulk buffers. A weak acid with high solubility has a higher concentration of the acid-base pair within the boundary layer, which leads to a higher self-buffering capacity and less susceptibility to the changes of bulk buffer.

Dissolution for QC or Bioequivalence

Dissolution tests are used to achieve two major objectives during drug product development: 1). to serve as quality control (QC) specification checking the reproducibility of manufacturing processes and products; and 2). to forecast the *in vivo*

performance of drug products. The experimental test conditions for QC are designed to detect manufacturing variables and stability changes on storage, whereas test conditions for BE should discriminate adequately among products/batches with different *in vivo* release behavior. For the QC testing of BCS II weak acids, the USP [13] suggests a wide range of dissolution media. For example, the media used in the USP monograph for indomethacin is 20% pH 7.2 phosphate and 80% water, for etodolac (pKa = 4.7) is pH 6.8 phosphate, and for sulindac (pKa = 4.5) is 0.1 M pH 7.2 phosphate. However, none of these pharmacopeial monograph phosphate buffers is physiologically relevant. They are primarily useful in checking reproducibility of products during manufacturing procedures to meet regulatory requirements, and they poorly predict the *in vivo* performance of a drug product. Therefore, an *in vitro* bioequivalence (BE) dissolution testing methodology, with which physiologically relevant conditions in the GI tract can be better reflected and the *in vivo* drug product dissolution can be better estimated, needs to be developed.

In addition, as demonstrated experimentally and theoretically in this work, the dissolution profiles for drugs with pKa < 5.5 are expected to show large differences in the monograph phosphate buffer from the physiological bicarbonates. The gap between the USP phosphate buffers and physiological bicarbonates may contribute largely to the dissolution discrepancy between the *in vitro* testing and the *in vivo* situation. Consequently, when *in vivo* dissolution is the rate limiting step to absorption of a BCS II drug, an expected IVIVC may not be observed. Across the industry, a lack of success has been seen in successfully developing an IVIVC for numerous BCS II immediate-release oral dosage forms. Additionally, if a dissolution medium is designed in order to reach

maximum or even 100% of release within the duration of the test, it may satisfy the dissolution specification of a product, but generally do not represent the *in vivo* condition and therefore may not be suitable for BE dissolution purposes. In a typical QC dissolution testing, more than 75-80% of the drug release has dissolved at the final evaluation time point. In contrast, a BE or biorelevant dissolution test for BCS II drugs should be aimed to reflect the extent of an *in vivo* dissolution.

Conclusions

In summary, this work has highlighted the importance of using physiological buffers when determining the drug intrinsic dissolution rates, particularly for BCS II weakly acidic drugs. Based on drug pKa, solubility and diffusivity, and buffer characteristics, theoretical analysis has successfully forecasted the drug flux in various phosphates and bicarbonates at least semi-quantitatively. Practical consideration leads to the utilization of surrogate buffers such as phosphate to mimic physiological bicarbonates. It is expected that the bicarbonate surrogate should better reflect the *in vivo* dissolution fluid, thus further improving the *in vitro* dissolution with the *in vivo* performance, in relative to FaSSIF or USP SIF.

Table 4.1. Commonly used pharmaceutical dissolution media/buffers for simulating upper small intestine.

Dissolution media	pH	Buffer components
USP SIF	6.8	Phosphate: 50 mM
		1% pancreatin
FaSSIF	6.5	Phosphate buffer: 29 mM
		Sodium taurocholate: 3 mM
		Lecithin: 0.75 mM
		NaOH: adjust pH to 6.5
		NaCl: adjust to isotonic

Table 4.2. Parameters used in theoretical analysis.

Species	pKa	D ($\times 10^6$), cm^2/s	M.W.	Solubility (M)
Ketoprofen	4.76[a]	9.3[b] for HA form 9.2[c] for A^-	254.3	9.95×10^{-4}, [a]
Indomethacin	4.17[d]	8.0[b] for HA form 7.9[c] for A^-	253.3	9.58×10^{-6}
$H_2PO_4^-$ /HPO_4^{2-}	7.21[e], 6.53[f]	11.5[g]	98	
H_2CO_3	6.37[e], 6.31[f]	19.2[h]	44.0	
HCO_3^-		12.3[g]		
H^+		104.9[i]		
OH^-		63.0[i]		

[a]: from the paper submitted to *Euro. J. Pharm. Sci*.; [b]: calculated using ADMET Predictor™ based on Einstein-Stokes equation for 37°C; [c]: calculated using harmonic average of HA and H^+ forms; [d]: from D.P. McNarmara et al., *Pharm. Res*., 2003, (20), 1641-1646.; [e]: at 25°C, from both Physical pharmacy, 4th edition, by A. Martin and Lange's handbook of chemistry, 5th edition, by J.A. Dean, McGraw-Hill, Inc., 1999.; [f]: calculated using Gribbs equation ($\ln Ka = \Delta G^0/RT$) with the consideration of temperature.; [g]: limiting ionic mobility for $H_2PO_4^-$, HPO_4^{2-} and HCO_3^- at 37°C is 41.6 and 44.5cm^2/O/equiv., being converted to D using the unit conversation factor from $D = 2.769 \times 10\text{-}6\lambda_i/Z_i$ (E.L. Cussler, Diffusion); [h]: at 25°C, from E.L. Cussler, 2nd ed., 1997, p 112; [i]: at 37°C, from Lange's handbook of chemistry, 5th edition, by J.A. Dean, McGraw-Hill, Inc., 1999, p 8.168.

Table 4.3. Intrinsic flux of ketoprofen in the phosphate and in the bicarbonate buffer systems, experimental and theoretical results.

Buffer components	pH	Experimental (N_{total}/N_0)	Reaction plane model (N_{total}/N_0)	Film model (N_{total}/N_0)
USP SIF, w/o pancreatin, 50 mM phosphate buffer	6.8	35.8	35.0	24.1
FaSSIF w/o bile salts, 29 mM phosphate buffer	6.5	17.6	18.8	12.6
5.0 mM bicarbonate buffer	6.5	6.14	9.67	6.4
15 mM bicarbonate buffer	6.5	10.5	16.5	13.6
20 mM bicarbonate buffer	6.5	14.2	19.4	16.5

Table 4.4. Intrinsic flux ratios of indomethacin in the phosphate versus in the bicarbonates, experimental and theoretical results.

Buffer components	pH	Experimental	Reaction plane model	Film model
USP SIF, 50 mM phosphate buffer: 5% CO_2, 6.4 mM bicarbonate	6.8	2.42	1.68	1.69
USP SIF, 50 mM phosphate buffer: 10% CO_2, 12.9 mM bicarbonate	6.8	1.67	1.34	1.28
USP SIF, 50 mM phosphate buffer: 15% CO_2, 19.3 mM bicarbonate	6.8	1.53	1.21	1.17
USP SIF, 50 mM phosphate buffer: 20% CO_2, 25.8 mM bicarbonate	6.8	1.39	1.14	1.09
USP SIF, 50 mM phosphate buffer: 15 mM bicarbonate	6.8:6.5	2.80	1.92	1.89

Table 4.5. Intrinsic dissolution rates of ketoprofen in 50mM pH 6.8 phosphate and bicarbonate buffers.

Buffer components	pH	Mean flux ($mg/cm^2/min$) (n = 3, S.D.)	Experimental (N_{total}/N_0)
USP SIF, 50 mM phosphate buffer	6.8	0.783 (0.010)	35.8
50 mM bicarbonate buffer	6.8	0.352 (0.003)	16.1
SGF, 0.1 N HCl	1.2	0.022 (0.001)	1.0

Table 4.6-1. Drug flux ratio in USP 50 mM phosphate and 15mM bicarbonate buffers: the impact of drug solubility and drug diffusion coefficient (drug pKa = 3).

	Drug diffusion coefficient ($\times 10^{-5}$ cm2/s)			
Drug Solubility (M)	0.1	0.5	1.0	5.0
1×10^{-8}	2.0	2.0	1.99	1.98
1×10^{-7}	1.99	1.99	1.95	1.92
1×10^{-6}	1.98	1.90	1.85	1.79
1×10^{-5}	1.85	1.79	1.81	1.90
1×10^{-4}	1.81	1.94	1.99	2.03
1×10^{-3}	1.99	2.02	1.99	1.81

Table 4.6-2. Drug flux ratio in USP 50 mM phosphate and 15 mM bicarbonate buffers: the impact of drug solubility and drug diffusion coefficient (drug pKa = 5).

Drug Solubility (M)	**Drug diffusion coefficient ($\times 10^{-5}$ cm2/s)**			
	0.1	0.5	1.0	5.0
1×10^{-8}	1.97	1.97	1.97	1.97
1×10^{-7}	1.97	1.99	1.97	1.97
1×10^{-6}	1.97	1.97	1.96	1.95
1×10^{-5}	1.96	1.96	1.93	1.88
1×10^{-4}	1.95	1.87	1.82	1.75
1×10^{-3}	1.82	1.74	1.74	1.73

Table 4.7-1. Drug flux ratio in USP 50 mM phosphate and 15 mM bicarbonate buffers: the impact of drug pKa and drug diffusion coefficient (drug solubility = 1×10^{-8} M).

	Drug diffusion coefficient (cm^2/s)			
Drug pKa	1×10^{-6}	5×10^{-6}	1×10^{-5}	5×10^{-5}
3.0	2.0	2.0	1.99	1.98
3.5	2.0	2.0	2.0	1.99
4.0	2.0	2.0	1.99	2.0
4.5	1.99	1.99	1.99	1.99
5.0	1.97	1.97	1.97	1.97
5.5	1.91	1.91	1.91	1.91
6.0	1.76	1.76	1.76	1.76
6.5	1.50	1.50	1.50	1.50
7.0	1.24	1.24	1.24	1.24
8.0	1.03	1.03	1.03	1.03

Table 4.7-2. Drug flux ratio in USP 50mM phosphate and 15 mM bicarbonate buffers: the impact of drug pKa and drug diffusion coefficient (drug solubility = 1×10^{-3} M).

	Drug diffusion coefficient (cm^2/s)			
Drug pKa	1×10^{-6}	5×10^{-6}	1×10^{-5}	5×10^{-5}
3.0	1.99	2.02	1.99	1.81
3.5	1.89	1.99	2.00	1.88
4.0	1.80	1.92	1.94	1.88
4.5	1.78	1.80	1.84	1.82
5.0	1.82	1.74	1.74	1.73
5.5	1.84	1.72	1.68	1.61
6.0	1.74	1.66	1.61	1.50
6.5	1.50	1.47	1.44	1.37
7.0	1.24	1.23	1.23	1.20
8.0	1.03	1.03	1.03	1.03

Table 4.8. Phosphate buffer as an equivalent substitute for 15 mM bicarbonate buffer.

Buffer components (pH 6.5)	Ketoprofen	Indomethacin
	Exp. Drug flux (S.D) ($mg/cm^2/min$)	Exp. Drug flux (S.D.) ($\mu g/cm^2/min$)
29 mM phosphate	0.386 (0.010)	40.0 (3.5)
15 mM bicarbonate	0.231 (0.002)	24.0 (4.8)
Theoretical analysis	Theoretical phosphate concentration (mM)	
Reaction plane model	12.0	< 3.0
Film model	13.7	~ 4.0
Exp. phosphate	13.0	3.5
Exp. drug flux (S.D.) using the bicarbonate substitute	0.198 (0.004)	26.0 (0.3)
Proficiency to bicarbonate	86%	108%

Table 4.9. pKa values, maximum dose, and salt forms of some BCS II weak acids.

Compound	pKa values	Maximum dose (mg)	Acid/salt form	Provisional BCS classification
Acetyl-salicylic acid	3.5 [45]	975	Free acid	BCS I or III
Atorvastatin	4.46 [45]	80	Calcium salt	BCS II [46]
Diacerein	4.74*	50	Free acid	non-us marketed drug
Diclofenac	4.2 [47]	50	K and Na salts	BCS II
Diflunisal	3.0 [45]	500	Free acid	BCS II
Etodolac	4.7 [45]	400	Free acid	BCS II
Epalrestat	3.2*	50	Free acid	non-us drug
Fenoprofen	4.5 [47]	600	Calcium salt	BCS II
Flurbiprofen	4.3 [47]	100	Free acid	BCS II
Fluvastatin	4.76*	40	Na salt	BCS II
Furosemide	3.88, 9.37*	80	Free acid	BCS II
Ibuprofen	4.4 [47]	800	Free acid	BCS II
Indomethacin	4.5 [47]	50	Free acid	BCS II
Ketoprofen	4.76 [47]	75	Free acid	BCS II
Ketorolac	3.5 [47]	20	Tromethamine salt	Salt form: BCS I
Mefenamic acid	4.2 [45]	250	Free acid	BCS II
Meloxicam	1.1, 4.2 [48]	15	Free acid	BCS II
Naproxen	4.2 [47]	500	Free acid	Acid: BCS II [49]
		500	Na salt	Na salt: BCS I [50]
Oxaprozin	4.3 [48]	600	Free acid	BCS II
Piroxicam	1.8, 5.1 [48]	20	Free acid	BCS II
Salicylic acid	3.0 [45]	750	Free acid	BCS I
Sulindac	4.5 [47]	200	Free acid	BCS II
Triflusal	4.15*	300	Free acid	non-us drug
Tolmetin [51]	3.5 [47]	600	Na salt	BCS II
Zaltoprofen	4.44*	80	Free acid	non-us drug
Warfarin	5.35*	10	Na salt [52]	BCS I

*: calculated using Program ADMET version 1.2.3,

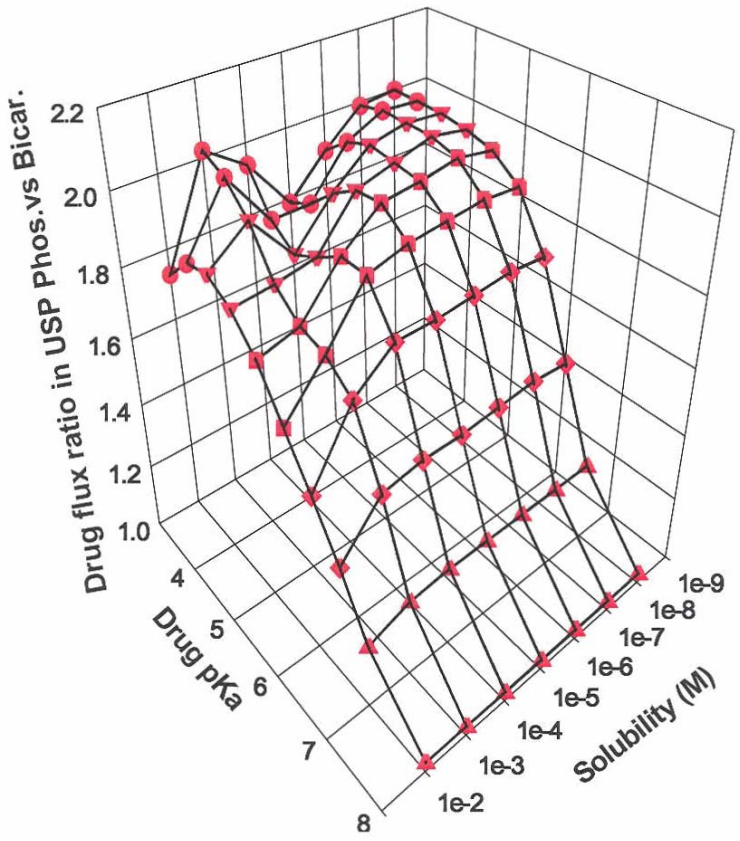

Figure 4.1. Dependence of drug flux ratio in the USP 50 mM phosphate buffer versus 15 mM bicarbonate buffer on drug pKa and solubility.

The drug diffusion coefficient is assumed to be 5×10^{-5} cm^2/s.

References.

1. Amidon GL, Lennernas H, Shah VP, Crison JR. **1995**. A theoretical basis for a biopharmaceutic drug classification: The correlation of in vitro drug product dissolution and in vivo bioavailability. Pharm Res 12:413-420.
2. Lindahl A, Ungell AL, Knutson L, Lennernas H. **1997**. Characterization of fluids from the stomach and proximal jejunum in men and women. Pharm Res 14:497-502.
3. Pedersen BL, Brondsted H, Lennernas H, Christensen FN, Mullertz A, Kristensen HG. **2000**. Dissolution of hydrocortisone in human and simulated intestinal fluids. Pharm Res 17:183-189.
4. Vertzoni M, Fotaki N, Kostewicz E, Stippler E, Leuner C, Nicolaides E, Dressman J, Reppas C. **2004**. Dissolution media simulating the intralumenal composition of the small intestine: Physiological issues and practical aspects. J Pharm Pharmacol 56:453-462.
5. Persson EM, Gustafsson AS, Carlsson AS, Nilsson RG, Knutson L, Forsell P, Hanisch G, Lennernas H, Abrahamsson B. **2005**. The effects of food on the dissolution of poorly soluble drugs in human and in model small intestinal fluids. Pharm Res 22:2141-2151.
6. Kalantzi L, Goumas K, Kalioras V, Abrahamsson B, Dressman JB, Reppas C. **2006**. Characterization of the human upper gastrointestinal contents under conditions simulating bioavailability/bioequivalence studies. Pharm Res 23:165-176.
7. Kalantzi L, Persson E, Polentarutti B, Abrahamsson B, Goumas K, Dressman JB, Reppas C. **2006**. Canine intestinal contents vs. Simulated media for the assessment of solubility of two weak bases in the human small intestinal contents. Pharm Res 23:1373-1381.
8. Dressman JB, Amidon GL, Reppas C, Shah VP. **1998**. Dissolution testing as a prognostic tool for oral drug absorption: Immediate release dosage forms. Pharm Res 15:11-22.
9. Sheng JJ, Kasim NA, Chandrasekharan R, Amidon GL. **2005**. Solubilization and dissolution of insoluble weak acid, ketoprofen: Effects of ph combined with surfactant. European Jounral of Pharmaceutical Sciences sumbitted.
10. Balakrishnan A, Rege BD, Amidon GL, Polli JE. **2004**. Surfactant-mediated dissolution: Contributions of solubility enhancement and relatively low micelle diffusivity. J Pharm Sci 93:2064-2075.
11. Jinno J, Oh D, Crison JR, Amidon GL. **2000**. Dissolution of ionizable water-insoluble drugs: The combined effect of ph and surfactant. J Pharm Sci 89:268-274.
12. Ozturk SS, Palsson BO, Dressman JB. **1988**. Dissolution of ionizable drugs in buffered and unbuffered solutions. Pharm Res 5:272-282.
13. USP. **2000**. The united states pharmacopeia usp 24, the national formulary nf19. ed., Rockville, Maryland: United States Pharmacopeial Convention, Inc. p 2236.
14. Lobenberg R, Kramer J, Shah VP, Amidon GL, Dressman JB. **2000**. Dissolution testing as a prognostic tool for oral drug absorption: Dissolution behavior of glibenclamide. Pharm Res 17:439-444.
15. Allen A, Flemstrom G. **2005**. Gastroduodenal mucus bicarbonate barrier: Protection against acid and pepsin. Am J Physiol Cell Physiol 288:C1-19.

16. Rune SJ. **1972**. The duodenal pco2 in duodenal ulcer patients and normal subjects. Acta Hepatogastroenterol (Stuttg) 19:386-387.
17. Rune SJ. **1972**. Acid-base parameters of duodenal contents in man. Gastroenterology 62:533-539.
18. Flemstrom G. **1994**. Gastric and duodenal mucosal secretion of bicarbonate. 3rd ed., New York: Raven Press. p 1285-1309.
19. Rees WD, Botham D, Turnberg LA. **1982**. A demonstration of bicarbonate production by the normal human stomach in vivo. Dig Dis Sci 27:961-966.
20. Isenberg JI, Hogan DL, Thomas FJ. **1986**. Duodenal mucosal bicarbonate secretion in humans: A brief review. Scand J Gastroenterol Suppl 125:106-109.
21. Hogan DL, Isenberg JI. **1988**. Gastroduodenal bicarbonate production. Adv Intern Med 33:385-408.
22. Kristensen M. **1975**. Titration curves for gastric secretion. A study on duodenal ulcer and gastric ulcer with particular reference to the effect of glycopyrronium. Scand J Gastroenterol Suppl 32:11-144.
23. Goodman LS, Hardman JG, Limbird LE, Gilman AG. **2001**. Goodman and gilman's the pharmacological basis of therapeutics. 10th ed., New York: McGraw-Hill, Medical Publishing Division. p xxvii, 2148 p. [2141] leaf of fold. plates.
24. Tietz NW. **1995**. Clinical guide to laboratory tests. 3rd ed., Philadelphia: W.B. Saunders Co. p xxxix, 1064 p.
25. Karr WG, Abbott WO, Sample AB. **1935**. Intubation studies of the human small intestine. Iv. Chemical characteristics of the intestinal contents in the fasting state and as influenced by the administration of acids, of alkalies and of water. J Clin Invest 14:893-900.
26. Repishti M, Hogan DL, Pratha V, Davydova L, Donowitz M, Tse CM, Isenberg JI. **2001**. Human duodenal mucosal brush border na(+)/h(+) exchangers nhe2 and nhe3 alter net bicarbonate movement. Am J Physiol Gastrointest Liver Physiol 281:G159-163.
27. McNamara DP, Whitney KM, Goss SL. **2003**. Use of a physiologic bicarbonate buffer system for dissolution characterization of ionizable drugs. Pharm Res 20:1641-1646.
28. Mooney KG, Mintun MA, Himmelstein KJ, Stella VJ. **1981**. Dissolution kinetics of carboxylic acids ii: Effect of buffers. J Pharm Sci 70:22-32.
29. Aunins JG, Southard MZ, Myers RA, Himmelstein KJ, Stella VJ. **1985**. Dissolution of carboxylic acids. Iii: The effect of polyionizable buffers. J Pharm Sci 74:1305-1316.
30. McNamara DP, Amidon GL. **1988**. Reaction plane approach for estimating the effects of buffers on the dissolution rate of acidic drugs. J Pharm Sci 77:511-517.
31. Litt M, Serad G. **1964**. Chemical reactions on a rotating disk. Chemical Engineering Science 19:867-884.
32. McNamara DP, Amidon GL. **1986**. Dissolution of acidic and basic compounds from the rotating disk: Influence of convective diffusion and reaction. J Pharm Sci 75:858-868.
33. Cussler EL. **1997**. Diffusion: Mass transfer in fluid systems. ed., New York: Cambridge University Press. p 65-67.
34. Riddiford AC. **1966**. Advances in electrochemistry and electrochemical engineering. ed., New York: Interscience. p 47-116.

35. Olander DR. **1960**. Simultaneous mass transfer and equilibrium chemical reaction. Aiche Journal 6:233-239.
36. Mooney KG, Mintun MA, Himmelstein KJ, Stella VJ. **1981**. Dissolution kinetics of carboxylic acids i: Effect of ph under unbuffered conditions. J Pharm Sci 70:13-22.
37. Banwell JG, Gorbach SL, Pierce NF, Mitra R, Mondal A. **1971**. Acute undifferentiated human diarrhea in the tropics. Ii. Alterations in intestinal fluid and electrolyte movements. J Clin Invest 50:890-900.
38. Davenport HW. **1982**. Physiology of the digestive tract: An introductory text. 5th ed., Chicago: Year Book Medical Publishers. p 201.
39. AOAC. **1995**. Methods of analysis of the association of official analytical chemists. 18th ed., Washington. p 1.46.
40. Caputi A, Ueda M, Walter P, Brown T. **1970**. Titrimetric determination of carbon dioxide in wine. American Journal of Enology and Viticulture 21:140-&.
41. Caputi A, Walker DR. **1987**. Titrimetric determination of carbon-dioxide in wine - collaborative study. Journal of the Association of Official Analytical Chemists 70:1060-1062.
42. Levich VG. **1962**. Physicochemical hydrodynamics. ed., Englewood Cliffs, N.J.: Prentice-Hall. p 700 p.
43. Sheng JJ, Kasim NA, Chandrasekharan R, Amidon GL. **2006**. Solubilization and dissolution of insoluble weak acid, ketoprofen: Effects of ph combined with surfactant. Eur J Pharm Sci 29:306-314.
44. AHFS. **2005**. Ahfs drug information. ed.: Copyright 2005 by the American Society of Health-System Pharmacists, Inc. p 24:06.08.
45. O'Neil MJ, Merck & Co. **2001**. The merck index: An encyclopedia of chemicals, drugs, and biologicals. 13th ed., Whitehouse Station, NJ: Published by Merck Research Laboratories Division of Merck. p 1 v. (various pagings).
46. Kearney AS, Crawford LF, Mehta SC, Radebaugh GW. **1993**. The interconversion kinetics, equilibrium, and solubilities of the lactone and hydroxyacid forms of the hmg-coa reductase inhibitor, ci-981. Pharm Res 10:1461-1465.
47. Jack DB. **1992**. Handbook of clinical pharmacokinetic data. ed., Basingstoke, Hants: Macmillan.
48. Medical Economics Company. **1995**. Pdr medical dictionary. ed., Montvale, N.J.: Medical Economics. p v.
49. Avdeef A, Berger CM, Brownell C. **2000**. Ph-metric solubility. 2: Correlation between the acid-base titration and the saturation shake-flask solubility-ph methods. Pharm Res 17:85-89.
50. Kim YS, Mendez del Rio JR, Rousseau RW. **2005**. Solubility and prediction of the heat of solution of sodium naproxen in aqueous solutions. J Pharm Sci 94:1941-1948.
51. Wishart DS, Knox C, Guo AC, Shrivastava S, Hassanali M, Stothard P, Chang Z, Woolsey J. **2006**. Drugbank: A comprehensive resource for in silico drug discovery and exploration. Nucleic Acids Res 34:D668-672.
52. Zingone G, Rubessa F. **2005**. Preformulation study of the inclusion complex warfarin-beta-cyclodextrin. Int J Pharm 291:3-10.

CHAPTER V

SUMMARY

So far, dissolution testing is one of the most widely employed quality control criteria for oral drug products. Using the current dissolution methods as a predictive tool for the *in vivo* performance of a drug product, however, is very difficult if not impossible. has been frequently encountered in pharmaceutical product development, with pharmacopeia dissolution testing often either over- or under- discriminating the *in vivo* dissolution behavior for an immediate drug product. Evidently, the gap between *in vitro* dissolution results and *in vivo* dissolution are largely caused by the discrepancy between *in vitro* dissolution design and *in vivo* GI environment. project was thus to focus on mechanistically investigating key *in vitro* dissolution parameters that can closely reflect *in vivo* drug dissolution, with the ultimate goal to design a bioequivalent dissolution methodology.

To achieve this goal we started investigating the effect of particle size and paddle speeds on the diffusional layer thickness h_{app} in a USP dissolution apparatus II. Fenofibrate, a neutral and poorly soluble drug with a single polymorph, was selected as the model compound. In the literature, the dependence of h_{app} on particle size assumes various relationships. Popular among them includes $h_{app} = r$ or h_{app} as a constant based on a rotating disk system, and h_{app} comparable to or larger than r in a

rotating bottle. One immediate goal of this work is to examine how h_{app} is related to particle radius r in a pharmaceutically relevant system such as a USP dissolution vessel. It is surprising that even with global usage of the USP paddle device, this relationship has not been experimentally determined through powder dissolution testing. It is well known that h_{app} is a function of fluid velocity. Unfortunately, the dependence of h_{app} on paddle speeds or fluid velocity has been largely ignored in pharmaceutical field. This work demonstrated that the dependence of h_{app} on particle size follows different functions in accordance with the paddle speed. At 50 rpm, the function of h_{app} is best described by a linear plot of $h_{app} = 9.91\sqrt{d} - 23.31$ ($R^2 = 0.98$) throughout the particle size range of 6.8-106 μm. In contrast, at 100 rpm a transitional particle radius of 23.7 μm exists, under which a linear relationship of $h_{app} = 1.59r$ ($R^2 = 0.98$) manifests, but above which h_{app} becomes a constant of 43.5 μm. Further, the effect of particle size and paddle speed on h_{app} was combined using dimensionless analysis. Within certain fluid velocity/particle size regime, linear correlation of $\frac{h_{app}}{d}$ with the square-root of Reynolds number $(\frac{d\varpi}{\upsilon})^{1/2}$, i.e., $\frac{h_{app}}{d} = 1.5207 - 9.25\times10^{-4}(\frac{d\varpi}{\nu})^{1/2}$ ($R^2 = 0.9875$), was observed. One unique finding of work is the independence of diffusional layer thickness on fluid velocity for the drug particles in micron range. certainly merits further investigation considering the current technological trend of micronizing and nanonizing. In addition, the application of apparent diffusion layer thickness h_{app} to the real drug powder namely polydispersed powder, should be investigated in the future. Further, in this work a non-ionized compound was used. Examination of the dependence of h_{app} on particle size and paddle

speed for ionizable BCS II drugs such as weak acids and bases is yet to be conducted. Conceivably, in addition to diffusion and convection, the reaction term can be included into the apparent h_{app}.

The other objective of this work is to design *in vitro* dissolution media closely reflecting *in vivo* GI fluids. To accomplish goal, two research investigations were conducted: 1). The combined effects of pH and surfactants in solubilization and dissolution of a BCS II acid ketoprofen; 2). The buffer differential between bicarbonate and phosphate in dissolution of ketoprofen and indomethacin. A lot of attention has been paid to the pH of dissolution media so that they match the pH changes along GI tract. Surfactants as economic substitute for bile salts have been examined by several investigators recently. When the effects of pH and surfactants were combined and compared, work revealed that pH is the far more important factor than surfactants (bile salts) in solubilization and dissolution of a BCS II weak acid with a pKa value within the GI pH range, mainly because pH has the log-scale effect whereas surfactant has a linear effect on ionizable drug dissolution. Surfactants are still important in constituting dissolution media especially for non-ionizable low-solubility drugs. Further, even at the same pH and with the same buffer concentration, BCS II weak acids still exhibit different dissolution rates depending on the buffer species. Therefore, bicarbonate as a key buffer species in dissolution medium was investigated. work demonstrated the buffer differential between bicarbonates and phosphates both experimentally using rotating disk method and theoretically using reaction plane model and film model. Specifically, the intrinsic dissolution rates of ketoprofen and indomethacin in USP and FaSSIF phosphate buffers are 50-200% faster than those in 15 mM bicarbonates, which is in good

agreement with the theoretical trendline. Using theoretical approach, the buffer differential was demonstrated to depend on the biopharmaceutical properties of API in the following decreasing order: drug pKa > drug solubility ∂ drug diffusivity. The significance of this finding is that for a given new drug candidate, the effects of buffer species can be forecasted and then appropriate buffer can be selected in dissolution testing. Even though bicarbonate is *in vivo* buffer system, its utilization in practice is inconvenient due to difficulty of maintaining CO_2 concentration in aqueous phase. Therefore, through theoretical prediction and experimental results a simple buffer such as phosphate buffer can be recommended, in which the dissolution rates of an API is equivalent to that in the bicarbonates. Specifically, in this work I showed that at pH 6.5 ketoprofen and indomethacin require 13 -14 mM and 3-4 mM phosphate buffer to match 85% and 108% of the dissolution rates in 15 mM bicarbonate buffer, respectively. Both phosphate concentrations are far below than the USP SIF and FaSSIF, suggesting that the current phosphates are very likely overestimate the true dissolution rates *in vivo*. Much work remains in designing the optimal dissolution media to mimic *in vivo* fluids. is because *in vivo* fluids inevitably change along the GI tract and vary among individuals. Therefore, one single dissolution medium can not possibly reflect the complexity and dynamic of GI fluids. I trust that this work will at least lead the colleagues' attention to and stimulate interest in bicarbonates or its surrogates when constituting a BE dissolution medium.

In the future, in order to establish a meaningful bioequivalent methodology, hydrodynamics, choice of dissolution media, and interplay between these two should be all carefully considered.